



University of Pennsylvania  
**ScholarlyCommons**

---

Publicly Accessible Penn Dissertations


---

2020

## Tumor-Derived Retinoic Acid Regulates Intratumoral Monocyte Differentiation To Promote Immune Suppression

Samirkumar S. Devalaraja  
*University of Pennsylvania*

Follow this and additional works at: <https://repository.upenn.edu/edissertations>

 Part of the [Allergy and Immunology Commons](#), [Immunology and Infectious Disease Commons](#), and the [Medical Immunology Commons](#)

---

### Recommended Citation

Devalaraja, Samirkumar S., "Tumor-Derived Retinoic Acid Regulates Intratumoral Monocyte Differentiation To Promote Immune Suppression" (2020). *Publicly Accessible Penn Dissertations*. 3801.  
<https://repository.upenn.edu/edissertations/3801>

This paper is posted at ScholarlyCommons. <https://repository.upenn.edu/edissertations/3801>  
For more information, please contact [repository@pobox.upenn.edu](mailto:repository@pobox.upenn.edu).

---

# Tumor-Derived Retinoic Acid Regulates Intratumoral Monocyte Differentiation To Promote Immune Suppression

## Abstract

The immunosuppressive tumor microenvironment (TME) is a major barrier to immunotherapy. Within solid tumors, why monocytes preferentially differentiate into immunosuppressive tumor associated macrophages (TAMs) but not immunostimulatory dendritic cells (DCs) remains unclear. Using multiple murine sarcoma models, we found that the TME induced tumor cells to produce retinoic acid (RA), which polarized intratumoral monocyte differentiation towards TAMs and away from DCs via suppression of DC-promoting transcription factor Irf4. Genetic inhibition of RA production by tumor cells or pharmacologic inhibition of RA signaling within the TME increased stimulatory monocyte-derived cells, enhanced T cell-dependent anti-tumor immunity and demonstrated striking synergy with immune checkpoint blockade. Further, an RA responsive gene signature in human monocytes correlated with an immunosuppressive TME in multiple human tumors. RA has been long considered as an anti-cancer agent, but our work demonstrates its tumorigenic capability via myeloid-mediated immune suppression and provides proof of concept for targeting this pathway for tumor immunotherapy.

## Degree Type

Dissertation

## Degree Name

Doctor of Philosophy (PhD)

## Graduate Group

Immunology

## First Advisor

Malay Haldar

## Keywords

cancer, dendritic cell, macrophage, monocyte, retinoic acid, sarcoma

## Subject Categories

Allergy and Immunology | Immunology and Infectious Disease | Medical Immunology

---

This dissertation is available at ScholarlyCommons: <https://repository.upenn.edu/edissertations/3801>

TUMOR-DERIVED RETINOIC ACID REGULATES INTRATUMORAL MONOCYTE  
DIFFERENTIATION TO PROMOTE IMMUNE SUPPRESSION

Samir Devalaraja

A DISSERTATION

In

Immunology

Presented to the Faculties of the University of Pennsylvania

in

Partial Fulfillment of the Requirements for the

Degree of Doctor of Philosophy

2020

Supervisor of Dissertation

---

Malay Haldar, M.D., Ph.D.

Assistant Professor of Pathology and Laboratory Medicine

Graduate Group Chairperson

---

David M. Allman, Ph.D.

Professor of Pathology and Laboratory Medicine

Dissertation Committee

George Cotsarelis, M.D., Milton Bixler Hartzell Professor of Dermatology

Jorge Heno-Mejia, M.D., Ph.D., Associate Professor of Pathology and Laboratory Medicine

Gerald P. Linette, M.D., Ph.D., Professor of Medicine

Anil K. Rustgi, M.D., Professor of Medicine

TUMOR-DERIVED RETINOIC ACID REGULATES INTRATUMORAL MONOCYTE  
DIFFERENTIATION TO PROMOTE IMMUNE SUPPRESSION

COPYRIGHT

2020

Samir Devalaraja

This work is licensed under the  
Creative Commons Attribution-  
NonCommercial ShareAlike 3.0  
License

To view a copy of this license, visit

<http://creativecommons.org/licenses/by-nc-sa/3.0/>

## ACKNOWLEDGEMENT

Thank you to all the members of the Haldar laboratory for helpful scientific discussion, technical assistance and consistent support during my Ph.D. In particular, I am forever indebted to my co-graduate students Ian Folkert and Jerrick To, without whom I would not have gotten through graduate school. Thanks also to the collegial community on the 4<sup>th</sup> floor of BRB, who have always been willing to share reagents and engage in friendly conversation. A special thank you to Ali Najj, who inspired me during undergrad to pursue a career as a physician-scientist. Very grateful for my supportive thesis committee, Jorge Henao-Mejia, Gerald Linette and Anil Rustgi. Thanks also to Celeste Simon and Ivan Maillard, whose guidance has been instrumental for my project. Thank you to the Immunology Graduate Group and MSTP Program, especially Dave Allman, Mary Taylor, Skip Brass and Maggie Krall for their help and support.

A huge thanks to George Cotsarelis, who has been an unwavering mentor since my first year as a combined degree student. His scientific and professional insights have proved invaluable over the years. And of course, thank you to my thesis mentor Malay Haldar. Despite me being his first graduate student, he has provided an exceptional environment in his laboratory for me to grow as a scientist. His passion for asking and answering fundamental questions has immeasurably enhanced the way that I approach science. Lastly, thank you to my friends and family for building the foundation for me to chase my dreams.

## ABSTRACT

### TUMOR-DERIVED RETINOIC ACID REGULATES INTRATUMORAL MONOCYTE DIFFERENTIATION TO PROMOTE IMMUNE SUPPRESSION

Samir Devalaraja

Malay Haldar

The immunosuppressive tumor microenvironment (TME) is a major barrier to immunotherapy. Within solid tumors, why monocytes preferentially differentiate into immunosuppressive tumor associated macrophages (TAMs) but not immunostimulatory dendritic cells (DCs) remains unclear. Using multiple murine sarcoma models, we found that the TME induced tumor cells to produce retinoic acid (RA), which polarized intratumoral monocyte differentiation towards TAMs and away from DCs via suppression of DC-promoting transcription factor *Irf4*. Genetic inhibition of RA production by tumor cells or pharmacologic inhibition of RA signaling within the TME increased stimulatory monocyte-derived cells, enhanced T cell-dependent anti-tumor immunity and demonstrated striking synergy with immune checkpoint blockade. Further, an RA responsive gene signature in human monocytes correlated with an immunosuppressive TME in multiple human tumors. RA has been long considered as an anti-cancer agent, but our work demonstrates its tumorigenic capability via myeloid-mediated immune suppression and provides proof of concept for targeting this pathway for tumor immunotherapy.

## TABLE OF CONTENTS

<b>ACKNOWLEDGEMENT</b>	<b>III</b>
<b>ABSTRACT</b>	<b>IV</b>
<b>LIST OF FIGURES</b>	<b>IX</b>
<b>CHAPTER 1: INTRODUCTION</b>	<b>1</b>
1.1: Overview of cancer immunotherapy	1
1.2: Tumor immunity cycle	4
1.3: Mononuclear phagocyte ontogeny and heterogeneity in solid tumors	5
1.4: Transcriptional and metabolic control of monocyte differentiation	9
1.5: Retinoic acid synthesis and metabolism	10
1.6: Role of retinoic acid in immune system and mononuclear phagocytes	11
1.7: Role of retinoic acid in tumorigenesis	12
1.8: Overview of sarcoma	13
<b>CHAPTER 2: TUMOR-DERIVED RETINOIC ACID PROMOTES MACROPHAGE AND BLOCKS DENDRITIC CELL DIFFERENTIATION FROM INTRATUMORAL MONOCYTES</b>	<b>15</b>
<b>2.1: TME promotes monocyte differentiation into immunosuppressive TAMs</b>	<b>15</b>
2.1.1: Distribution of mononuclear phagocytes in sarcoma	15
2.1.2: Ontogeny of mononuclear phagocytes in sarcoma	16
2.1.3: Suppressive function of mononuclear phagocytes in sarcoma	18
2.1.4: TME promotes intratumoral monocytes to differentiate into suppressive macrophages	20
2.1.5: Intratumoral monocytes retain capacity for dendritic cell differentiation	22
<b>2.2: Tumor cells produce retinoic acid in response to T cell derived Interleukin 13</b>	<b>24</b>
2.2.1: Sarcomas harbor elevated levels of RA	24
2.2.2: Tumor cells produce majority of RA in sarcoma	27
2.2.3: TME is required for tumor cell RA production	29
2.2.4: T cell derived IL-13 promotes tumor cell RA production	31

**2.3: RA-RAR signaling promotes macrophage but suppresses DC differentiation from monocytes via *Irf4*** **33**

2.3.1: RA inhibits DC and promotes macrophage differentiation from mouse and human monocytes 33

2.3.2: RA inhibits DC and promotes macrophage differentiation from tumor monocytes 37

2.3.3: RA enhances suppressive function of mouse and human monocyte derived APCs 39

2.3.4: *Irf4* is required for the effects of RA on monocyte differentiation 43

**CHAPTER 3: INHIBITING RETINOIC ACID PRODUCTION OR RETINOIC ACID RECEPTOR SIGNALING IN THE TUMOR MICROENVIRONMENT AUGMENTS ANTI-TUMOR IMMUNITY** **47**

**3.1: Reducing tumor RA production enhances intratumoral stimulatory APCs** **47**

3.1.1: CRISPR-Cas9 mediated deletion of RA producing enzymes 47

3.1.2: Reducing tumor RA production decreases intratumoral suppressive macrophage and increases stimulatory DC 49

3.1.3: Unbiased single cell RNA sequencing of immune compartment in RA inhibited tumors 51

3.1.4: Reducing tumor RA production augments intratumoral T cell responses 54

3.1.5: Additional models to validate the effects of inhibiting RA production on intratumoral APCs and anti-tumor immune responses 57

3.1.6: Reducing tumor RA production enhances T cell-dependent anti-tumor immunity 59

3.1.7: Reducing tumor RA production synergizes robustly with immune checkpoint blockade 62

**3.2: Inhibiting RAR signaling in TME or monocytes enhances anti-tumor immune responses** **64**

3.2.1: RAR inhibition enhances intratumoral stimulatory APCs and T cell responses in multiple murine cancer models 64

3.2.2: RAR inhibition synergizes with immune checkpoint blockade selectively in RA producing tumors 67

3.2.3: Additional models to validate the effects of RAR inhibition on intratumoral APCs and anti-tumor immune responses 69



3.2.4: Monocyte-specific RAR inhibition increases intratumoral DC and augments anti-tumor immunity	71
<b>3.3: Human tumors display evidence of RA-mediated immunosuppression</b>	<b>73</b>
3.3.1: Tumor cells upregulate RA producing enzymes in human sarcomas	73
3.3.2: Analysis of RA production across the TCGA mRNA dataset	75
3.3.3: Generation and analysis of “RA response score” in sarcoma	77
3.3.4: Analysis of “RA response score” across TCGA mRNA dataset	79
<b>CHAPTER 4: DISCUSSION</b>	<b>83</b>
4.1: Targeting myeloid differentiation in the tumor microenvironment	83
4.2: Dual functions of retinoic acid in tumorigenesis	84
4.3: Ontological specificity of metabolic control of differentiation	87
4.4: Varied roles of Th2 cytokines in solid tumor biology	88
<b>CHAPTER 5: MATERIALS AND METHODS</b>	<b>93</b>
<b>5.1: Experimental models and subject details:</b>	<b>93</b>
5.1.1: Mouse models	93
5.1.2: Tumor cells	94
5.1.3: Human samples	94
<b>5.2: Method details:</b>	<b>95</b>
5.2.1: “RA response score” computation and TCGA analysis	95
5.2.2: Analysis of microarray	96
5.2.3: Implantation of tumor cells, tumor growth measurements and survival analyses	96
5.2.4: Flow cytometry of murine samples	97
5.2.5: T cell IFNg <i>ex vivo</i> assay	98
5.2.6: <i>In vitro</i> tumor cell proliferation assay	98
5.2.7: ALDEFLUOR assay	98
5.2.8: Cell sorting	99
5.2.9: LC-MS for ATRA	99
5.2.10: Bone marrow monocyte isolation	99
5.2.11: Intratumoral monocyte transfer	100
5.2.12: <i>In vitro</i> and <i>ex vivo</i> mouse and human monocyte differentiation assays	100
5.2.13: Mouse and human T cell suppression assays	101

5.2.14: Depletion of CD4+ or CD8+ T cells <i>in vivo</i>	101
5.2.15: <i>In vivo</i> reagents	101
5.2.16: RNA isolation and qPCR analysis for gene expression	102
5.2.17: CRISPR mediated gene deletion in tumor cells	103
5.2.18: Overexpression of target genes in tumor cells	103
5.2.19: Single cell sequencing preparation	104
5.2.20: Single cell RNA sequencing analysis	104
5.2.21: Quantification and statistical analysis	105
<b>BIBLIOGRAPHY</b>	<b>106</b>

## LIST OF FIGURES

- 1.1.1: Ontogeny of mononuclear phagocytes in tumor microenvironment
- 1.1.2: Representative murine models of sarcoma
- 2.1.1: Distribution of mononuclear phagocytes in sarcoma
- 2.1.2: Ontogeny of mononuclear phagocytes in sarcoma
- 2.1.3: Suppressive function of mononuclear phagocytes in sarcoma
- 2.1.4: TME promotes intratumoral monocytes to differentiate into suppressive macrophages
- 2.1.5: Intratumoral monocytes retain capacity for dendritic cell differentiation
- 2.2.1: Sarcomas harbor elevated levels of RA
- 2.2.2: Tumor cells produce majority of RA in sarcoma
- 2.2.3: TME is required for tumor cell RA production
- 2.2.4: T cell derived IL-13 promotes tumor cell RA production
- 2.3.1: RA inhibits DC and promotes macrophage differentiation from mouse and human monocytes
- 2.3.2: RA inhibits DC and promotes macrophage differentiation from tumor monocytes
- 2.3.3: RA enhances suppressive function of mouse and human monocyte derived APCs
- 2.3.4: *Irf4* is required for the effects of RA on monocyte differentiation
- 3.1.1: CRISPR-Cas9 mediated deletion of RA producing enzymes

3.1.2: Reducing tumor RA production decreases intratumoral suppressive macrophage and increases stimulatory DC

3.1.3: Unbiased single cell RNA sequencing of immune compartment in RA inhibited tumors

3.1.4: Reducing tumor RA production augments intratumoral T cell responses

3.1.5: Additional models to validate the effects of inhibiting RA production on intratumoral APCs and anti-tumor immune responses

3.1.6: Reducing tumor RA production enhances anti-tumor immunity

3.1.7: Reducing tumor RA production synergizes robustly with immune checkpoint blockade

3.2.1: RAR inhibition enhances intratumoral stimulatory APCs and T cell responses in multiple murine cancer models

3.2.2: RAR inhibition synergizes with immune checkpoint blockade selectively in RA producing tumors

3.2.3: Additional models to validate the effects of RAR inhibition on intratumoral APCs and anti-tumor immune responses

3.2.4: Monocyte-specific RAR inhibition increases intratumoral DC and augments anti-tumor immunity

3.3.1: Tumor cells upregulate RA producing enzymes in human sarcomas

3.3.2: Analysis of RA production across the TCGA mRNA dataset

3.3.3: Generation and analysis of “RA response score” in sarcoma

3.3.4: Analysis of “RA response score” across TCGA mRNA dataset

#### 4.1.1: Unifying model of findings described in Devalaraja et al. 2020

## CHAPTER 1: INTRODUCTION

### 1.1: Overview of cancer immunotherapy

The infiltration of neoplastic tissue with leukocytes, first reported by Rudolf Virchow in the 19<sup>th</sup> century, provided initial evidence that the immune system may interact with cancer (Balkwill and Mantovani, 2001). Virchow hypothesized that “irritation” of normal tissue associated with a lymphoreticular infiltrate may contribute to the origin of tumors (Balkwill and Mantovani, 2001). We now understand that the immune system does indeed engage with malignant tissue, and that inadequate tumor immunity fundamentally contributes to the tumor progression (Motz and Coukos, 2013).

In an effort to restore immune control of cancer, a multitude of immunotherapy strategies have been discovered and developed over the years. One of the earliest attempts of cancer immunotherapy dates back more than 100 years to the Memorial Hospital in New York, where surgeon scientist William B. Coley subcutaneously injected bacterial products (colloquially known as “Coley’s Toxins”) into patients with sarcomas and other types of solid tumors to boost anti-tumor immune responses (Coley, 1891). Although his approach was reported to demonstrate considerable activity in clinical trials, it was deemed at the time to have limited therapeutic value (van den Boorn and Hartmann, 2013).

Over the past few decades, however, the scientific community has made significant progress in our understanding of how the immune system interacts with cancer (Chen and Mellman, 2013). Indeed, a strong body of literature demonstrates that the immune system plays an active role in shaping the immunogenicity of growing tumors (Schreiber and Podack, 2009). Spontaneously induced immune responses were clearly shown by Schreiber and others to protect from carcinogen-induced sarcoma and epithelial carcinomas in mice (Dunn et al., 2004). Further, over the course of tumorigenesis, it is now understood that immune pressure is required to generate the growth of selected tumor cell clones with enhanced resistance to immune-mediated deletion, in part due to deficiencies in immunogenic antigens (Motz and Coukos, 2013). On the flip side, these studies emphasize the importance of tumor heterogeneity and genetic instability in shaping the anti-tumor immune response. Collectively, the aforementioned interactions in which cancer cells attempt to thwart immune-mediated clearance are termed immune evasion. The eventual failure of the immune response against cancer leading to tumor outgrowth has been termed immune escape (Dunn et al., 2004).

Tumor infiltrating T cells are a hallmark of ongoing anti-tumor immune surveillance. Although anti-tumor T cells can be spontaneously generated in tumors, the sustained deletion of tumor cells which express targets of T cell attack enable tumors to escape T cell-mediated clearance

(van den Boorn and Hartmann, 2013). Nevertheless, overcoming immune suppressive factors in the tumor microenvironment and lymphoid organs has led to augmented anti-tumor T cell immune responses, suggesting the presence of immune evasion mechanisms beyond antigen escape in solid tumors (Benci et al., 2016). Along these lines, fundamental discoveries into the regulation and function of T cells have led to the development of an arsenal of T cell-based immunotherapies. Most prominently, insight into the negative regulation of T cell activation and effector function has led to the clinical development of “immune checkpoint” inhibitors in a multitude of cancers. These include monoclonal antibodies against programmed cell death protein 1 (PD-1) and cytotoxic T lymphocyte associated protein 4 (CTLA-4). Though the clinical success of alleviating T cell suppression by anti-PD-1 and anti-CTLA-4 monoclonal antibodies highlight the therapeutic potential of targeting immune evasion pathways for the treatment of solid tumors, the majority of patients demonstrate inadequate clinical responses, suggesting the presence of additional immune evasion mechanisms (Broz and Krummel, 2015). My thesis work sought to uncover additional ways in which tumor cells thwart the immune system and prevent immune-mediated control of solid tumors. In particular, my work focused on the contributions of myeloid cells as critical regulators of anti-tumor T cell responses. Myeloid cells are amongst the most abundant cell types in sarcomas and the majority of solid tumors. Therefore, a deeper understanding of their biology



in the context of tumorigenesis may provide opportunities for improved therapeutic approaches for the treatment of cancer.

## 1.2: Tumor immunity cycle

Tumor immunity involves (1) the capture and processing of tumor antigens by antigen presenting cells (APCs), (2) migration of APCs to draining lymph nodes to prime T cells, and (3) migration of primed T cells to the tumor where they exert cytotoxic anti-tumor effects (cytotoxic T cells or CTLs) (Coley, 1891). APCs are important at multiple steps of this cycle; dendritic cells (DCs) process tumor antigens to prime anti-tumor T cells, DCs and immunostimulatory (M1-polarized) tumor-associated macrophages (TAMs) support CTL function, while immunosuppressive (M2-polarized) TAMs counteract CTL function (Chen and Mellman, 2013).

DCs are sentinel cells of the immune system that are required to identify and eliminate threats (Mildner and Jung, 2014a). While the scientific community has a good understanding of mechanisms by which pathogens activate DCs, how tumors are sensed and subsequently eliminated by DCs is poorly understood. Mice deficient in DCs display defects in anti-tumor immunity, demonstrating that DCs can detect tumors and orchestrate anti-tumor immune responses (Fuentes et al., 2011; Hildner et al., 2008a). Recent studies have supported the concept that tumors can alter DC function or prevent DC recruitment. For example, Wnt/ $\beta$ -catenin activation

was shown in a subset of melanoma tumors to block DC and recruitment into the tumor microenvironment. In turn, defective DC recruitment resulted in a lack of cytotoxic T cell priming, poor CD8 T cell infiltration into tumor, and ultimately to resistance to immune checkpoint blockade (Spranger et al., 2015a). Furthermore in ovarian cancer, lipid peroxidation products were demonstrated to activate the ER stress response pathway and thereby disable critical functions of DCs in the tumor bed and draining lymph node, such as antigen presentation (Juan R. Cubillos-Ruiz et al., 2015).

The aforementioned examples serve to not only emphasize the importance of DCs in the generation and maintenance of anti-tumor T cell responses, but also to exemplify the diversity of immune evasion mechanisms that solid tumors may utilize. Indeed, immunosuppression within the tumor microenvironment (TME) has emerged as a key barrier for the immunotherapy of solid tumors. The TME promotes suppressive TAMs and inhibits DCs, thereby impeding the generation and maintenance of functional anti-tumor CTLs (Veglia and Gabrilovich, 2017). Therefore, identifying pathways that polarize APC distribution in the TME is critical for developing new treatment approaches for cancer immunotherapy.

### 1.3: Mononuclear phagocyte ontogeny and heterogeneity in solid tumors

The tumor microenvironment (TME) contains two major types of antigen presenting cells (APCs) – tumor associated macrophages (TAMs) and dendritic cells (DCs). DCs are required to generate effective anti-tumor immunity as they process and present tumor associated antigens to initiate anti-tumor T cell responses (Broz and Krummel, 2015; Veglia and Gabrilovich, 2017). Currently, several subsets of DCs have been identified based on their ontogeny and dependence on specific transcription factors. Under steady state conditions, the vast majority of DCs in tissues develop from common dendritic cell precursors (CDPs), hardwired DC precursors that have committed to the DC fate before entering the periphery (Mildner and Jung, 2014b). CDPs give rise to classical dendritic cells (cDCs), which in tumors can be classified into two subsets: CD103<sup>+</sup> CD11b<sup>-</sup> cDC1s dependent on transcription factors BATF3 and IRF8, and CD103<sup>-</sup> CD11b<sup>+</sup> cDC2s dependent on IRF4 (Broz et al., 2014; Merad et al., 2013). Studies performed using genetically engineered mice that are deficient in cDC1s (BATF3 KO) or have a functional defect in cDC1 cross presentation (WDFY4 KO) have demonstrated that these cells are critical to the generation of anti-tumor CD8 T cell immunity (Hildner et al., 2008b; Theisen et al., 2018). However, cDCs are exceedingly rare and often dysfunctional in solid tumor microenvironments (Herber et al., 2010). To this end, efforts to augment cDC functionality have shown moderate promise in generating de novo adaptive anti-tumor immunity for specific tumor types (Juan R. Cubillos-Ruiz et al., 2015; Spranger et al., 2015b).

Macrophages can originate from early embryonic precursors or from circulating monocytes (Halder and Murphy, 2014). Likewise, DCs differentiate from bone-marrow derived DC-precursors (conventional DCs or cDCs) or from circulating monocytes (monocyte-derived DCs or moDCs) (Mildner and Jung, 2014b). While cDCs are required for both spontaneous and therapy-induced antitumor immune responses, the role of moDCs in tumor immunity is less clear (Veglia and Gabrilovich, 2017). Circulating monocytes are vastly more abundant than cDC precursors, and under inflammatory conditions can readily differentiate into moDCs (Merad et al., 2013). Within solid tumors, however, monocytes do not appear to generate moDCs and instead differentiate into immunosuppressive TAMs (Richards et al., 2012). The molecular basis for this is largely unknown (Salmon et al., 2019).

Under inflammatory conditions such as cancer, monocytes migrate into peripheral tissues and can undergo local differentiation into DCs (Merad et al., 2013; Segura and Amigorena, 2013). Although the transcriptional programs and local factors that drive the differentiation of monocyte-derived DCs (moDCs) are likely distinct from those that drive cDCs, the specific transcription factors and environmental cues that control moDC differentiation remain unclear (Briseño et al., 2016a; Daro et al., 2000; Greter et al., 2012; Menezes et al., 2016; Merad et al., 2013). moDCs have

been shown to play important functions in anti-tumor immunity, such as cross-presenting tumor antigens, migrating to tumor-draining lymph nodes to activate T cells, and providing stimulatory signals to maintain effector T cell responses, among others (Kuhn et al., 2015; Kumar et al., 2016, p. 45; Ma et al., 2013; Mach et al., 2000; Marigo et al., 2016; Segura et al., 2013; Segura and Amigorena, 2013). The relative frequency moDCs has been correlated with CD8 T cell activation and favorable treatment responses to chemotherapy and immunotherapy in various mouse and human tumors (Kuhn et al., 2013; Marigo et al., 2016; Rich et al., 2012).

However, the majority of monocytes that enter the TME undergo local differentiation into immunosuppressive TAMs (Noy and Pollard, 2014; Qian and Pollard, 2010). Indeed, circulating monocytes are a highly abundant immune cell type in a variety of solid tumors and have emerged as the major precursors for TAMs (Franklin and Li, 2016; Ginhoux and Jung, 2014; Lim et al., 2016; Richards et al., 2012). Immunosuppressive TAMs are abundant and pose a major barrier to successful tumor immunotherapy in part by dampening T cell effector function (Noy and Pollard, 2014; Qian and Pollard, 2010). The polarization of APCs toward TAMs and away from DCs is considered an important immune evasion strategy utilized by solid tumors (Broz and Krummel, 2015; Vinay et al., 2015). Importantly, circulating monocytes enter the TME and have the ability to differentiate into TAMs or

DCs – however, why the majority of monocytes differentiate into TAMs and not DCs is largely unknown.

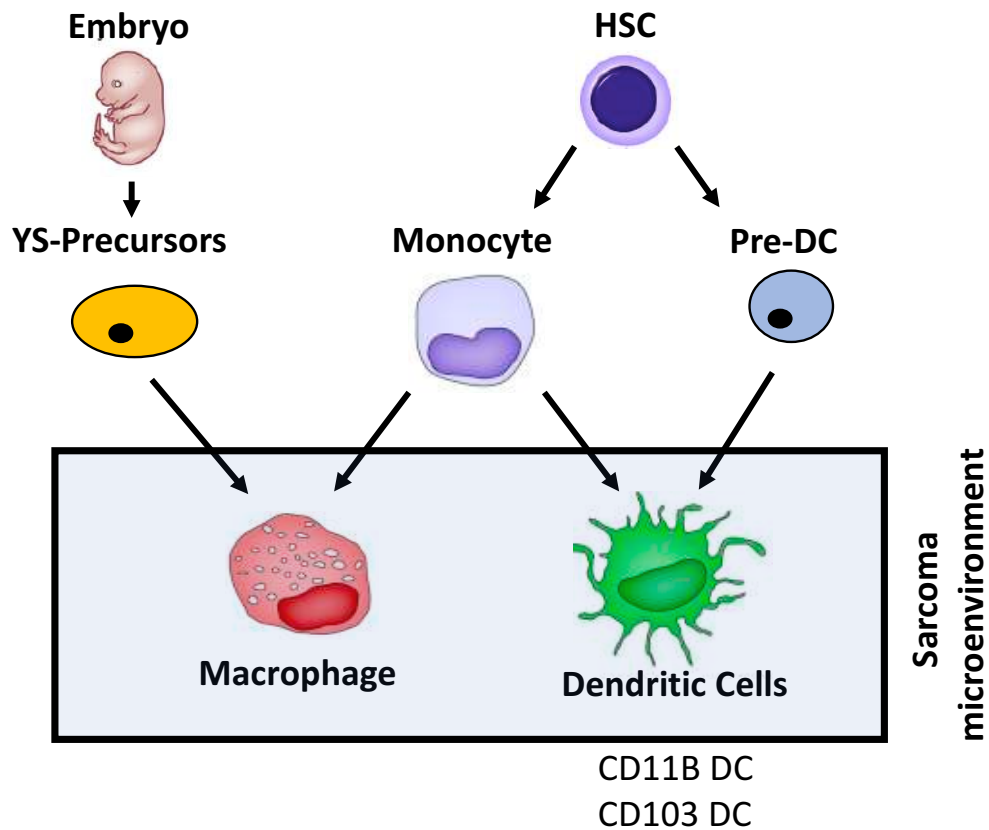


**Figure 1.1.1 Ontogeny of mononuclear phagocytes in the tumor microenvironment.** Tissue macrophages can arise from either yolk-sac progenitors or bone-marrow-derived monocytes. Similarly, DCs can arise from bone marrow derived monocytes or committed pre-DC progenitors.

#### 1.4: Transcriptional and metabolic control of monocyte differentiation

Recent studies have begun to elucidate the transcriptional circuitry controlling monocyte differentiation into distinct APC subtypes (Briseño et al., 2016b). As an example, the transcription factors *Irf4* and *MafB* were shown to have key roles in regulating monocyte differentiation into DC vs. macrophage respectively (Goudot et al., 2017). However, microenvironmental factors that control the selective induction of these transcription factors to induce alternative fate commitment of monocytes remain to be elucidated.

Tissue metabolites may play a key role in this process, as evidenced by the role of environmental heme in inducing the differentiation of monocytes into splenic iron-recycling macrophages via induction of transcription factor *SpiC* (Haldar et al., 2014). Likewise, retinoic acid (RA), a metabolite of vitamin A, has been previously shown to play a role in the development and functional specification of peritoneal macrophages via induction of transcription factor *Gata6* (Gundra et al., 2017; Okabe and Medzhitov, 2014). However, how tumor metabolites may impact monocyte differentiation into APCs is unclear.

### 1.5: Retinoic acid synthesis and metabolism

RA is a small molecule generated from vitamin A-derivative retinol through a series of enzyme-catalyzed intermediary steps (Duester, 2008). The first step in RA synthesis is the oxidation of retinol to retinaldehyde, and is

catalyzed by a group of alcohol dehydrogenase enzymes (Duester, 2008). The expression of these alcohol dehydrogenase enzymes is overlapping and wide ranging throughout almost every tissue in the human body. The second step of RA synthesis is the the rate limiting step, which is the conversion of retinaldehyde to RA via retinaldehyde dehydrogenases (Raldh1, 2, or 3) (Duester, 2008). These enzymes exhibit non-overlapping expression in tissues and are thought to play a critical role in the regulation of RA synthesis, although the regulation of the expression of the enzymes themselves is largely unknown (Duester, 2008). The oxidization and subsequent degradation of RA is executed by three cytochrome P450 enzymes, CYP26A1, CYP26B1 and CYP26C1. Similar to Raldh enzymes, these CYP enzymes also display non-overlapping expression and tissue specificity, suggesting that they may play a role in the regulation of the biological roles of RA (Kumar et al., 2012).

#### 1.6: Role of retinoic acid in immune system and mononuclear phagocytes

RA is a powerful morphogen with well-established roles in development (Erkelens and Mebius, 2017). Though RA has diverse functions in both innate and adaptive immunity, it is generally known to promote tolerance via multiple immune cell types (Erkelens and Mebius, 2017). Several studies have examined the impact of RA on peripheral monocyte differentiation with conflicting conclusions. While some studies have



reported that RA promotes DC differentiation, others have reached the opposite conclusion (Jin et al., 2010; Mohty et al., 2003). Similarly, though RA is known to induce Foxp3<sup>+</sup> T regulatory cells and Arg1 producing anti-inflammatory macrophages, it has also been reported to promote anti-tumor Th1 or Th17 T cell responses and dampen myeloid derived suppressor cell function (Bhatt et al., 2014; Bhattacharya et al., 2016; Hill et al., 2008; Nefedova et al., 2007; Vellozo et al., 2017). Factors contributing to these discrepancies include the exclusive reliance on cell surface markers to represent cellular identity and function, the use of inconsistent or supra-physiological doses of RA in experimentation, and the presence of additional environmental factors that modulate RA's effects (Duester, 2017). Further, the impact of RA on tumor-associated APCs remains unclear.

### 1.7: Role of retinoic acid in tumorigenesis

Raldh enzymes are highly expressed in many human tumors (Khoury et al., 2012; Li et al., 2010, 2014; Marcato et al., 2015; Wei et al., 2015; Zhang et al., 2013, p. 3). Indeed, given RA's critical role as a pro-differentiation agent during development, the effect of RA to promote tumor cell differentiation and suppress tumor growth has been studied for decades, albeit with limited clinical translation outside of promyelocytic leukemia (Tang and Gudas, 2011). However, solid tumors represent a complex niche comprising of many different cell types other than malignant cells (Binnewies et al., 2018).

Hence, we wanted to explore whether RA could act on immune cells in the TME to promote immune suppression and facilitate tumor growth, a concept that has not been adequately explored.

## 1.8: Overview of sarcoma

Soft tissue sarcoma (STS) is a rare but heterogeneous collection of fatal malignancies that arise from mesenchymal tissue such as fat, muscle, cartilage, etc (Blay and Ray-Coquard, 2016). Though surgery and radiation are mainstay therapies for localized disease, metastasis is common and often fatal, with metastatic STS exhibiting a 5 year survival rate of less than 15% (Linch et al., 2014). Recent efforts to utilize immunotherapies such as immune checkpoint blockade in STS have demonstrated efficacy only in a small percentage of patients; unfortunately, the vast majority of patients remain refractory (Ghosn et al., 2017). Uncovering novel immune evasion mechanisms in STS is thus critical to develop efficacious immunotherapies for this fatal disease.

Human sarcomas are heterogeneous with over 70 diagnostic subtypes, but can be broadly classified based on their underlying genetic aberrations: (1) unique translocations resulting in fusion oncogenes, (2) mutations in tumor suppressors or oncogenes and (3) genomic instability without a consistent mutation (Taylor et al., 2011). We utilize a representative mouse model for each of these genetic categories: synovial sarcoma (SS) (driven by SYT-

SSX fusion oncogene), undifferentiated pleomorphic sarcoma (UPS) (driven by loss of p53 and activation of KRAS), and fibrosarcoma (FS) (syngeneic transplant of sarcoma cell lines derived from methylcholanthrene induced murine fibrosarcomas) (Haldar et al., 2007; Kirsch et al., 2007; Schreiber and Podack, 2009).

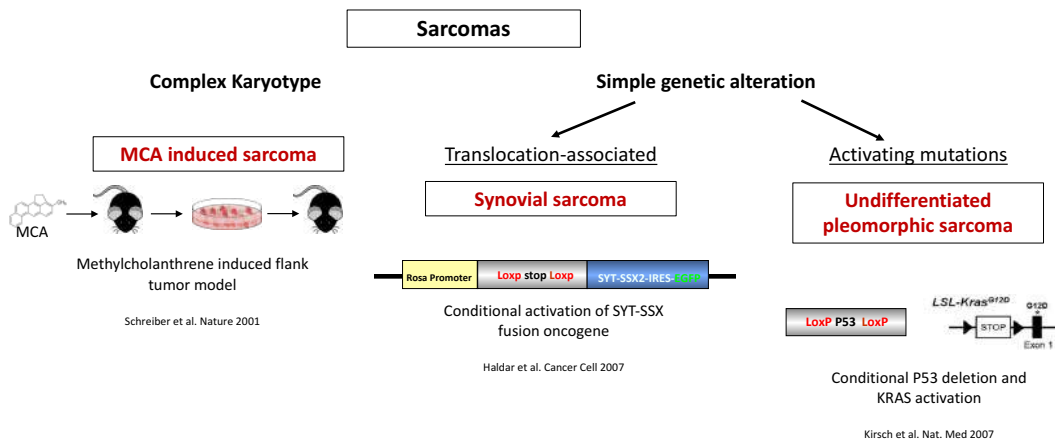


**Figure 1.1.2. Representative mouse models of diverse sarcomas.** Sarcomas can be classified genetically into broad categories – those with a complex karyotype and sarcomas with simple genetic alterations, which are further subclassified into translocation-associated sarcomas or sarcomas with other specific mutations. We utilize representative mouse models for each of these genetic subtypes.

CHAPTER 2: TUMOR-DERIVED RETINOIC ACID PROMOTES  
MACROPHAGE AND BLOCKS DENDRITIC CELL DIFFERENTIATION  
FROM INTRATUMORAL MONOCYTES

2.1: TME promotes monocyte differentiation into immunosuppressive TAMs

2.1.1: Distribution of mononuclear phagocytes in sarcoma

The distribution, function and ontogeny of mononuclear phagocytes (MPs) have been described in common solid tumors such as breast, lung, colon and melanoma (Broz et al., 2014; Broz and Krummel, 2015; Laoui et al., 2011). In contrast, MPs have been sparsely studied in sarcoma (Ehnman and Larsson, 2015). In fibrosarcoma, undifferentiated pleomorphic sarcoma and synovial sarcoma mouse models, monocytes and TAMs comprised the majority of intratumoral leukocytes (Fig. 2.1.1A and 2.1.1C). In contrast, CD11b<sup>+</sup> DCs were rare and CD103<sup>+</sup> DCs exceedingly rare (Fig. 2.1.1B, 2.1.1D, 2.1.1E). These results are in concordance with the aforementioned studies which also concluded that though the frequency of leukocytes may differ based on tumor type, the majority of leukocytes in solid tumors are mononuclear phagocytes. Of mononuclear phagocytes, the vast majority are monocytes and macrophages, with bonafide dendritic cells being much rarer.

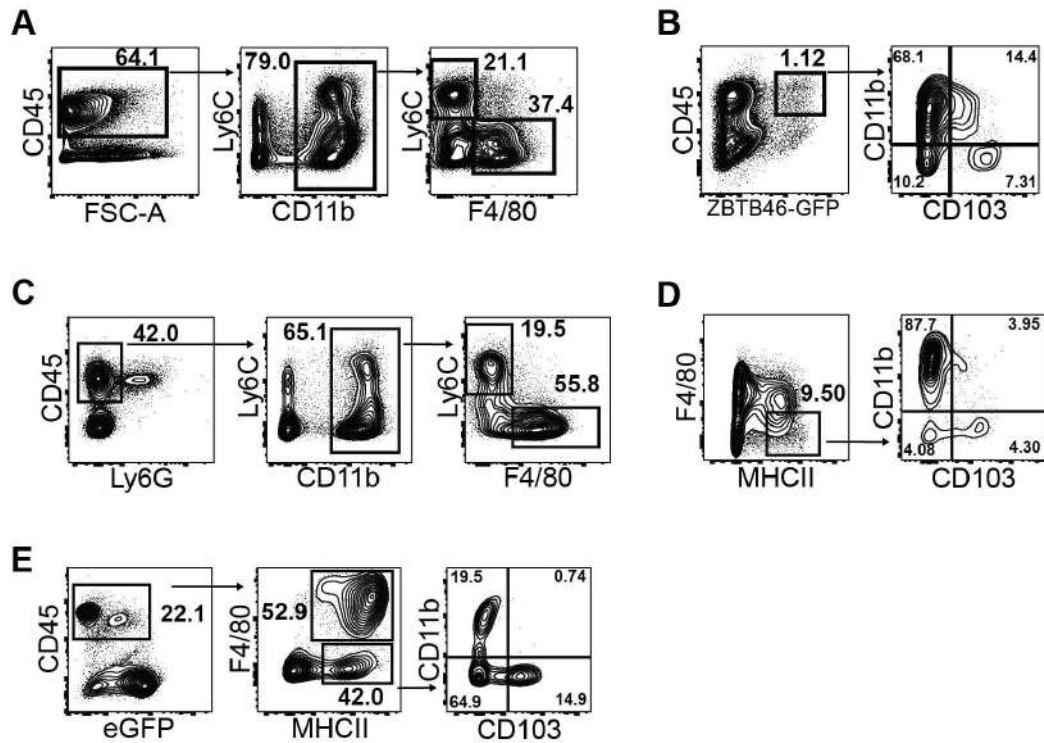


**Figure 2.1.1: Distribution of mononuclear phagocytes in sarcoma. A and B,** Representative contour plots of monocyte (CD45<sup>+</sup>CD11b<sup>+</sup>Ly6C<sup>+</sup>), TAM (CD45<sup>+</sup>CD11b<sup>+</sup>F4/80<sup>+</sup>Ly6C<sup>-</sup>) and DC (CD45<sup>+</sup>ZBTB46<sup>+</sup>) distributions in FS tumors (n>20 tumors). **C and D,** Representative contour plots of monocytes, TAMs and DCs in UPS tumors (n=8 tumors). **E,** Representative contour plots of TAM and DC distribution in SS tumors (n=6 tumors).

### 2.1.2: Ontogeny of mononuclear phagocytes in sarcoma

Studies in other solid tumors have shown monocytes to be the major source of TAMs (Richards et al., 2012). However, this may depend on the type of solid tumor, as recent studies have suggested that yolk-sac derived macrophages may be the source of TAMs in pancreatic ductal adenocarcinoma. To identify monocyte progenies in the sarcoma TME, we

used monocyte lineage-tracing by generating FS tumors (syngeneic transplant) in  $LysM^{Cre}; Rosa26^{tdT}$  hosts (Abram et al., 2014).  $LysM$  marks monocytes and neutrophil ontogeny (Abram et al., 2014). The majority of TAMs were indeed tdTomato positive and thus derived from monocytes in this setting (Fig. 2.1.2A). In contrast, monocytes generated a minor fraction of DCs (Fig. 2.1.2A). We further corroborated these findings in a monocyte-deficient autochthonous mouse model of UPS generated by breeding the murine UPS model to  $Ccr2^{-/-}$  mice (Fig. 2.1.2B and 2.1.2C). In  $Ccr2^{-/-}$  mice, which have approximately a three-fold reduction in circulating monocytes in addition to a defect in monocyte egress into tissues, tumor macrophages (but not tumor DCs) were reduced approximately two fold, suggesting a monocytic origin for tumor macrophages (Fig. 2.1.2B and 2.1.2C).

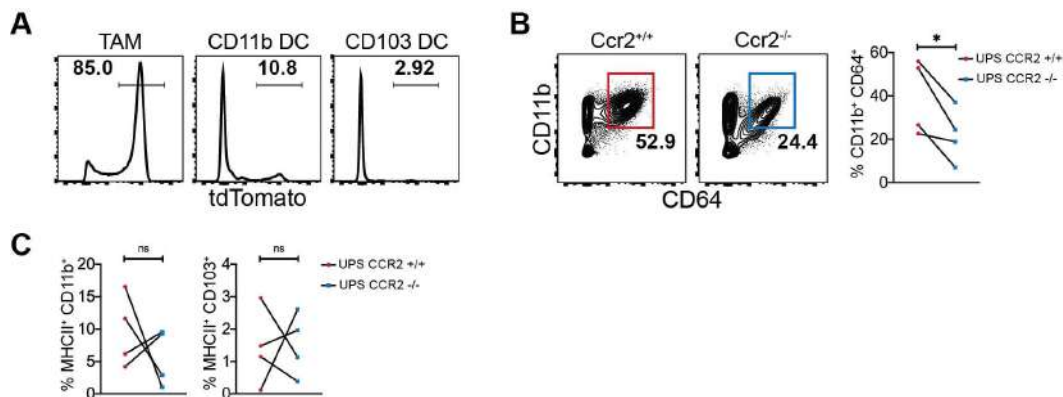


**Figure 2.1.2: Ontogeny of mononuclear phagocytes in sarcoma. A,**  $LysM$  lineage tracing. FS tumors were implanted into  $LysM^{Cre}; Rosa26^{tdT}; Zbtb46^{GFP}$  hosts. Histogram of tdT expression in  $F4/80^{+}$  TAMs,  $CD11b^{+}$  DCs or  $CD103^{+}$  DCs. Data are representative of  $n > 15$  tumors across three independent experiments. **B and C,** Comparison of TAM,  $CD11b^{+}$  DC and

CD103<sup>+</sup> DC frequency in Ccr2 deficient (Ccr2<sup>-/-</sup>) and control (Ccr2<sup>+/+</sup>) UPS tumors (n=4 tumors per group). \*p<0.05, Two-tailed t test. All error bars represent SEM. Events shown are pregated on live singlets unless otherwise specified.

### 2.1.3: Suppressive function of mononuclear phagocytes in sarcoma

Though monocytes, macrophages and DCs can impact T cell function in the tumor microenvironment, the relative ability for each of these cell types to stimulate or suppress T cell responses remains unclear. To assess the impact of the different MP subsets on T cell proliferation we isolated monocytes, TAMs, or DCs from tumors and co-cultured them with aCD3/28 stimulated splenic T cells (Fig. 2.1.3A). DC isolation was greatly facilitated by use of the Zbtb46<sup>GFP</sup> mouse that allowed clear distinction of DCs from TAMs, which can be challenging by using surface markers alone (Satpathy et al., 2012, p. 46). In both FS and UPS, TAMs and monocytes suppressed T cell proliferation, with TAMs displaying greater suppression (~2-3x) (Fig. 2.1.3B, 2.1.3C, 2.1.3D). In stark contrast, DCs stimulated T cell proliferation (Fig. 2.1.3E). Hence, the abundant TAMs were the most immunosuppressive MP cell in the sarcoma TME.

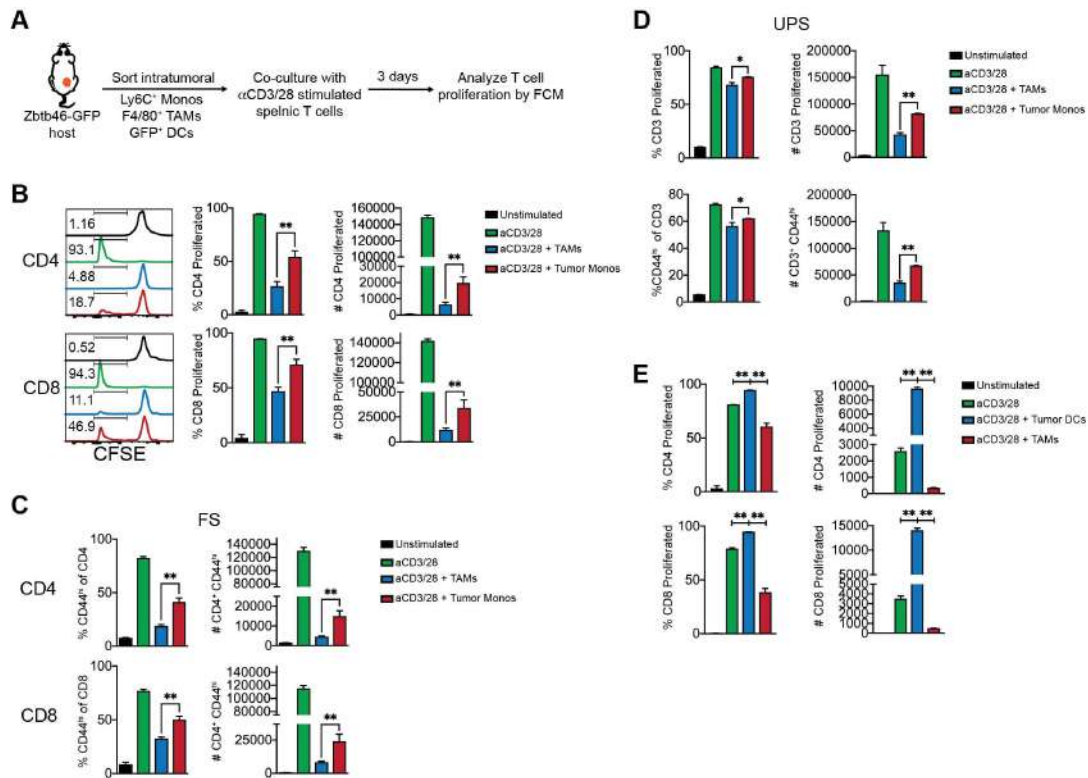


**Figure 2.1.3: Suppressive function of mononuclear phagocytes in sarcoma.** **A**, Experimental outline of T cell suppression assay (D, E) performed with tumor MPs (gating scheme shown in A, B). FS flank tumors were established in Zbtb46-GFP hosts. At 14d post-transplant, specified MP populations were sorted and co-cultured for 3d with αCD3/28 stimulated splenic T cells obtained from non-tumor bearing hosts. T cells were labelled with CFSE and assayed for proliferation. **B**, Results of T cell suppression assay with tumor monocytes or TAMs (n=5 tumors, pooled). Shown are frequency and absolute number of proliferated CD4 and CD8 T cells. Data are representative of three independent experiments. **C**, Frequency and absolute number of CD4<sup>hi</sup> T cells following co-culture with Ly6C<sup>+</sup> tumor monocytes or F4/80<sup>+</sup> TAMs from FS. MPs were sorted from n=5 tumors.



Data are representative of three independent experiments. **D**, T cell suppression assay using MPs from autochthonous UPS. Ly6C<sup>+</sup> monocytes or F4/80<sup>+</sup> TAMs were sorted from n=3 tumors. Shown are frequency and absolute number of proliferated T cells. **E**, Frequency and absolute number of proliferated T cells following co-culture with DCs or TAMs (n=3 tumors, pooled). Data are representative of two independent experiments. \*p<0.05, \*\*p<0.01. One-way ANOVA with Tukey's post hoc test. All error bars represent SEM. Events shown are pregated on live singlets unless otherwise specified.

#### 2.1.4: TME promotes intratumoral monocytes to differentiate into suppressive macrophages

Our results thus far show that monocytes undergo TAM but not DC differentiation within TME. Monocytes are heterogeneous with regards to their differentiation potential into DCs vs. macrophages (Briseño et al., 2016b; Menezes et al., 2016; Olingy et al., 2019). Therefore, one explanation for the skewed monocyte differentiation within TME may be the selective recruitment of monocyte subsets that are primed for macrophage differentiation. Alternatively, factors in the TME may drive macrophage differentiation from “uncommitted” monocytes. To address this, we first isolated bulk monocytes from the bone marrow of LysM<sup>Cre</sup>: Rosa26<sup>tdT</sup>: Zbtb46<sup>GFP</sup> mice, transplanted them into FS tumors, and analyzed their differentiation over time (Fig. 2.1.4A). Progenies of transplanted monocytes

were identified by tdT fluorescence while DC and TAM differentiation was assessed by a combination of GFP (Zbtb46) expression and surface markers (Fig. 2.1.4B). In this setting, the majority of monocytes differentiated into TAMs, whereas a very small fraction differentiated into DCs (Fig. 2.1.4C). Hence, the TME appears to polarize monocyte differentiation toward TAMs and away from DCs.

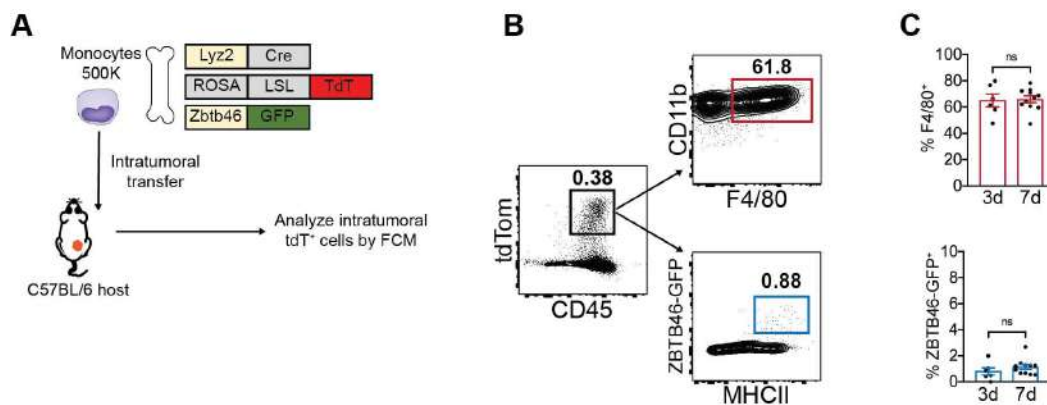


**Figure 2.1.4: TME promotes intratumoral monocytes to differentiate**

**into suppressive macrophages. A**, Experimental outline of intratumoral monocyte transfer to track monocyte differentiation within the TME. Monocytes were isolated from bone marrow of  $Lyz2^{Cre}; Rosa26^{tdT}; Zbtb46^{GFP}$  hosts using negative selection on magnetic columns (Miltenyi™).  $5 \times 10^5$  monocytes were injected directly into FS flank tumors (7d post-transplant). Tumors were harvested and analyzed by FCM at specified time points. **B**, Representative contour plots of  $tdT^+$  cells (derived from transplanted monocytes) in FS tumors at 3d or 7d post-monocyte transplant. **C**, Frequency of  $F4/80^+$  or  $Zbtb46-GFP^+$  cells within the  $tdT^+$  fraction at

indicated time points. Data aggregated from three independent experiments. Each dot represents an individual mouse. Two-tailed t test. All error bars represent SEM. Events shown are pregated on live singlets unless otherwise specified.

### 2.1.5: Intratumoral monocytes retain capacity for dendritic cell differentiation

Though the aforementioned results demonstrate that tumor monocytes exclusively differentiate into macrophages within the tumor microenvironment, it remains unexplored whether tumor monocytes still have the ability to differentiate into DCs. Indeed, in many other settings of infection and inflammation, abundant monocytes have been shown to generate large numbers of DCs. To ask whether intratumoral monocytes retain the ability to differentiate into DCs, we isolated tumor monocytes and cultured them *ex vivo* with DC promoting cytokines GM-CSF and IL-4 (Fig. 2.1.5A and 2.1.5B). Remarkably, in this setting the vast majority of monocytes differentiated into DCs while a minor fraction differentiated into macrophages (Fig. 2.1.5C). Furthermore, we observed that the major subsets of circulating monocytes (Ly6Chi and Ly6Clo monocytes) are also present within the sarcoma TME (Fig. 2.1.5D). Taken together, these findings suggest that TME-associated factors promote monocyte differentiation into suppressive TAMs but not DCs.

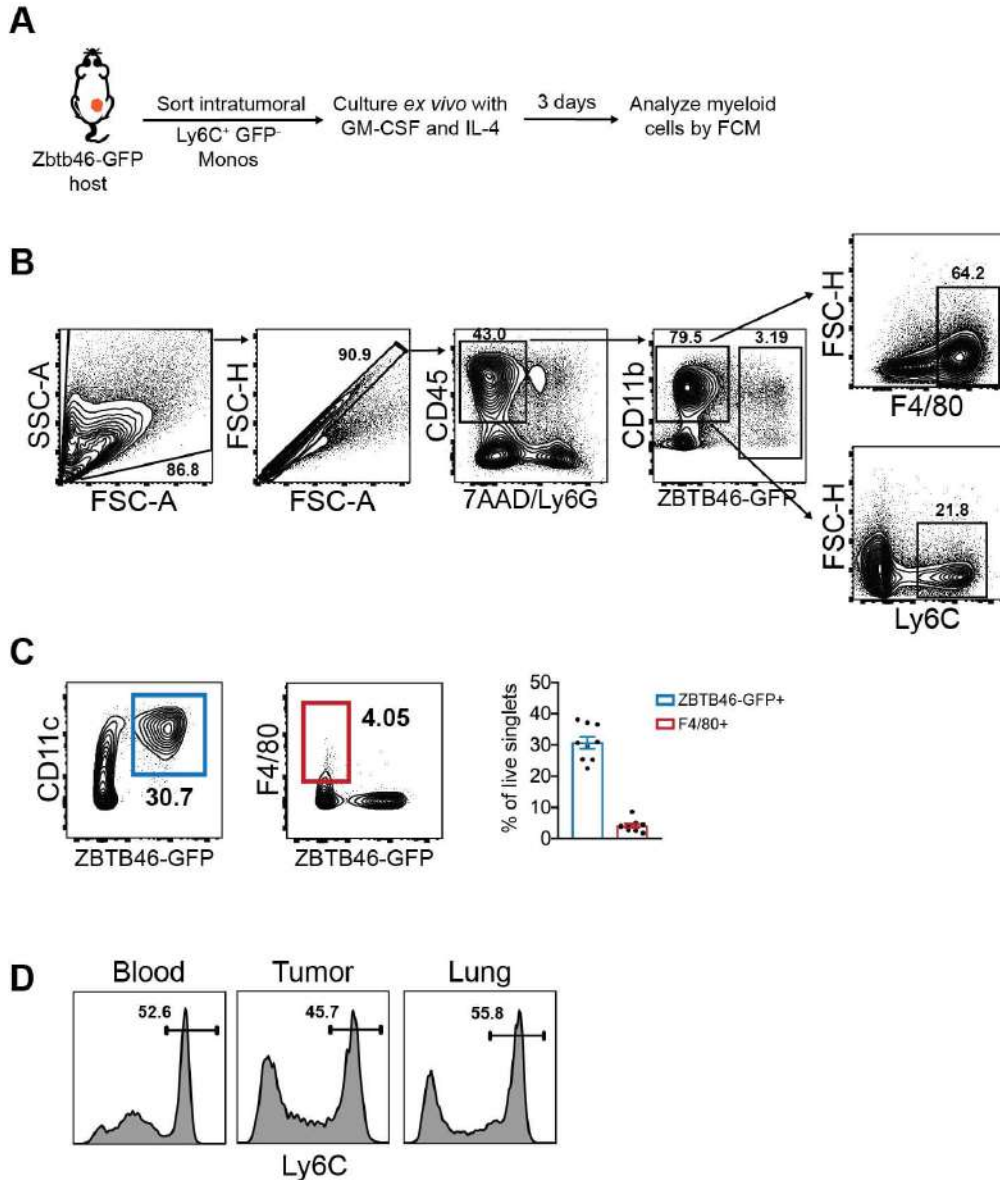


**Figure 2.1.5: Intratumoral monocytes retain capacity for dendritic cell differentiation.** **A**, Experimental outline of tumor monocyte *ex vivo* DC differentiation system. FS flank tumors were established in Zbtb46<sup>GFP</sup> hosts. Ly6C<sup>+</sup> Zbtb46-GFP<sup>-</sup> monocytes were sorted from 14d tumors and cultured for 3d with GM-CSF and IL-4. **B**, Sorting scheme to isolate tumor monocytes from FS tumors generated in Zbtb46<sup>GFP</sup> hosts. **C**, Contour plots and frequencies of DC and macrophage markers in tumor monocytes

differentiated *ex vivo*. Monocytes were sorted from n=8 tumors over three independent experiments. Each dot represents an individual mouse. **D**, Histograms depicting the frequency of Ly6C<sup>hi</sup> monocytes in mouse peripheral blood, FS flank tumor, and naïve lung. Cells were pregated on live singlets, CD45<sup>+</sup> Ly6G<sup>-</sup> CD11b<sup>+</sup> F4/80<sup>-</sup> CD11c<sup>-</sup> MHCII<sup>-</sup> to exclude neutrophils, macrophages and DCs. Histograms shown are representative of at least 5 independent experiments. All error bars represent SEM. Events shown are pregated on live singlets unless otherwise specified.

## 2.2: Tumor cells produce retinoic acid in response to T cell derived Interleukin 13

### 2.2.1: Sarcomas harbor elevated levels of RA

To identify factors within the TME driving monocyte differentiation into TAMs, we performed microarray-based gene expression profiling of TAMs isolated from our murine sarcoma models. Compared to tissue resident macrophages, we found that TAMs expressed high levels of cellular retinoic acid binding proteins (CRABPs) (Fig. 2.2.1A, 2.2.1B and 2.2.1C). High CRABP expression was independently validated by isolating monocytes, macrophages, and DCs from tumors and normal tissues (Fig. 2.2.1D). Further, gene expression profiling of bulk tumor revealed higher expression of enzymes catalyzing the rate-limiting step of RA synthesis (retinaldehyde dehydrogenases or Raldhs) compared to surrounding normal muscle (Fig. 2.2.1E). These unbiased transcriptomic studies suggested that sarcomas

may produce and respond to elevated RA. To directly quantify RA, we performed liquid chromatography / mass spectrometry for the major bioactive isoform of RA, *all-trans* retinoic acid (ATRA), and found elevated ATRA in all three mouse sarcoma models compared to normal mesenchymal tissues such as muscle, subcutaneous fat and endothelial cells (Fig. 2.2.1F).

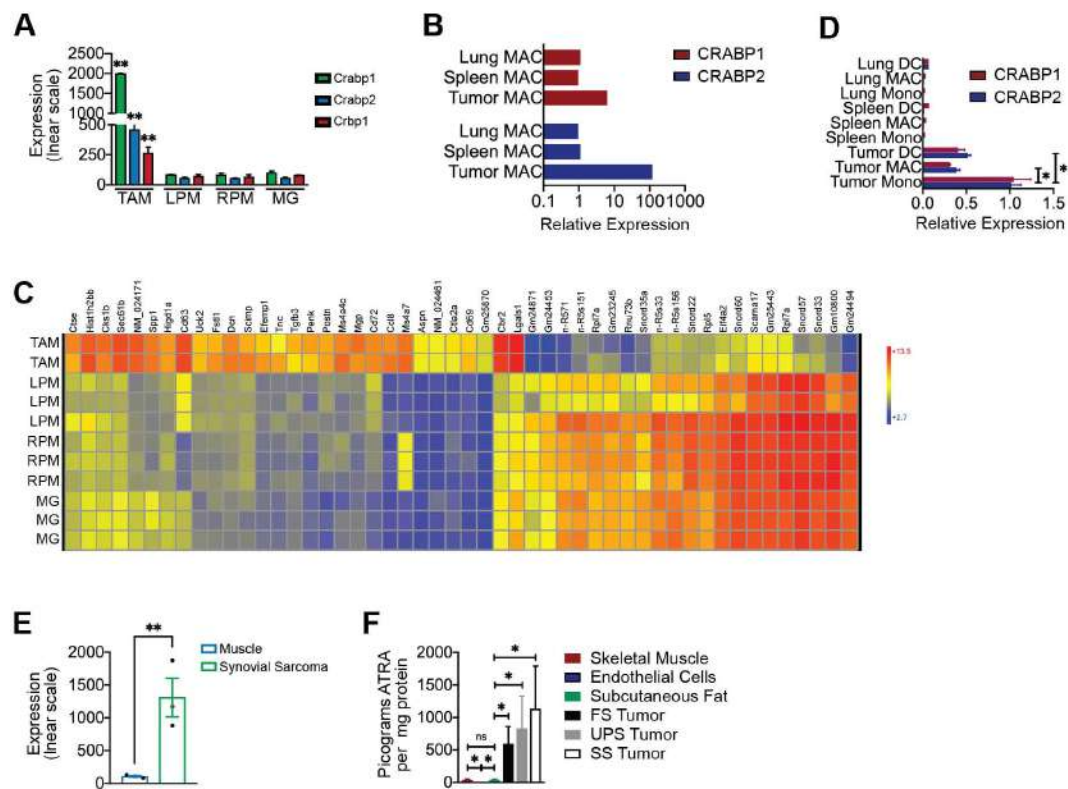


**Figure 2.2.1: Sarcomas harbor elevated levels of RA.** **A**, Microarray (Affymetrix, mouse gene 1.0ST) based gene expression profiling was performed on CD45<sup>+</sup> F4/80<sup>+</sup> CD11c<sup>-</sup> TAMs FACsorted from autochthonous UPS. Shown are the expression (y-axis, linear scale) of cellular retinoic acid binding proteins (CRABPs) in TAMs compared to selected tissue resident

macrophages (expression values downloaded from ImmGen database). LPM: large peritoneal macrophage; RPM: red pulp macrophage; MG: microglia. **B**, Relative expression of *Crabp1* and *Crabp2* in sorted TAMs (CD11b<sup>+</sup> F4/80<sup>+</sup>) from SS tumors (n=6, pooled) compared to lung or spleen macrophages from non-tumor bearing mice (n=3, pooled). **C**, Heatmap of the top 50 differentially expressed genes in TAMs (microarray described in 2A) to selected tissue resident macrophages (expression values downloaded from ImmGen database). LPM: large peritoneal macrophage; RPM: red pulp macrophage; MG: microglia. **D**, Relative expression of *Crabp1* and *Crabp2* in sorted monocyte (CD45<sup>+</sup> CD11b<sup>+</sup> F4/80<sup>-</sup> Ly6C<sup>+</sup>), macrophage (CD45<sup>+</sup> CD11b<sup>+</sup> F4/80<sup>+</sup>) and DC (CD45<sup>+</sup> Ly6C<sup>-</sup> F4/80<sup>-</sup> CD11c<sup>+</sup> MHCII<sup>+</sup>) populations from lung (n=3 mice, pooled), spleen (n=3 mice, pooled) or FS tumor (n=5 tumors). **E**, Microarray (Affymetrix mouse gene 1.0ST) based expression of *Aldh1a2* (*Raldh2*) in autochthonous SS compared to surrounding skeletal muscle. Each dot represents an individual mouse tumor (n=3 per group). **F**, Liquid chromatography / mass spectrometry for *all-trans* retinoic acid (ATRA) was performed on snap frozen subcutaneous adipose tissue (n=3), pelleted and snap frozen mouse primary lung microvascular endothelial cells (n=3), FS tumors (n=10), UPS tumors (n=5) or SS tumors (n=5). All expression normalized to *Hprt*. \*p<0.05, \*\*p<0.01. Two-tailed t test. (A), and (E) were analyzed with one-way ANOVA with Tukey's post hoc test. All error bars represent SEM. Events shown are pregated on live singlets unless otherwise specified.

### 2.2.2: Tumor cells produce majority of RA in sarcoma

To identify the cellular source of RA in the TME, we used a fluorescence-based assay that quantitates the enzymatic activity of aldehyde dehydrogenases (Aldh), a larger family of enzymes which includes Raldh (Ginestier et al., 2009). RA production was largely restricted to tumor cells in all of our murine models (Fig. 2.2.2A, 2.2.2B and 2.2.2C). To assess whether Aldh activity in this assay was indicative of Raldh activity, we performed unbiased gene expression profiling on sorted Aldh<sup>+</sup> and Aldh<sup>-</sup> tumor cells. Raldh transcripts were the only members of the Aldh enzymatic family that were upregulated (data not shown). Additionally, there was differential upregulation of Raldh isoforms between sarcoma subtypes, with synovial sarcoma upregulating *Raldh2*, and fibrosarcoma upregulating *Raldh3* (Fig. 2.2.2D and 2.2.2E). Though unique regulatory mechanisms of the Raldh family members remain unclear, the three enzymes are thought to perform redundant catalytic function by oxidizing retinaldehyde to RA (Kumar et al., 2012). These data demonstrate that tumor cells produce the vast majority of RA in the TME.



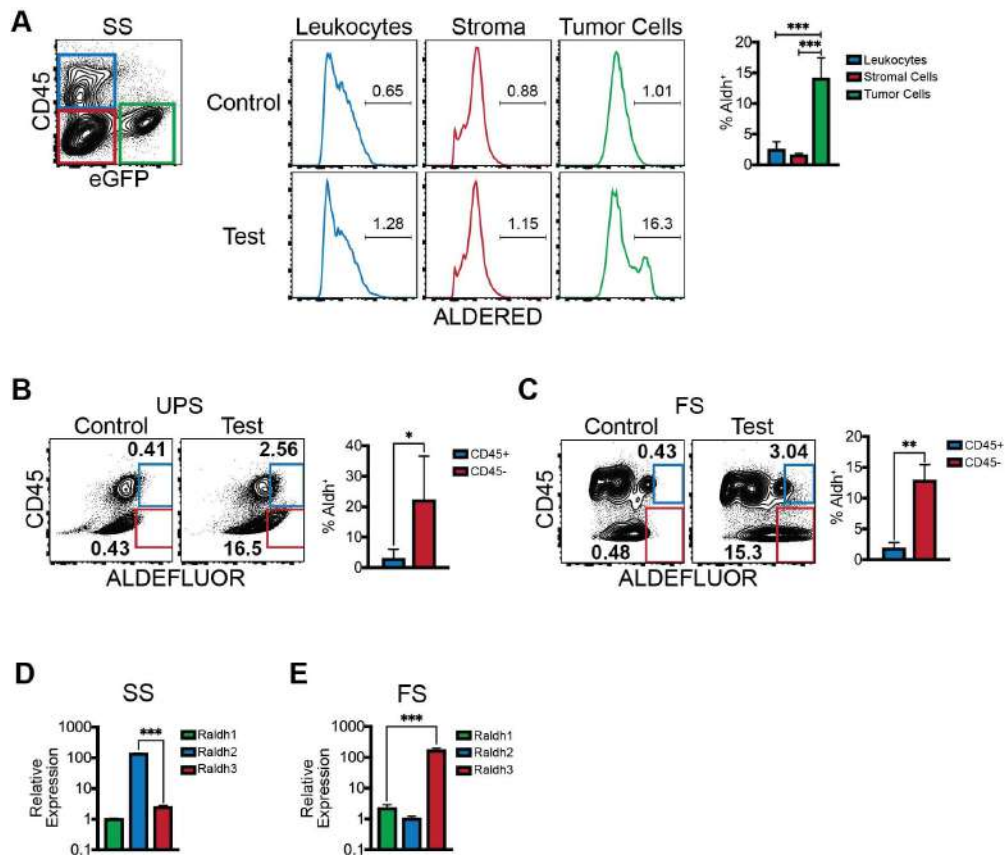


**Figure 2.2.2: Tumor cells produce majority of RA in sarcoma. A,** ALDERED assay was performed on mouse SS. Representative contour plot of eGFP<sup>+</sup> tumor cells, CD45<sup>+</sup> leukocytes and stromal cells (left). Representative histograms of ALDERED fluorescence in the aforementioned populations (right). “Control” samples (top) show ALDERED fluorescence in the presence of a potent Aldh inhibitor (DEAB) while “test” samples (bottom) show the same without the inhibitor, which allows accurate identification of fluorescence imparted by Aldh activity. Bar graph shows frequency of Aldh<sup>+</sup> cells within indicated parent populations (n=6 tumors). **B and C,** ALDEFLUOR assay was performed on mouse UPS or FS. Shown are representative contour plots of “control” and “test”

samples along with frequency (bar graph) of Aldh<sup>+</sup> cells within indicated parent populations (n=4 UPS and n=10 FS tumors). **D**, Aldh<sup>+</sup> or Aldh<sup>-</sup> cells were sorted from mouse SS (n=3) tumors. Relative expression of *Raldh* isoforms were quantified by qPCR. Normalized to *Hprt* expression. Data representative of two independent experiments. **E**, Aldh<sup>+</sup> or Aldh<sup>-</sup> cells were sorted from mouse FS (n=5) tumors. Relative expression of *Raldh* isoforms were quantified by qPCR. Data representative of two independent experiments. \*p<0.05, \*\*p<0.01, \*\*\*p<0.001. Two-tailed t test. (D) and (E) analyzed with one-way ANOVA with Tukey's post hoc test. All error bars represent SEM. Events shown are pregated on live singlets unless otherwise specified.

### 2.2.3: TME is required for tumor cell RA production

Of note, only a subset of tumor cells exhibited RA production in murine sarcomas. We also found that FS tumor cells massively upregulated *Raldh* *in vivo* compared to the *in vitro* cell line (Fig. 2.2.3A), prompting us to wonder whether RA production is induced by the TME. To further address this, we isolated Aldh<sup>+</sup> (RA-producing) and Aldh<sup>-</sup> (RA-negative) tumor cells from FS tumors, cultured the cells separately for 7 days *in vitro*, and re-transplanted them each into syngeneic recipients (Fig. 2.2.3B). We found that Aldh<sup>+</sup> tumor cells ceased to display Aldh activity when cultured *in vitro* (Fig. 2.2.3C). Further, re-transplantation of Aldh<sup>+</sup> or Aldh<sup>-</sup> cells resulted in similar proportions Aldh<sup>+</sup> tumor cells in *in vivo* tumors (Fig. 2.2.3D). Hence, RA-

producing tumor cells cease RA production *in vitro* while RA-negative cells regain the capacity to produce RA *in vivo*. These results suggest that TME-associated factors induce tumor cells to produce high levels of RA.

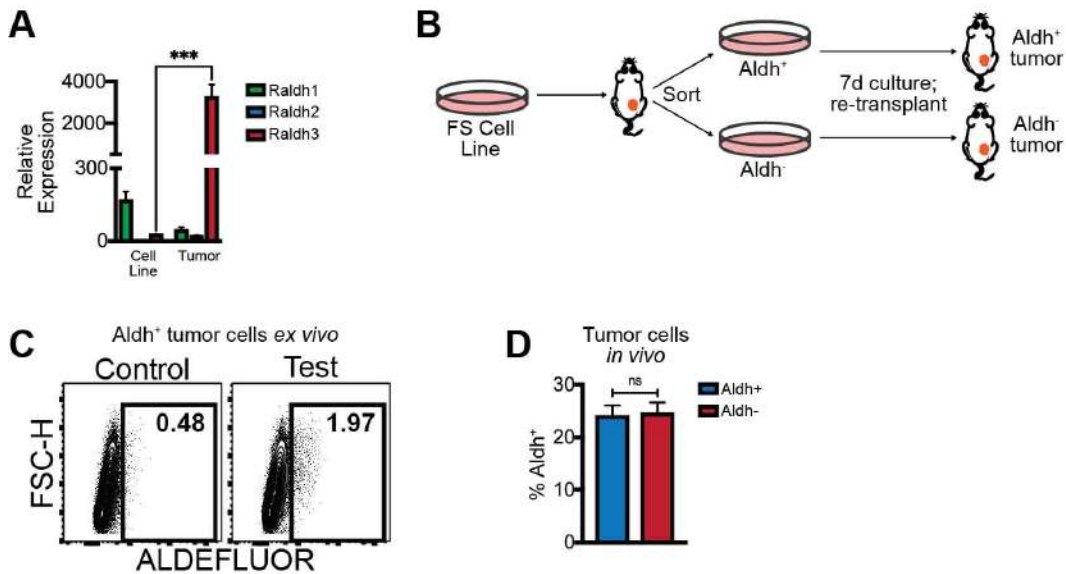


**Figure 2.2.3: TME is required for tumor cell RA production. A,** qPCR analysis of *Raldh* expression in FS tumor cell line *in vitro* compared to FS tumors *in vivo* (n=4 FS tumors). Results shown are normalized to *Hprt* expression and representative of three independent experiments. **B,** Experimental outline of RA producing vs. RA negative FS re-transplant experiment. Aldh<sup>+</sup> or Aldh<sup>-</sup> cells were isolated from 14d FS tumors and cultured for 7d *in vitro*. Subsequently, *in vitro* cultured Aldh<sup>+</sup> or Aldh<sup>-</sup> tumor cells were re-transplanted into flanks of naïve C57BL/6 hosts. **C,** ALDEFLUOR assay was performed on FS Aldh<sup>+</sup> tumor cells that were sorted and cultured for 7d *in vitro* as described above. Shown are representative contour plots of “control” and “test” samples, which show

significant loss of Aldh activity when cultured *in vitro*. **D**, Aldh<sup>+</sup> or Aldh<sup>-</sup> re-transplanted tumors (as described in (G)) were harvested 14d post-transplant and assayed by ALDEFLUOR. Frequency of ALDEFLUOR<sup>+</sup> cells is shown (n= 5 tumors per group). Data are representative of two independent experiments. \*\*\*p<0.001. Two-tailed t test. (A) was analyzed with one-way ANOVA with Tukey's post hoc test. All error bars represent SEM. Events shown are pregated on live singlets unless otherwise specified.

#### 2.2.4: T cell derived IL-13 promotes tumor cell RA production

To identify the TME-associated factor that might induce RA production, we revisited the microarray data from Aldh<sup>+</sup> and Aldh<sup>-</sup> tumor cells. Interleukin 13 (IL-13) receptor alpha 2 (IL13Ra2), which is known to be strongly induced by IL-13 signaling (Suzuki et al., 2015), was significantly higher in Aldh<sup>+</sup> cells (confirmed by qPCR in sorted ALDH<sup>+</sup> vs ALDH<sup>-</sup> tumor cells from FS and UPS mouse models) (Fig. 2.2.4A). Addition of recombinant IL-13 (and to a lesser extent IL-4) to FS and UPS mouse cancer cell lines was sufficient to upregulate *Raldh* expression (Fig. 2.2.4B). Next, because IL-13 receptor alpha 1 (IL13Ra1) transduces IL-13 signaling (Suzuki et al., 2015), we generated IL13Ra1 knockout sarcoma cell lines using CRISPR-Cas9. Upon treatment with IL-13 *in vitro*, IL13Ra1 KO tumor cells did not upregulate *IL13Ra2* and strikingly, also did not upregulate *Raldh3* (Fig. 2.2.4C). Consistent with our *in vitro* findings, syngeneic transplants of IL13Ra1 knockout tumor cells demonstrated significantly reduced *Raldh3*

*in vivo* (Fig. 2.2.4D). Finally, we identified T cells as the primary source of IL-13 in TME, while the expression of IL-13 receptors was largely restricted to myeloid and tumor cells (Fig. 2.2.4E). Taken together, these findings suggest that T cell-derived IL-13 can induce RA production by tumor cells.

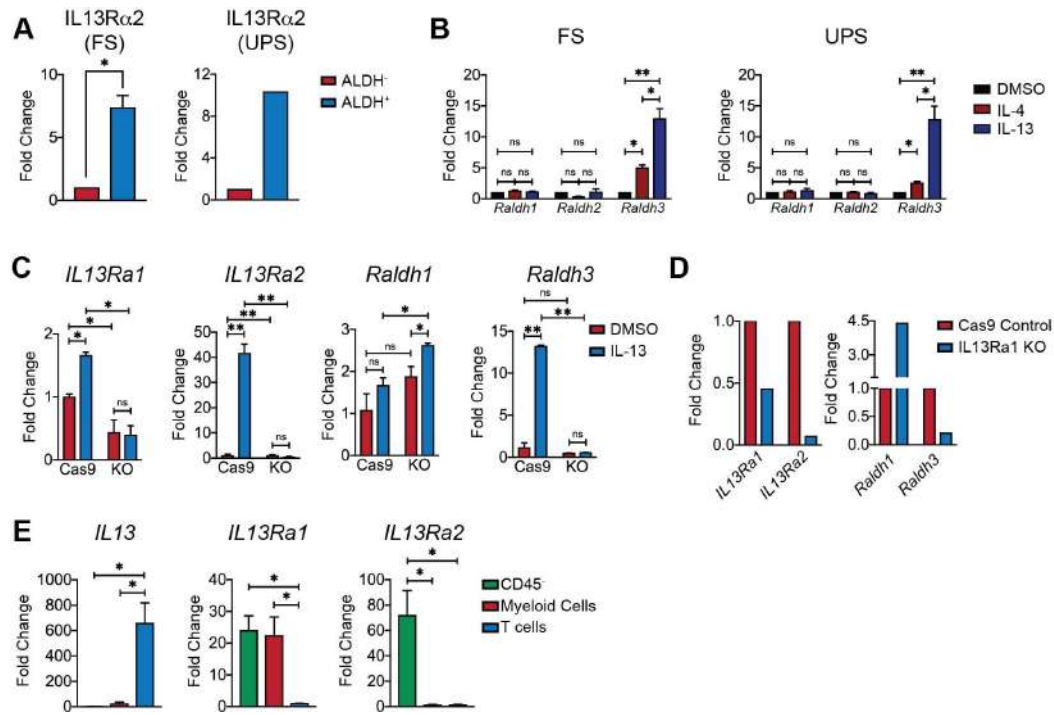


**Figure 2.2.4: T cell derived IL-13 promotes tumor cell RA production.**

**A**, ALDH<sup>+</sup> or ALDH<sup>-</sup> tumor cells were sorted from FS or UPS flank tumors. Relative expression of *IL13Ra2* was quantified by qPCR (n=3 FS tumors individually sorted; n=5 UPS tumors pooled and sorted). **B**, FS or UPS tumor cell lines were treated *in vitro* with recombinant IL-4 (20ng/mL), IL-13 (20ng/mL), or DMSO. Relative expression of *Raldh1* and *Raldh3* were quantified by qPCR. **C**, Cas9 Control or IL13Ra1 KO UPS cell lines were treated *in vitro* with recombinant IL-13 (20ng/mL) or DMSO. Relative

expression of *Il13ra1*, *Il13ra2*, *Raldh1* and *Raldh3* were quantified by qPCR. **D**, UPS tumors were generated in C57BL/6 hosts by subcutaneous implantation of Cas9 Control or IL13Ra1 KO UPS cell lines. Tumors were harvested 11d post-implantation and tumor cells FACsorted for qPCR analysis. Relative expression of *Il13ra1*, *Il13ra2*, *Raldh1* and *Raldh3* in sorted tumor cells is shown. **E**, Relative expression of *Il13*, *Il13ra1* and *Il13ra2* in sorted CD45<sup>-</sup> cells, CD11b<sup>+</sup> myeloid cells, or CD3<sup>+</sup> CD11b<sup>-</sup> T cells from orthotopic FS tumors (n=10 tumors). All expression normalized to *Hprt*. \*p<0.05, \*\*p<0.01, \*\*\*p<0.001. Two-tailed t test. (B), (C) and (E) were analyzed with one-way ANOVA with Tukey's post hoc test. All error bars represent SEM. Events shown are pregated on live singlets unless otherwise specified.

### 2.3: RA-RAR signaling promotes macrophage but suppresses DC differentiation from monocytes via *Irf4*

#### 2.3.1: RA inhibits DC and promotes macrophage differentiation from mouse and human monocytes

Results described above show (1) high levels of RA production by sarcomas, (2) evidence of RA exposure in TAMs, and (3) skewed differentiation of monocytes into TAMs within TME. Therefore, we explored whether RA might impact monocyte differentiation in the TME. Though RA has been previously implicated as a pro-differentiation agent for myeloid derived suppressor cells, its precise influence on the differentiation and progeny of

tumor infiltrating monocytes remains unclear (Bauer et al., 2018; Nefedova et al., 2007).

To start, we utilized a well-established assay of *in vitro* monocyte differentiation with GM-CSF and IL-4 that yields a mixture of macrophages and DCs (Helft et al., 2015). Addition of RA at the onset of culture significantly impaired DC differentiation of both murine and human monocytes (Fig. 2.3.1A and 2.3.1B). The *in vitro* doses of RA were based on published literature and in-house data demonstrating that plasma RA levels range from ~5-20 nM (Duester, 2017). These effects were recapitulated by RAR agonist CH55 and blocked by pan-RAR inverse agonist BMS493, suggesting that RA acts on monocytes via the RAR signaling pathway (Fig. 2.3.1C). Conversely, RA promoted macrophage differentiation from both mouse and human monocytes (Fig. 2.3.1D and 2.3.1E). Interestingly, these effects of RA on monocyte differentiation were even more striking in a modified monocyte-DC differentiation culture involving GM-CSF and IL-13 (Fig. 2.3.1F and 2.3.1G). A brief bioinformatics-based analysis of human tumors suggested that the levels of IL-13 may be higher than IL-4 in many solid tumors including sarcomas (Fig. 2.3.1H) (Suzuki et al., 2015). These findings along with our aforementioned observations of IL-13 inducing RA support an important role of this cytokine in MP cell differentiation and function within solid tumors.

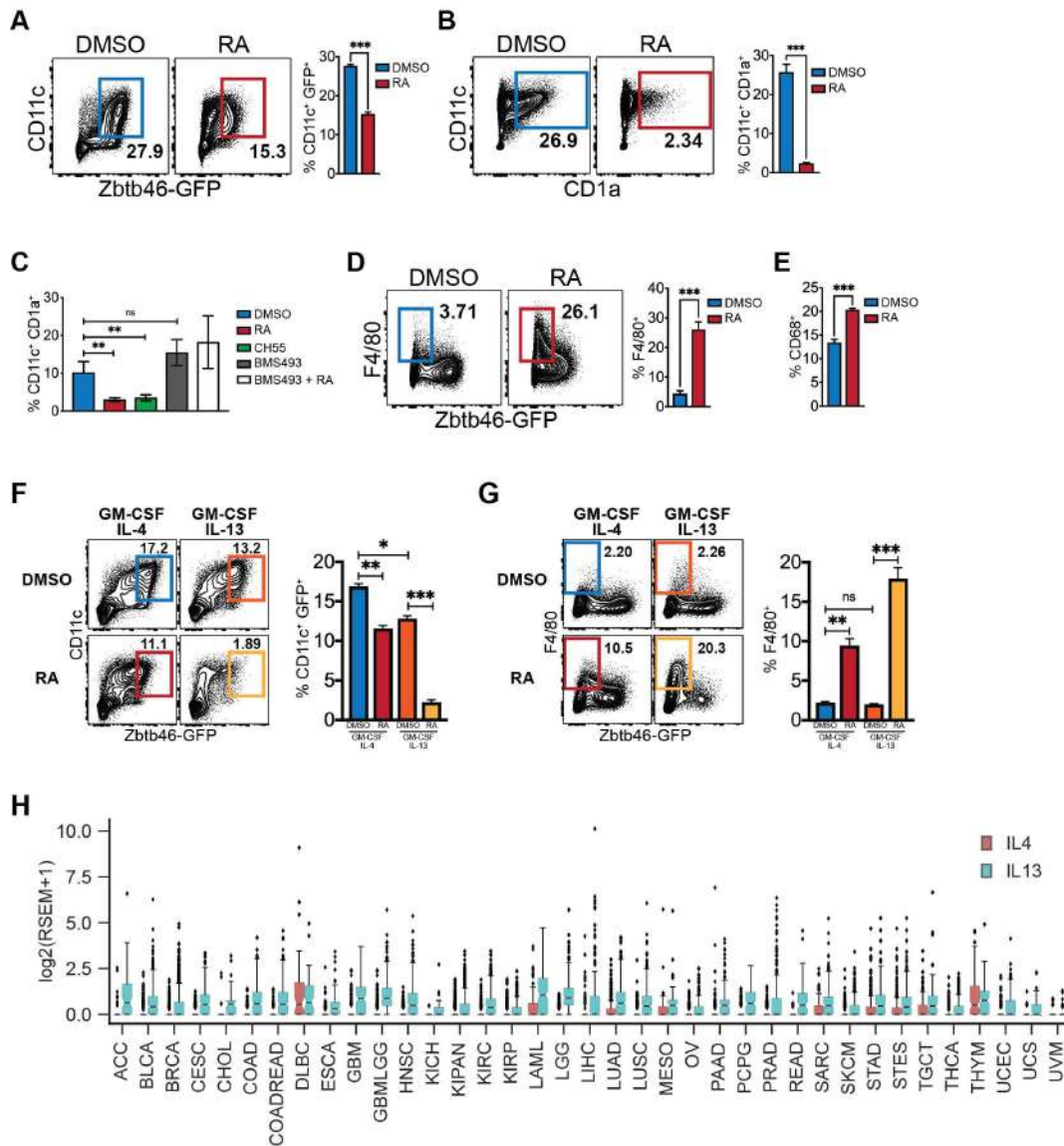


**Figure 2.3.1: RA inhibits DC and promotes macrophage differentiation from mouse and human monocytes. A**, BM monocytes were isolated from Zbtb46<sup>GFP</sup> mice and subsequently cultured for 3d with GM-CSF and IL-4. RA (100nM) or DMSO was added at Day 0. Representative contour plots and cumulative frequencies are shown. BM monocytes were harvested from n=3 mice and data are representative of five independent experiments. **B**, Human monocytes obtained from normal donors were



cultured for 5d with GM-CSF and IL-4. RA (20nM) or DMSO were added at Day 0. Representative contour plots and cumulative frequencies are shown. Data are representative of three independent experiments. **C**, Frequency of CD11c<sup>+</sup> CD1a<sup>+</sup> cells in human monocytes cultured for 5d with GM-CSF and IL-4 with either DMSO, RA (20nM), CH55 (RAR agonist; 10nM), BMS493 (pan-RAR inverse agonist; 1uM) or RA + BMS493. Data are representative of two independent experiments. **D**, Representative contour plots and frequencies of F4/80<sup>+</sup> cells; mouse monocytes were differentiated with GM-CSF and IL-4 with DMSO or RA. BM monocytes were harvested from three Ztb46<sup>GFP</sup> mice and data are representative of five independent experiments. **E**, Frequency of CD68<sup>+</sup> cells in human monocytes cultured for 3d with GM-CSF and IL-4 with DMSO or RA. Data are representative of three independent experiments. **F and G**, BM monocytes were isolated from Zbtb46<sup>GFP</sup> mice (Miltenyi negative selection kit) and subsequently cultured for 3d with GM-CSF and IL-4 or GM-CSF and IL-13. RA (100nM) or DMSO was added at Day 0. Representative contour plots and cumulative frequencies are shown. BM monocytes were harvested from n=3 mice and data are representative of two independent experiments. **H**, Comparison of *IL4* and *IL13* expression (log<sub>2</sub>(RSEM+1)) expression across all TCGA cancer types. \*p<0.05, \*\*p<0.01, \*\*\*p<0.001. Two-tailed t test. (C), (F) and (G) were analyzed with one-way ANOVA with Tukey's post hoc test. All error bars represent SEM. Events shown are pregated on live singlets unless otherwise specified.

### 2.3.2: RA inhibits DC and promotes macrophage differentiation from tumor monocytes

Next, we tested whether RA also impacted the differentiation of monocytes that exist within tumors. We isolated tDT<sup>+</sup> GFP<sup>-</sup> intratumoral monocytes from FS tumors generated in LysM<sup>Cre</sup>: Rosa26<sup>tdT</sup>: Zbtb46<sup>GFP</sup> mice and cultured them with GM-CSF and IL-4 with or without RA. Consistent with results above, RA significantly inhibited DC and promoted macrophage differentiation from tumor monocytes (Fig. 2.3.2A, 2.3.2B and 2.3.2C). We also tested whether tumor-associated conditions affect RA's ability to influence monocyte differentiation by culturing monocytes *in vitro* (with GM-CSF + IL-4) in the presence of tumor-conditioned media. The aforementioned effects of RA on monocyte differentiation were significantly augmented in the presence of tumor-conditioned media (Fig. 2.3.2D).

Finally, we tested whether tumor-derived RA can regulate monocyte differentiation in human cancers. Although most tumors we tested produced very little RA *in vitro*, only inducing its production *in vivo* as described above, we were able to find a human cancer cell line (hepatocellular carcinoma SNU398) that expressed high levels of *RALDH1* *in vitro* (Fig. 2.3.2E). Thus, we co-cultured human monocytes with SNU398 in the presence or absence of BMS493. Consistent with our observations above, DC differentiation was suppressed from monocytes in the presence of SNU398. Strikingly,

BMS493 completely rescued this effect, suggesting that tumor-derived RA was largely responsible for the skewed monocyte differentiation (Fig. 2.3.2F). Together, these results demonstrate that RA-RAR signaling inhibits tumor monocyte differentiation into DC and promotes differentiation into macrophage.

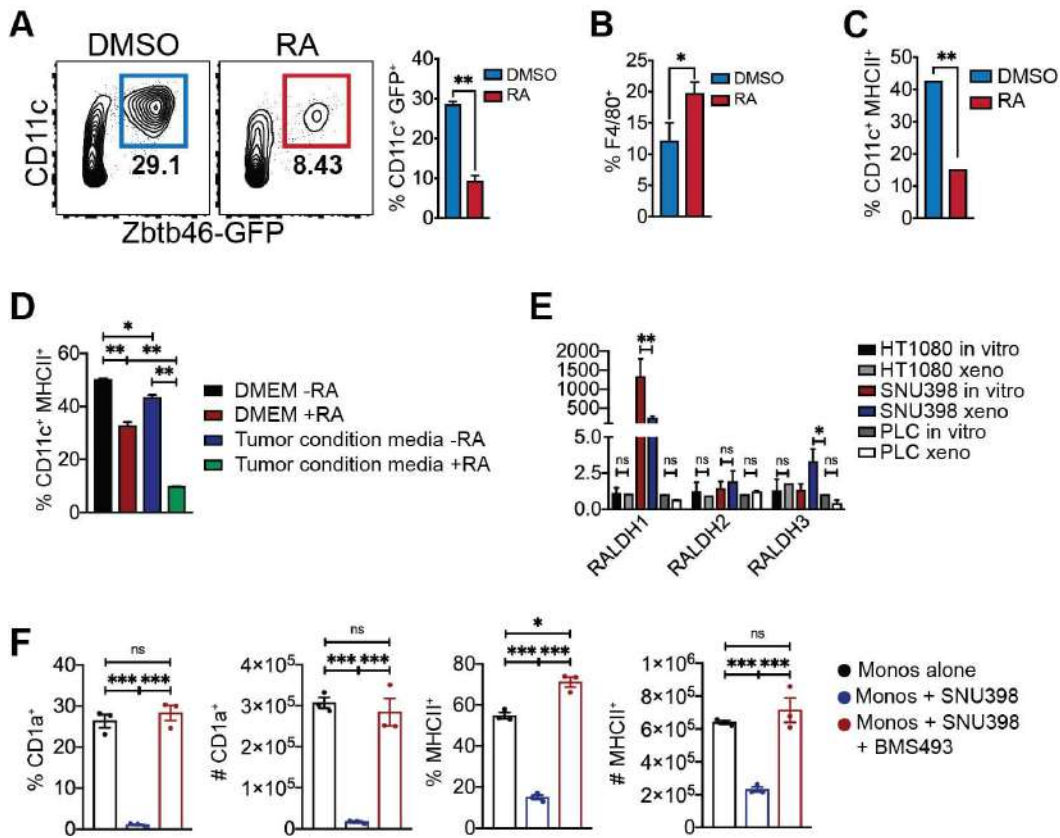


**Figure 2.3.2: RA inhibits DC and promotes macrophage differentiation from tumor monocytes.** **A - C**, Ly6C<sup>+</sup> Zbtb46-GFP<sup>+</sup> monocytes were isolated from FS tumors and cultured for 3d with GM-CSF and IL-4. DMSO or RA (100nM) was added at the onset of culture. Contour plots and frequencies are shown (n=3 FS tumors, data representative of three independent experiments). **D**, BM monocytes were cultured for 3d with GM-

CSF and IL-4, in the presence or absence of 50% filtered tumor conditioned media from subconfluent *in vitro* FS cell line. RA (100nM) or DMSO was added at Day 0. Shown are the frequencies of CD11c<sup>+</sup> MHCII<sup>+</sup> DCs. **E**, Relative expression of *RALDH1*, *RALDH2*, *RALDH3* in human cell lines HT1080 (liposarcoma), SNU398 (hepatocellular carcinoma) and PLC (hepatoma) *in vitro* culture and *in vivo* xenograft into NU/J hosts. Normalized to *Hprt* expression. **F**, Human monocytes were differentiated for 5 days with GM-CSF and IL-4 (50ng/mL) with or without SNU398 (hepatocellular carcinoma) cells at a 1:1 ratio. BMS493 was added at Day 0. Shown are frequencies and absolute numbers of CD1a<sup>+</sup> or MHCII<sup>+</sup> cells at Day 5. \*p<0.05, \*\*p<0.01, \*\*\*p<0.001. Two-tailed t test. (D), (E) and (F) were analyzed with one-way ANOVA with Tukey's post hot test. All error bars represent SEM. Events shown are pregated on live singlets unless otherwise specified.

### 2.3.3: RA enhances suppressive function of mouse and human monocyte derived APCs

TAMs are generally immunosuppressive while DCs are stimulatory. Hence, we examined whether RA affects the immunosuppressive capacity of APCs generated from monocytes. We co-cultured GM-CSF and IL-4 differentiated APCs with aCD3/28 stimulated splenic T cells and measured APC suppressive function by T cell proliferation and activation. As expected, the addition of RA during monocyte differentiation enhanced APC suppressive

function, which was likely due to polarized monocyte differentiation towards suppressive macrophages and away from stimulatory DCs (Fig. 2.3.3A and 2.3.3B). We found similar effects in an additional monocyte differentiation system involving GM-CSF alone (Fig. 2.3.3C and 2.3.3D). Furthermore, we found that RA more dramatically induces suppressive function of monocyte derived APCs in the presence of tumor condition media from fibrosarcoma (Fig. 2.3.3E). Next, to test whether RA induces additional suppressive capability on fully differentiated macrophages, we co-cultured aCD3/28 stimulated T cells with mature macrophages, which were derived *in vitro* by culturing monocytes with M-CSF. Addition of RA to the macrophage T cell co-culture significantly increased macrophage suppressive function (Fig. 2.3.3F and 2.3.3.G). This finding was consistent in human macrophage T cell co-cultures (Fig. 2.3.3H). Of note, the addition of RA to T cells in the absence of macrophages did not significantly impact T cell proliferation (Fig. 2.3.3I), suggesting that the effects of RA on T cell suppression in co-cultures were largely mediated via macrophages. Together, these results demonstrated that RA polarizes monocyte differentiation towards suppressive APCs, and additionally induces suppressive functionality on mature macrophages.

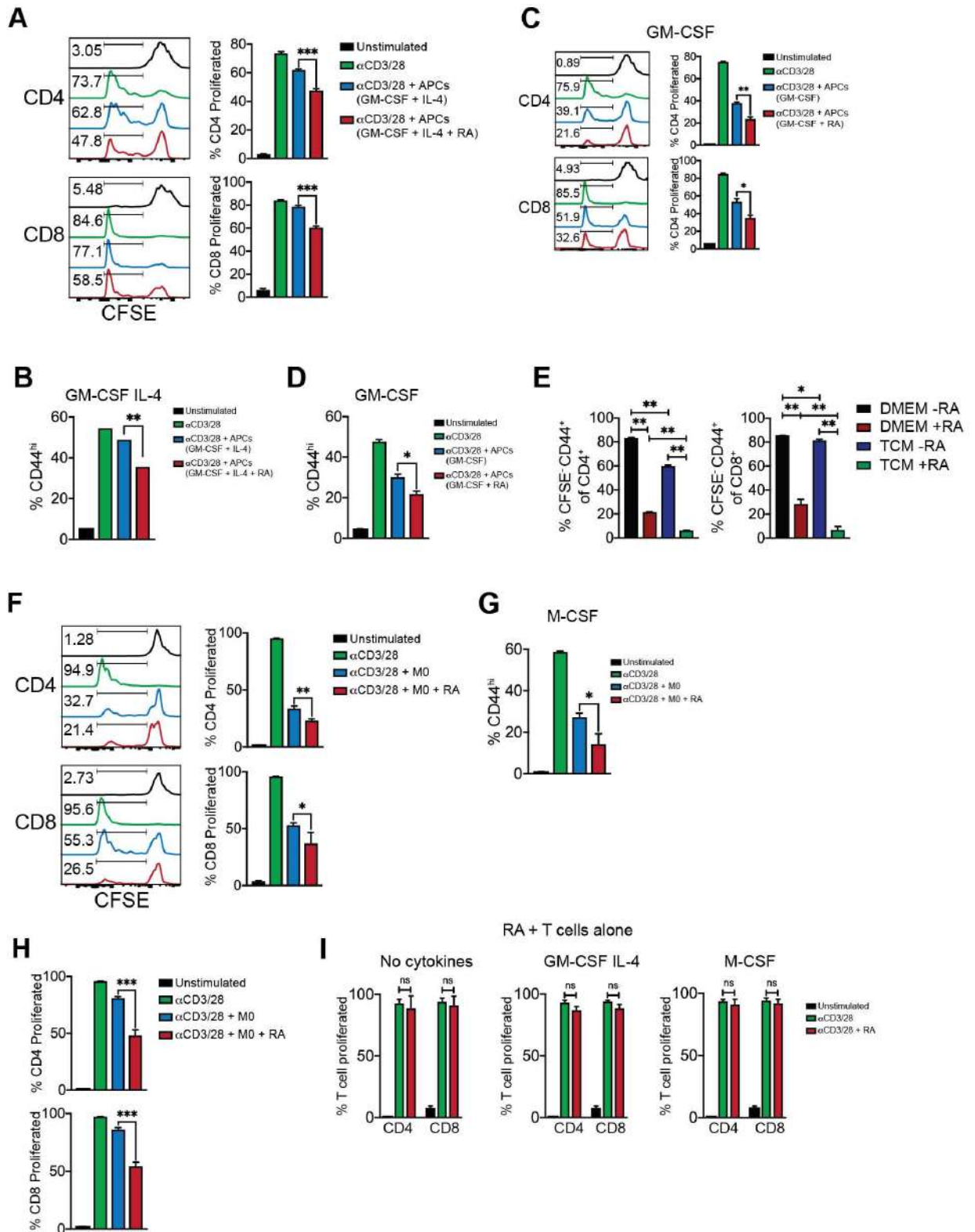


**Figure 2.3.3: RA enhances suppressive function of mouse and human monocyte derived APCs. A, BM monocytes were cultured for 3d with GM-**

CSF and IL-4. RA (100nM) or DMSO was added at Day 0. Subsequently, differentiated APCs were harvested, washed, and co-cultured for 3d with CFSE labeled aCD3/28 stimulated splenic T cells. Shown are histograms and frequency of proliferated T cells. Data are representative of four independent experiments. **B**, Frequency of CD44<sup>hi</sup> T cells in T cell suppression assay using GM-CSF and IL-4 +/- RA differentiated APCs. **C**, BM monocytes were cultured for 3d with GM-CSF alone. RA (100nM) or DMSO was added at Day 0. Subsequently, differentiated APCs were harvested, washed, and co-cultured for 3d with CFSE labeled aCD3/28 stimulated splenic T cells. Shown are histograms and frequency of proliferated T cells. **D**, Frequency of CD44<sup>hi</sup> T cells in T cell suppression assay using GM-CSF alone +/- RA differentiated APCs. **E**, Differentiated APCs (from Fig. 2.3.2D tumor condition media experiment) were harvested, washed, and co-cultured for 3d with CFSE labeled aCD3/28 stimulated splenic T cells. Shown are frequencies of proliferated CD4<sup>+</sup> or CD8<sup>+</sup> T cells. **F**, BM monocytes were cultured for 3d with M-CSF. Subsequently, differentiated macrophages were harvested, washed and co-cultured for 3d with CFSE labeled aCD3/28 stimulated splenic T cells. RA or DMSO was added to the co-culture at Day 0. Shown are histograms and frequency of proliferated T cells. Data are representative of three independent experiments. **G**, Frequency of CD44<sup>hi</sup> T cells in T cell suppression assay using M-CSF differentiated macrophages (M0). RA or DMSO was added during macrophage T cell co-culture. **H**, Human monocytes obtained from

normal donors were cultured with M-CSF for 5d. Subsequently, differentiated macrophages were harvested, washed and co-cultured for 3d with CFSE labeled aCD3/28 stimulated T cells (freshly obtained from a separate human donor). RA or DMSO was added to the co-culture at Day 0. Shown is frequency of proliferated T cells. Data are representative of two independent experiments. I, T cell proliferation assay in the absence of APCs/MPs. CFSE labeled aCD3/28 stimulated splenic T cells were cultured with either GM-CSF + IL-4, M-CSF or no cytokines for 3d. RA (100nM) or DMSO was added to each cytokine condition at Day 0. Shown is frequency of proliferated T cells. Data are representative of four independent experiments. \* $p < 0.05$ , \*\* $p < 0.01$ , \*\*\* $p < 0.001$ . One-way ANOVA with Tukey's post hoc test. All error bars represent SEM. Events shown are pregated on live singlets unless otherwise specified.

#### 2.3.4: *Irf4* is required for the effects of RA on monocyte differentiation

We next sought to probe transcriptional mechanisms downstream of RA-RAR signaling in MPs. RA is known to exert its effects on gene expression by binding to cognate nuclear receptors, a heterodimer of RAR/RXR (retinoic acid receptor/retinoid X receptor), which activate or repress transcription of a wide variety of genes (Duester, 2008). We performed gene expression profiling of mouse or human monocytes treated with RA, which revealed that RA induced the expression of key genes associated with



macrophage differentiation, while downregulating genes associated with moDC differentiation (Fig. 2.3.4A and 2.3.4B).

Of particular interest, RA downregulated *Irf4*, a transcription factor known to regulate monocyte differentiation into DCs (Briseño et al., 2016b; Lehtonen et al., 2005). Therefore, we tested whether the effects of RA on MP differentiation are dependent on *Irf4*. We first confirmed by qPCR that RA indeed downregulated *Irf4* in both mouse and human monocytes, and that this effect was dependent on RAR signaling (Fig. 2.3.4C and 2.3.4D). Further, similar to RA treated WT APCs, *Irf4*-deficient APCs ( $LysM^{Cre}; Irf4^{fl/fl}$ ) demonstrated heightened T cell suppression (Fig. 2.3.4E). Importantly, the addition of RA to *Irf4*-deficient monocytes did not further enhance suppressive capacity of these APCs (Fig. 2.3.4E). We also performed the complementary experiment of overexpressing *IRF4* in human monocytes, which rescued RA-mediated suppression of DC differentiation (Fig. 2.3.4F). Taken together, these findings suggest that RA impacts monocyte differentiation by regulating key transcription factors such as *Irf4*.

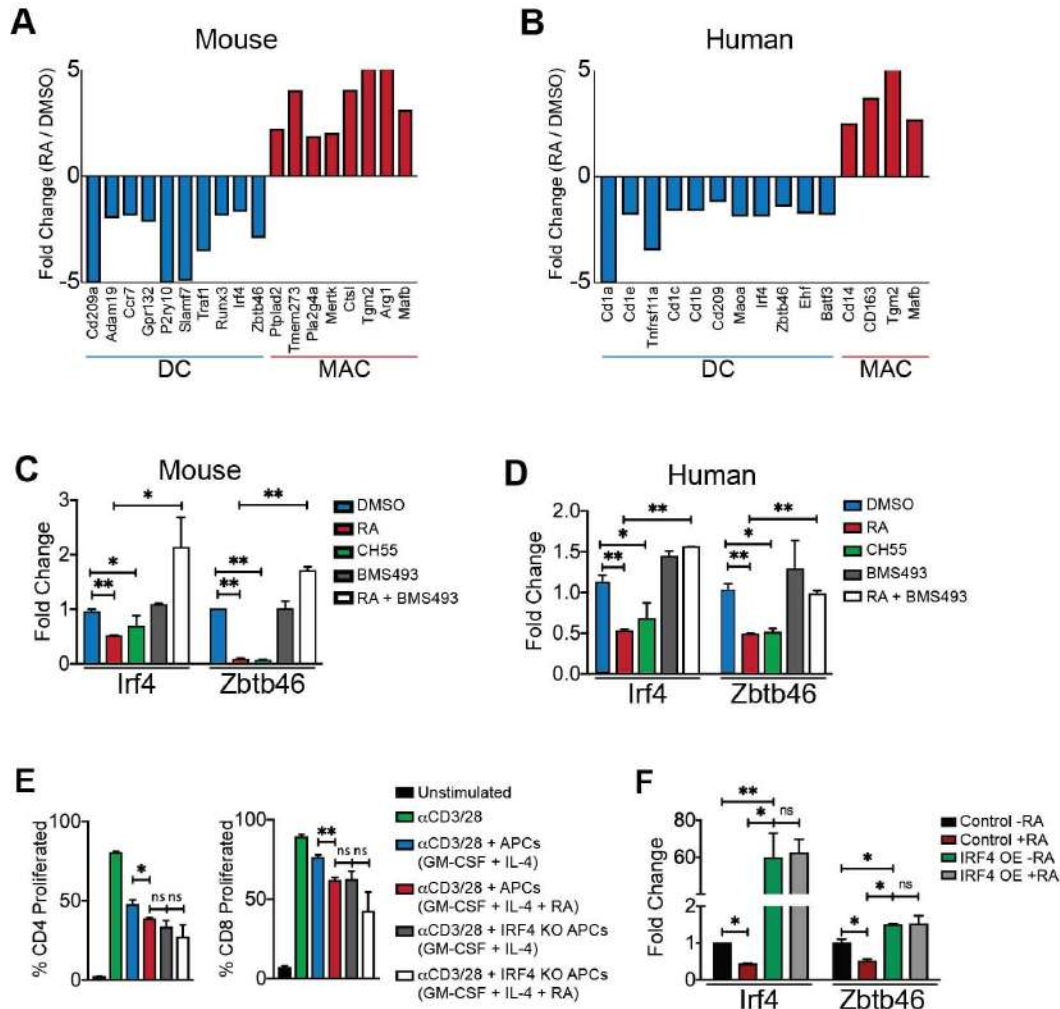


**Figure 2.3.4: *Irf4* is required for the effects of RA on monocyte differentiation.** **A and B**, Mouse BM monocytes from C57BL/6 mice (K), or human monocytes obtained from normal donors (L), were cultured with GM-CSF and IL-4 with DMSO or RA. Cells were harvested 1d later, RNA was extracted, and microarray (Affymetrix Mouse Gene 2.0ST) analysis was performed. Shown are fold changes of selected macrophage and DC signature genes in RA treated compared to DMSO treated mouse or human monocytes. **C**, Mouse BM monocytes were cultured for 3d with GM-CSF and IL-4 with either RA, CH55 (RAR agonist), BMS493, or DMSO. RNA was

extracted and expression of *Irf4* and *Zbtb46* was measured by qPCR. Expression normalized to *Hprt*. Data are representative of two independent experiments. **D**, Human monocytes obtained from normal donors were cultured for 5d with GM-CSF and IL-4. RNA was extracted and expression of *Irf4* and *Zbtb46* was measured by qPCR. Expression normalized to *Hprt*. Data are representative of two independent experiments. **E**, Mouse BM monocytes were isolated from  $\text{LysM}^{\text{Cre}}: \text{Irf4}^{\text{fl/fl}}$  or  $\text{LysM}^{\text{Cre}}: \text{Irf4}^{+/+}$  mice and cultured for 3d with GM-CSF and IL-4. RA or DMSO was added at Day 0. Subsequently, differentiated APCs were harvested, washed and co-cultured for 3d with CFSE labeled aCD3/28 stimulated splenic T cells. Shown is frequency of proliferated T cells. Data shown are aggregated from three independent experiments. **F**, Human monocytes were transfected with empty plasmid (control, pMax-GFP (Lonza)) or *IRF4* overexpression (*IRF4*-IRES2-eGFP (GeneCopoeia)) using Human Monocyte Nucleofector Kit (Lonza).  $2 \times 10^6$  cells were transfected with 1ug plasmid. Expression of *IRF4* and *ZBTB46* is shown. Normalized to *Hprt* expression. Data are aggregated from 2 independent experiments with n=3 technical replicates per experiment. \*p<0.05, \*\*p<0.01. One-way ANOVA with Tukey's post hoc test. All error bars represent SEM. Events shown are pregated on live singlets unless otherwise specified.

CHAPTER 3: INHIBITING RETINOIC ACID PRODUCTION OR  
RETINOIC ACID RECEPTOR SIGNALING IN THE TUMOR  
MICROENVIRONMENT AUGMENTS ANTI-TUMOR IMMUNITY

3.1: Reducing tumor RA production enhances intratumoral stimulatory  
APCs

3.1.1: CRISPR-Cas9 mediated deletion of RA producing  
enzymes

Our data thus far show high levels of RA production by tumor cells and the ability of RA to promote monocyte differentiation into immunosuppressive TAMs. Hence, we next sought to determine the impact of decreasing tumor-cell derived RA on the distribution and function of intratumoral APCs *in vivo*. Using CRISPR-Cas9, we generated a *Raldh3* KO FS cell line, given that *Raldh3* was specifically upregulated in RA producing FS cells *in vivo*. However, deletion of *Raldh3* alone resulted in compensatory increase in *Raldh1* expression (Fig. 3.1.1A). Thus, we generated a *Raldh1/3* double KO (DKO) cell line, which showed >80% reduction in *Raldh1* and *Raldh3* transcripts (Fig 3.1.1B), modestly reduced Aldh enzymatic activity *in vivo* (Fig. 3.1.1C), and significantly reduced ATRA levels compared to control tumors (Fig. 3.1.1D).

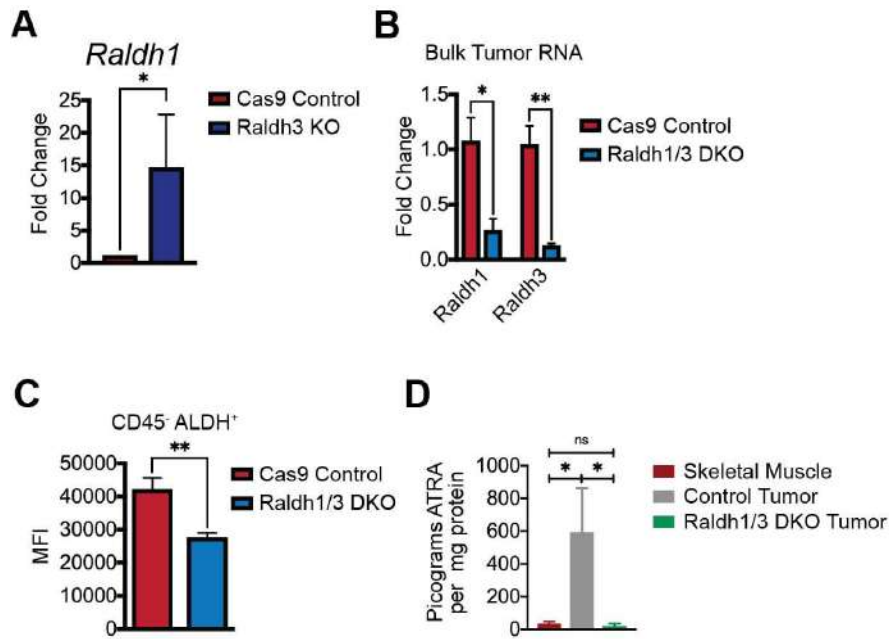


**Figure 3.1.1: CRISPR-Cas9 mediated deletion of RA producing enzymes.** **A**, Relative expression of *Raldh1* measured by qPCR in Raldh3 single KO or Cas9 Control FS cell line. Expression normalized to *Hprt*. **B**, Expression of *Raldh1* and *Raldh3* by qPCR in Raldh1/3 DKO vs. Cas9 Control bulk FS tumors (n=5 tumors per group harvested 11d post-transplant). Expression normalized to *Hprt*. Data are representative of two independent experiments. **C**, Median fluorescence intensity of Aldh activity in CD45<sup>-</sup> Aldh<sup>+</sup> cells assessed by ALDEFLUOR assay in Raldh1/3 DKO vs. Cas9 Control FS tumors (n=5 tumors per group harvested 11d post-transplant). Data are representative of two independent experiments. **D**, Liquid chromatography / mass spectrometry for *all-trans* retinoic acid (ATRA) on snap frozen tissue from skeletal muscle (n=8) control FS tumors (parental and Cas9 controls, n=10) or Raldh1/3 DKO FS tumors (n=5). Two-tailed t test. (B) and (D) were analyzed with one-way ANOVA. All error bars

represent SEM. Events shown are pregated on live singlets unless otherwise specified.

### 3.1.2: Reducing tumor RA production decreases intratumoral suppressive macrophage and increases stimulatory DC

DKO tumors showed reduced TAMs and increased CD11b<sup>+</sup> DCs, while CD103<sup>+</sup> DCs remained largely unchanged (Fig. 3.1.2A, 3.1.2B and 3.1.2C). Notably, a significantly higher fraction of F4/80<sup>+</sup> TAMs in DKO tumors were CD11c<sup>+</sup> MHCII<sup>+</sup> and expressed higher levels of activation markers CD40, CD86 and TNFa (Fig. 3.1.2D, 3.1.2E and 3.1.2F).

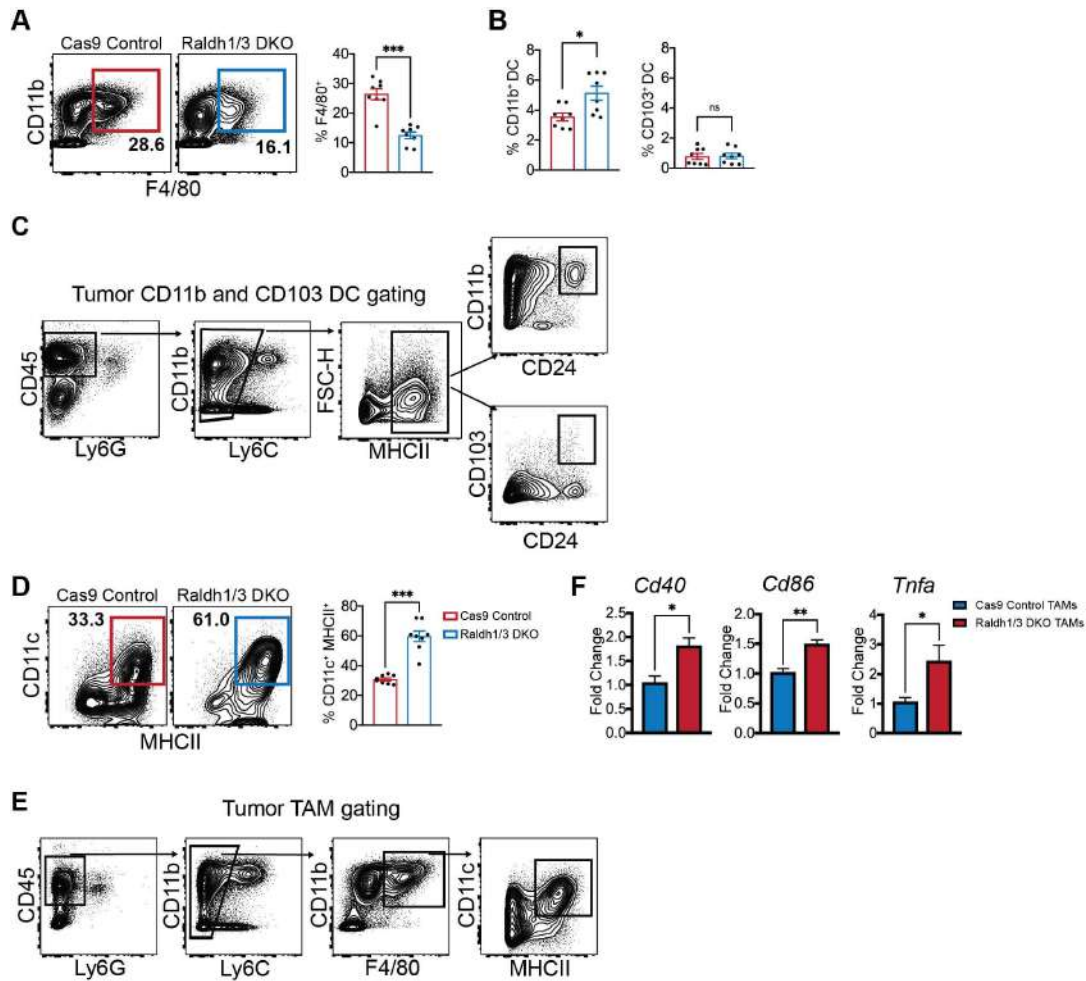


**Figure 3.1.2: Reducing tumor RA production decreases intratumoral suppressive macrophage and increases stimulatory DC.** **A**, Frequency of CD11b<sup>+</sup> F4/80<sup>+</sup> TAMs in Raldh1/3 DKO or Cas9 Control FS tumors (n=8 tumors harvested 11d post-transplant). Data representative of three independent experiments. **B**, Frequency of CD11b<sup>+</sup> or CD103<sup>+</sup> DCs in Raldh1/3 DKO or Cas9 Control tumors (n=8 tumors harvested 11d post-transplant). Data representative of three independent experiments. **C**, Gating strategy to identify CD11b<sup>+</sup> DC and CD103<sup>+</sup> DC subsets in FS tumors. **D**, Frequency of TAMs expressing both CD11c and MHCII (pregated on CD11b<sup>+</sup> F4/80<sup>+</sup>) in Raldh1/3 DKO or Cas9 Control FS tumors

(n=8 tumors per group harvested 11d post-transplant). Data are representative of three independent experiments. **E**, Gating strategy to evaluate CD11c and MHCII expression on CD11b<sup>+</sup> F4/80<sup>+</sup> TAMs in FS tumors (used in Fig. 4C). **F**, Relative expression of *Cd40*, *Cd86* and *Tnfa* in CD11b<sup>+</sup> F4/80<sup>+</sup> TAMs sorted from Raldh1/3 DKO or Cas9 Control FS tumors (n=5 tumors harvested 11d post-transplant). \*p<0.05, \*\*p<0.01, \*\*\*p<0.001. Two-tailed t test. All error bars represent SEM. Events shown are pregated on live singlets unless otherwise specified.

### 3.1.3: Unbiased single cell RNA sequencing of immune compartment in RA inhibited tumors

We further characterized RA driven changes in intratumoral leukocytes by using single cell RNA-sequencing; comparing tumor-infiltrating CD45<sup>+</sup> leukocytes in DKO to Cas9 Control tumors (Fig. 3.1.3A). Remarkably, the largest differences were observed in the myeloid compartment, with DKO tumors harboring reduced TAMs with immunosuppressive markers (TAM 1), increased TAMs with immunostimulatory markers (TAM 2), and increased DCs (Fig. 3.1.3B, 3.1.3C and 3.1.3D). Intriguingly, the majority of the DC cluster expressed *Ccr2*, suggesting a monocyte origin (Fig. 3.1.3B). Consistent with this reduction in immunosuppressive TAM by ScRNA-Seq, we found that F4/80<sup>+</sup> TAMs from DKO tumors were significantly less suppressive to T cell proliferation and activation *in vitro* (Fig. 3.1.3E, 3.1.3F and 3.1.3G). Of note, the distribution of blood neutrophils and monocytes



were similar in mice harboring control or DKO tumors, suggesting that the effects of decreasing tumor cell RA production on immune responses are mostly confined to the TME (Fig. 3.1.3H and 3.1.3I).

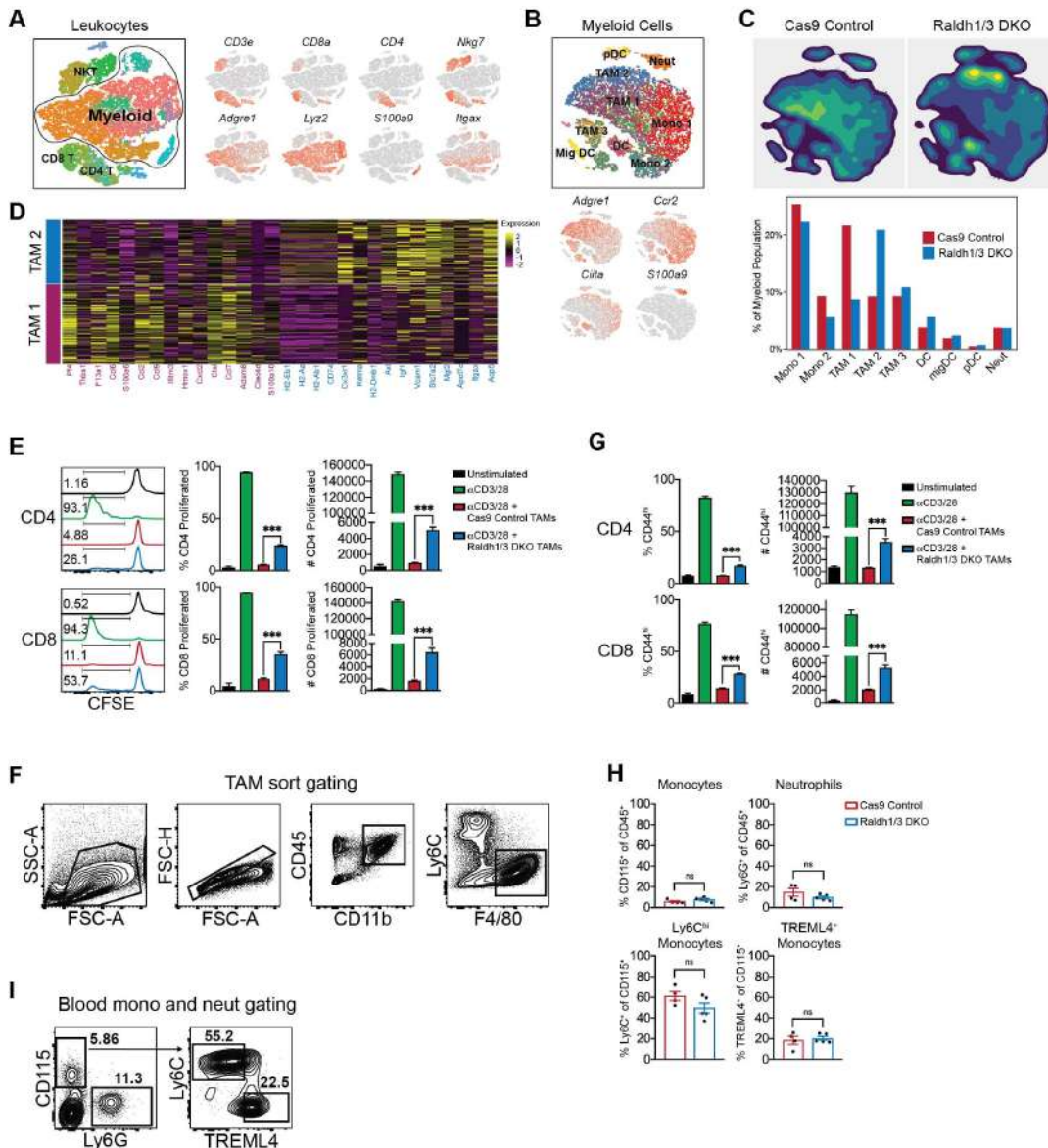


**Figure 3.1.3: Unbiased single cell RNA sequencing of immune compartment in RA inhibited tumors. A,** CD45<sup>+</sup> leukocytes from Raldh1/3 DKO or Cas9 Control FS tumors were profiled by scRNAseq (n=4

tumors per group). Shown are merged tSNE plots of identified immune populations (left) and selected marker gene expression (right) **B**, Merged tSNE plot of reclustered myeloid populations (top) and selected marker gene expression (bottom). **C**, Density plots (top) and relative frequencies (bottom) of myeloid clusters in Raldh1/3 DKO or Cas9 Control tumors. **D**, Heatmap of top 15 differentially expressed genes in TAM 1 compared to TAM 2 myeloid populations. **E**, T cell suppression assay using CD11b<sup>+</sup> F4/80<sup>+</sup> TAMs sorted from Raldh1/3 DKO or Cas9 Control tumors. Sorted TAMs were co-cultured with CFSE labeled aCD3/28 stimulated splenic T cells obtained from a non-tumor bearing host. Representative histograms, frequencies, and absolute numbers of proliferated T cells are shown. Data are representative of two independent experiments. **F**, Sorting scheme to purify CD11b<sup>+</sup> F4/80<sup>+</sup> TAMs from FS tumors. **G**, Frequency of CD44<sup>hi</sup> T cells in T cell suppression assay using CD11b<sup>+</sup> F4/80<sup>+</sup> TAMs sorted from Raldh1/3 DKO or Cas9 Control tumors. Data are representative of two independent experiments. **H**, Frequencies of specified monocyte and neutrophil populations in peripheral blood of C57BL/6 hosts bearing Raldh1/3 DKO or Cas9 control tumors (n=5 mice per group). Data are representative of two independent experiments. **I**, Gating strategy to identify CD115<sup>+</sup> peripheral blood monocyte and Ly6G<sup>+</sup> neutrophil populations in C57BL/6 mice. CD115<sup>+</sup> monocytes were further divided into Ly6C<sup>hi</sup> TREML4<sup>-</sup> and Ly6C<sup>-</sup> TREML4<sup>+</sup>. \*p<0.05, \*\*p<0.01, \*\*\*p<0.001. Two-tailed t test. (E) and (G) were analyzed with one-way ANOVA. All error bars

represent SEM. Events shown are pregated on live singlets unless otherwise specified.

### 3.1.4: Reducing tumor RA production augments intratumoral T cell responses

Additional immunophenotyping of intratumoral T cells revealed that the frequency of CD4<sup>+</sup> T cells was increased in DKO tumors (Fig. 3.1.4A and 3.1.4B). Importantly, both CD4<sup>+</sup> and CD8<sup>+</sup> T cells in DKO tumors produced significantly more IFN $\gamma$  compared to those from control tumors (Fig. 3.1.4C). Concomitant with a more stimulatory myeloid and T cell compartment, DKO FS demonstrated markedly decreased tumor volume and weight, which also translated into extended survival (Fig. 3.1.4D, 3.1.4E, 3.1.4F and 3.1.4G).

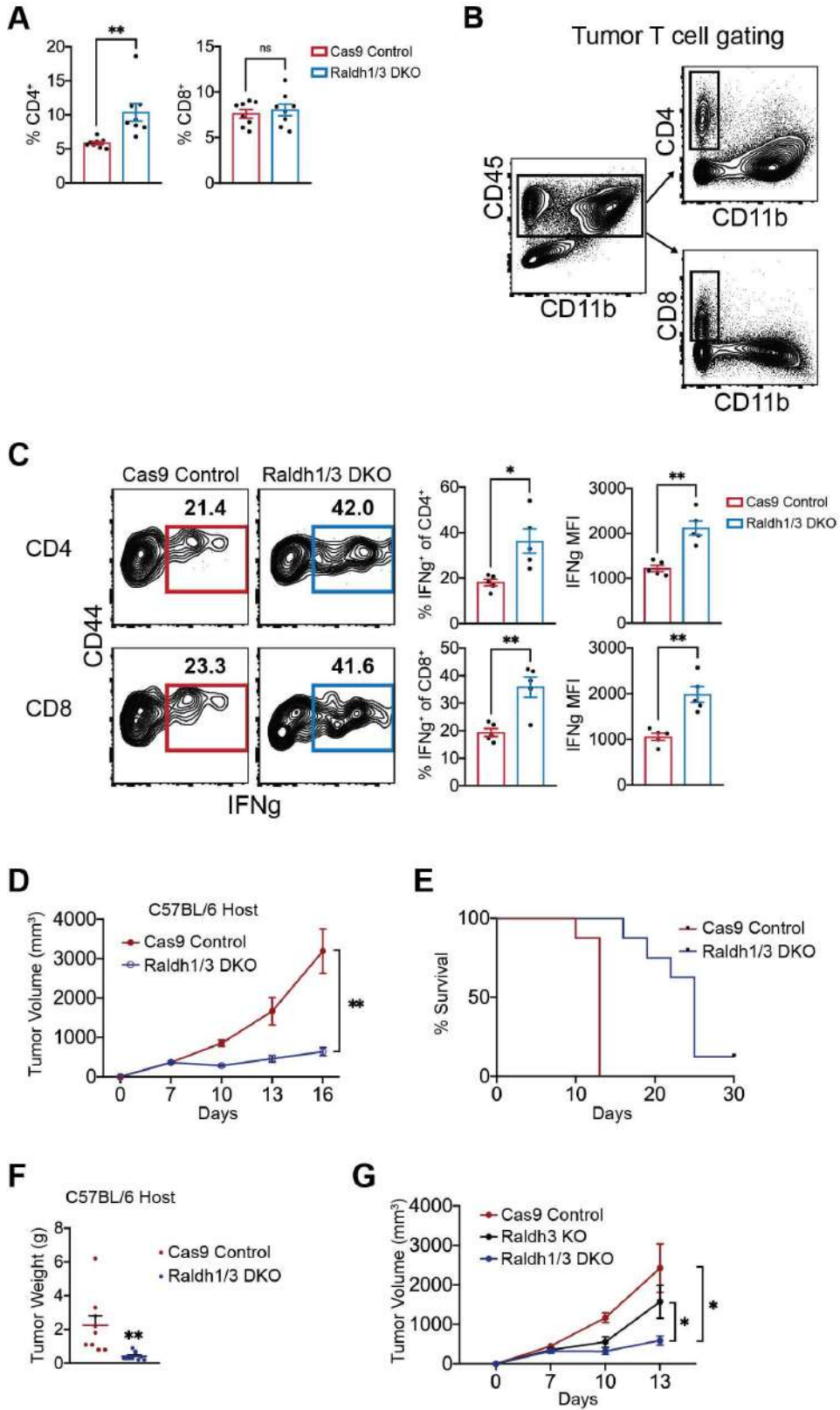


**Figure 3.1.4: Reducing tumor RA production augments intratumoral T cell responses.** **A**, Frequencies of CD4<sup>+</sup> or CD8<sup>+</sup> T cells within CD45<sup>+</sup> leukocytes in Raldh1/3 DKO or Cas9 Control tumors (n=8 tumors per group harvested 11d post-transplant). Data are representative of three independent experiments. **B**, Gating strategy to identify tumor infiltrating CD4<sup>+</sup> and CD8<sup>+</sup> T cells. **C**, IFN $\gamma$  cytokine production in T cells from Raldh1/3 DKO or Cas9 Control tumors. Intratumoral T cells were incubated with GolgiStop and stimulated for 4h with PMA/ionomycin. Shown are representative contour plots (left) and frequencies (right) of IFN $\gamma$ <sup>+</sup> CD4 or CD8 T cells (n=5 tumors per group harvested 11d post-transplant). Data are representative of two independent experiments. **D**, Tumor growth curve of Raldh1/3 DKO or Cas9 Control FS tumors implanted s.c. in C57BL/6 mice. Tumor volume was measured every three days starting at 7d post-implantation (n=8 tumors per group and data are representative of three independent experiments). **E**, Survival curve of mice bearing Raldh1/3 DKO or Cas9 Control FS tumors implanted s.c. in C57BL/6 mice (n=12 tumors per group and data are aggregated from three independent experiments). **F**, Tumor weight was measured in Raldh1/3 DKO or Cas9 Control tumors implanted s.c. into C57BL/6 mice. Tumors were harvested 16d post-implantation (n=8 tumors per group and data are representative of three independent experiments). **G**, Tumor growth curve of Raldh1/3 DKO, Raldh3 single KO or Cas9 Control FS tumors implanted s.c. in C57BL/6 mice. Tumor volume was measured every three days starting at 7d post-

implantation (n=5 tumors per group and data are representative of two independent experiments). \*p<0.05, \*\*p<0.01, \*\*\*p<0.001. Two-tailed t test. (D), (E) and (G) were analyzed with linear mixed-effects modeling with Tukey's HSD post-test or Kaplan-Meier with log-rank test. All error bars represent SEM. Events shown are predated on live singlets unless otherwise specified.

### 3.1.5: Additional models to validate the effects of inhibiting RA production on intratumoral APCs and anti-tumor immune responses

The effects of *Raldh1/3* DKO on immune cells and tumor size were also consistent in an intramuscular orthotopic transplant-based model, suggesting that the impact of RA deficiency is independent of the anatomical location of the tumor (Fig. 3.1.5A, 3.1.5B, 3.1.5C and 3.1.5D). To confirm that the observed effects in DKO tumors were driven by reduced RA production, we overexpressed *Raldh2* in the *Raldh1/3* DKO cell line to restore RA production (Fig. 3.1.5E). Overexpression of *Raldh2* restored tumor growth rate in DKO FS (Fig. 3.1.5F). Correspondingly, *Raldh2* overexpression reversed the stimulatory myeloid compartment of DKO tumors (Fig. 3.1.5G). Together, these findings demonstrated that reducing tumor cell RA production engenders a stimulatory APC compartment, augments intratumoral T cell responses and inhibits tumor progression.

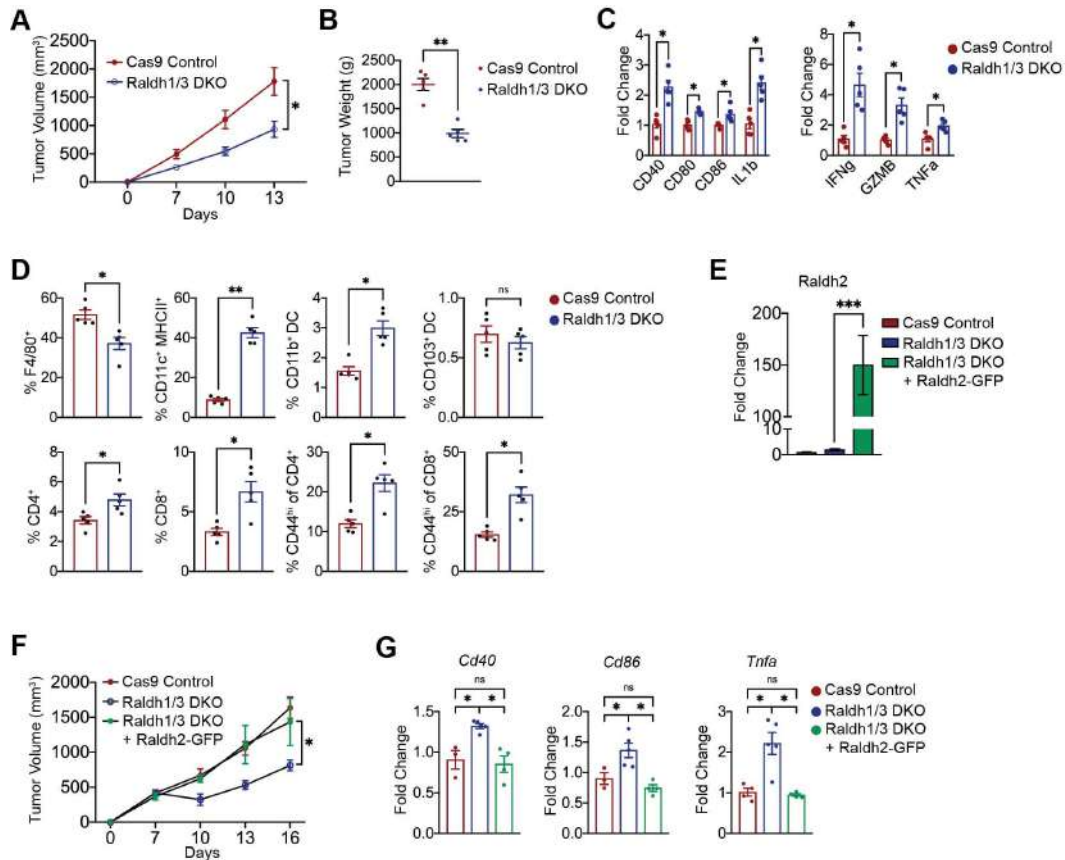


**Figure 3.1.5: Additional models to validate the effects of inhibiting RA production on intratumoral APCs and anti-tumor immune responses.**

**A**, Tumor growth curve of Raldh1/3 DKO or Cas9 Control FS tumors implanted orthotopically into hindlimb muscle of C57BL/6 mice. Tumor volume was measured every three days starting at 7d post-implantation (n=5 tumors per group and data are representative of two independent experiments). **B**, Tumor weight was measured in orthotopic Raldh1/3 DKO tumors or Cas9 Control tumors (harvested at Day 13 post-implantation; n=5 tumors per group). **C**, Relative expression of *Cd40*, *Cd80*, *Cd86*, *IL1b*, *IFNg*, *Gzmb*, *Tnfa* in bulk Raldh1/3 DKO tumors or Cas9 Control tumors (n=5 tumors per group harvested 13d post-implantation) Normalized to *Hprt*

expression. Each dot represents an individual mouse tumor. **D**, Frequency of specified myeloid and lymphoid populations in *Raldh1/3* DKO tumors or Cas9 Control tumors. **E**, Relative expression of *Raldh2* quantified by qPCR in indicated FS tumors. n=5 tumors per group were harvested 14d post-implantation. Data are representative of two independent experiments. **F**, Tumor growth curve of *Raldh1/3* DKO overexpressing *Raldh2*-GFP (*Raldh* rescue), *Raldh1/3* DKO, or Cas9 Control FS tumors implanted s.c. in *Lyz2*<sup>Cre</sup>: *Rosa26*-LSL<sup>Cas9-IRES-GFP</sup> mice. These mice were used as hosts to minimize potential immune responses against Cas9 and GFP. Tumor volume was measured every three days starting at 7d post-implantation (n=10 tumors per group and data are representative of two independent experiments). **G**, Relative expression of *Cd40*, *Cd86* and *Tnfa* quantified by qPCR in indicated FS tumors (n=5 tumors per group harvested 14d post-implantation). Data are representative of two independent experiments. \*p<0.05, \*\*p<0.01, \*\*\*p<0.001. Two-tailed t test. (G) was analyzed with one-way ANOVA with Tukey's post hoc test. (A) and (F) were analyzed with linear mixed-effects modeling with Tukey's HSD post-test or Kaplan-Meier with log-rank test. All error bars represent SEM. Events shown are pregated on live singlets unless otherwise specified.

### 3.1.6: Reducing tumor RA production enhances T cell-dependent anti-tumor immunity



We next asked whether the observed tumor growth defects with reduced RA production reflect tumor cell autonomous effects or anti-tumor immune responses. DKO tumor cells did not demonstrate a significant proliferation defect *in vitro* (Fig. 3.1.6A). Further, in contrast to the results seen in immunocompetent mice, depletion of either CD4<sup>+</sup> or CD8<sup>+</sup> T cells allowed for rapid growth of DKO tumors (Fig. 3.1.6B). Thus, impaired tumor progression upon RA reduction is dependent on CD4<sup>+</sup> and CD8<sup>+</sup> T cell immunity. Additionally, DKO tumors grew significantly faster in Batf3 KO mice (deficient in cDC1s) compared to WT controls, suggesting that anti-tumor immune responses upon RA reduction required the presence of cDC1s which cross-present tumor antigens to prime CD8<sup>+</sup> T cells (Fig. 3.1.6C and 3.1.6D).

Next, we sought to examine tumor-specificity of T cell responses induced by RA-deficiency by further engineering our Cas9-control and DKO FS cell lines to express the model antigen ovalbumin (OVA). We confirmed higher frequency and number of OVA (hence tumor)-specific splenic CD8<sup>+</sup> T cells in mice harboring DKO-OVA tumors (Fig. 3.1.6E).

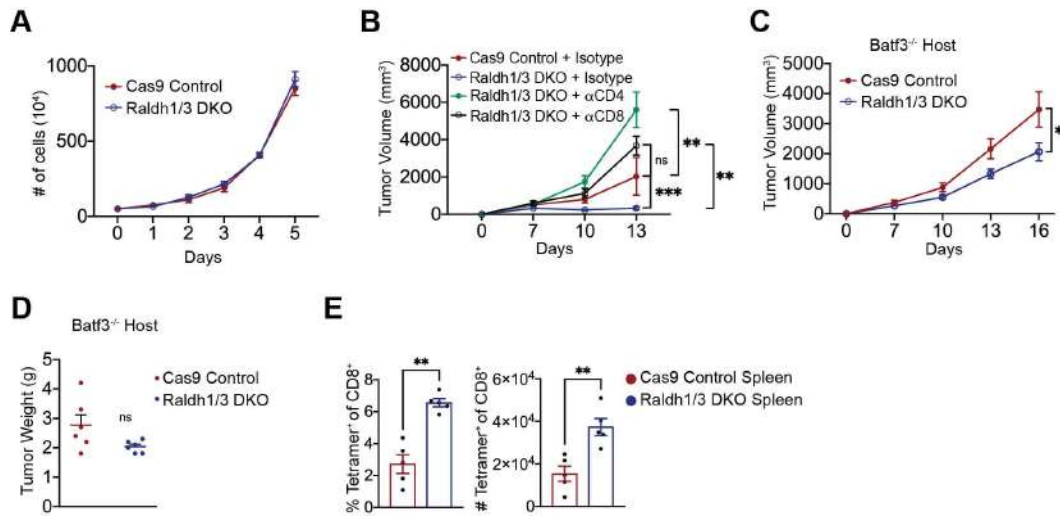


**Figure 3.1.6: Reducing tumor RA production enhances T cell-dependent anti-tumor immunity.** **A**, *In vitro* proliferation assay of Raldh1/3 DKO or Cas9 Control FS cell line.  $5 \times 10^4$  cells were seeded and total number of live cells were measured daily for five days. **B**, Tumor growth curve following CD4<sup>+</sup> or CD8<sup>+</sup> T cell depletion. αCD4, αCD8 or isotype control antibody was administered to C57BL/6 mice starting three days before s.c. implantation of Raldh1/3 DKO or Cas9 Control FS tumors. Depleting antibodies were administered i.p. every three days. (n=5 tumors per group). **C**, Tumor growth curve of Raldh1/3 DKO or Cas9 Control FS tumors implanted s.c. in in Batf3<sup>-/-</sup> hosts (n=7 mice per group). **D**, Tumor weight was measured in Raldh1/3 DKO or Cas9 Control tumors implanted into Batf3<sup>-/-</sup> mice. Tumors were harvested at 16d post-implantation. n=7 tumors per group. **E**, Raldh1/3 DKO or Cas9 Control FS tumor cell lines were transfected with plasmid encoding cytoplasmic OVA-ZsGreen. 3d later, cells were FACsorted for ZsGreen to ensure equal expression of OVA-ZsGreen between cell lines. Subsequently, Raldh1/3 DKO OVA-ZsGreen

or Cas9 Control OVA-ZsGreen FS tumors were generated in C57BL/6 hosts. Shown are frequency and number of H-2kb/SINFEKL tetramer positive splenic CD8<sup>+</sup> T cells at 11d post tumor implantation. \*p<0.05, \*\*p<0.01. Two-tailed t test. (A), (B) and (C) were analyzed with linear mixed-effects modeling with Tukey's HSD post-test or Kaplan-Meier with log-rank test. All error bars represent SEM. Events shown are pregated on live singlets unless otherwise specified.

### 3.1.7: Reducing tumor RA production synergizes robustly with immune checkpoint blockade

Given this evidence of tumor-specific CD8<sup>+</sup> T cell response, we tested whether RA reduction can synergize with PD-1 blockade for further tumor control. Consistent with published data, parental (control) FS were poorly responsive to aPD1 monotherapy (Fig. 3.1.7A) (Gubin et al., 2018). Strikingly, administration of aPD1 in established DKO tumors lead to complete tumor regression in 100% of mice (Fig. 3.1.7B and 3.1.7E). Mice that experienced complete regression of DKO tumors rejected re-challenge with parental FS but not unrelated tumor cells (Fig. 3.1.7C). Finally, reducing RA levels in the primary tumor (Raldh1/3 DKO) enhanced the sensitivity to aPD-1 in a distant (contralateral) Cas9 Control tumor, providing additional evidence of enhanced priming and systemic anti-tumor T cell immunity upon tumor RA reduction (Fig. 3.1.7D, 3.1.7E and 3.1.7F). Together, these results show that reducing tumor RA production engenders

a strong anti-tumor T cell response that synergizes with checkpoint blockade to control murine sarcoma.

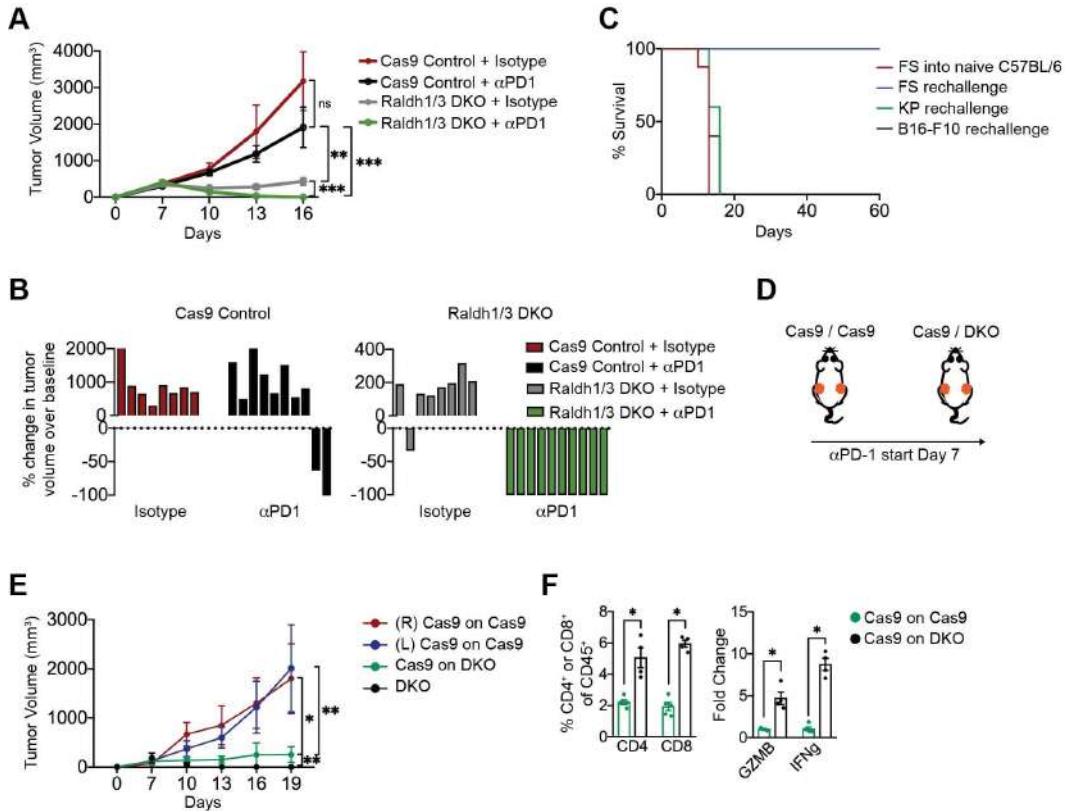


**Figure 3.1.7: Reducing tumor RA production synergizes robustly with immune checkpoint blockade.** **A and B**, αPD1 or isotype control antibody was administered to C57BL/6 mice starting 7d post-implantation of Raldh1/3 DKO or Cas9 Control tumors. Three doses (200ug i.p.) were given at Days 7, 10 and 13. Shown are tumor growth curves (A) and waterfall plots (B) of change in tumor volume after 12d of therapy. **C**, Parental FS, KP sarcoma, or B16-F10 melanoma tumor cell lines were implanted s.c. into mice that that previously experienced complete regression of Raldh1/3 DKO tumors upon αPD1 therapy (or into naïve C57BL/6 mice as control).

Implantation was performed 60d after complete regression (n=10 FS, n=5 KP, n=5 B16-F10). Shown is the survival curve for indicated groups. Mice were immune to re-challenge with parental FS, but not other tumors. **D**, C57BL/6 hosts were implanted with dual flank tumors: either dual Cas9 Control tumors, or Cas9 Control and Raldh1/3 DKO tumors. Once the tumors were established (Day 7), aPD-1 was administered (200ug i.p. on Days 7, 10, 13). **E**, Tumor growth curves for experiment outlined in K. Tumor volume was measured every three days starting at 7d post-implantation (n=5 tumors per group). **F**, Frequencies of CD4<sup>+</sup> or CD8<sup>+</sup> T cells in Cas9 tumors contralateral to Cas9 tumors, or Cas9 tumors contralateral to Raldh1/3 DKO tumors (left). Relative expression of *Gzmb* and *Ifnγ* in bulk tumors (right). Normalized to *Hprt* expression. \*p<0.05, \*\*p<0.01, \*\*\*p<0.001. Two-tailed t test. (A), (C) and (E) were analyzed with linear mixed-effects modeling with Tukey's HSD post-test or Kaplan-Meier with log-rank test. All error bars represent SEM. Events shown are predated on live singlets unless otherwise specified.

### 3.2: Inhibiting RAR signaling in TME or monocytes enhances anti-tumor immune responses

#### 3.2.1: RAR inhibition enhances intratumoral stimulatory APCs and T cell responses in multiple murine cancer models

Though pharmacologic approaches to specifically inhibit Raldh enzymes are not available, potent antagonists of RAR signaling exist (Chiba et al.,

2016). We first asked whether RAR signaling blockade could recapitulate the aforementioned effects of reducing tumor RA production. Because RAR antagonism has pleiotropic effects on myelopoiesis and peripheral immunity, we restricted RA-signaling blockade to the TME via intratumoral administration of BMS493. This resulted in similar changes to the intratumoral immune compartment as observed in RA deficient DKO tumors, including decreased frequency of TAMs, increased activation markers on APCs, and increased frequency of T cells (Fig. 3.2.1A, 3.2.1B and 3.2.1C). Strikingly, intratumoral BMS493 robustly synergized with systemic aPD1 therapy in FS (Fig. 3.2.1D and 3.2.1E). Of interest, *Raldh1* and *Raldh3* were significantly upregulated in tumors treated with BMS493, suggesting a potential resistance mechanism whereby tumors upregulate RA production in response to RA signaling blockade (Fig. 3.2.1F). However, administration of BMS493 to DKO tumors (in which this resistance mechanism cannot operate), did not show superior response compared to administration of DMSO control, suggesting the existence of additional potential resistance mechanisms (Fig. 3.2.1G).

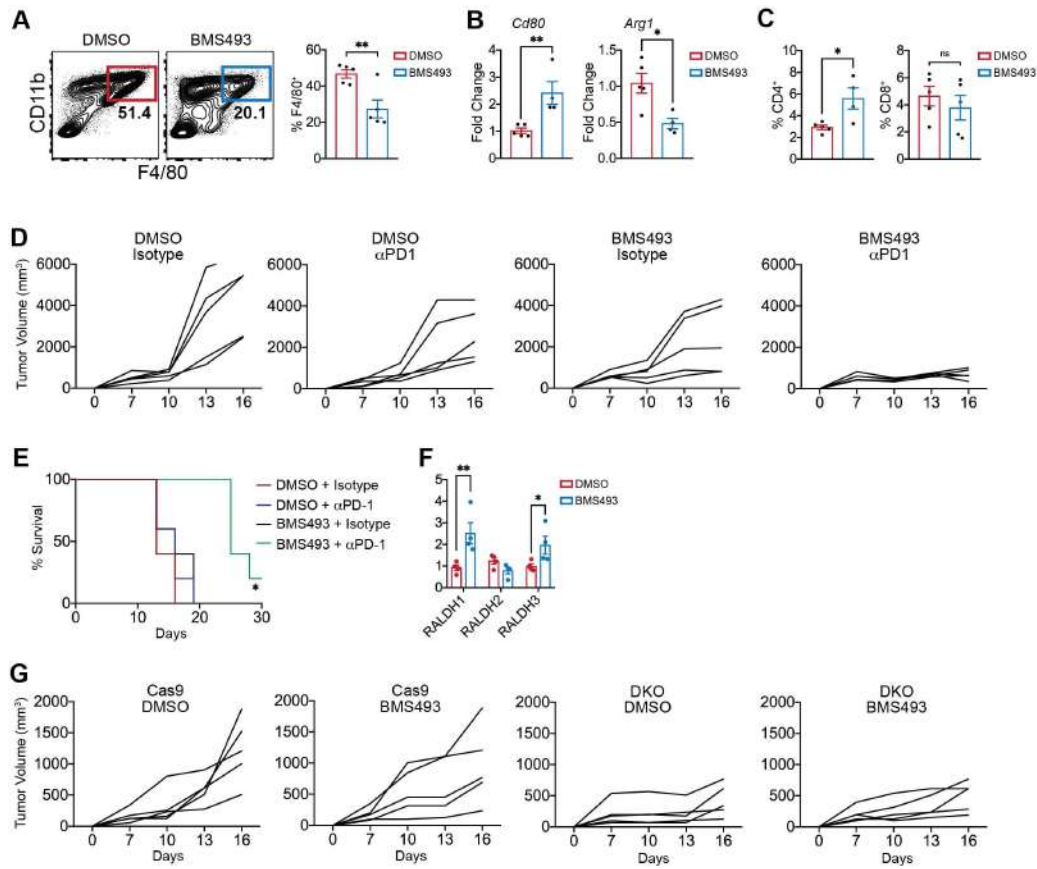


**Figure 3.2.1: RAR inhibition enhances intratumoral stimulatory APCs and T cell responses in multiple murine cancer models.** **A**, Frequency of CD11b<sup>+</sup> F4/80<sup>+</sup> TAMs in FS tumors treated with intratumoral BMS493 or DMSO. Three doses (200ug intratumorally) were given at Days 7, 10 and 13. n=5 tumors per group were harvested 15d post-transplant. **B**, Relative expression of *Cd80* and *Arg1* measured by qPCR in FS tumors treated with intratumoral BMS493 or DMSO. Expression normalized to *Hprt*. (n=5 tumors per group) **C**, Frequencies of CD4<sup>+</sup> or CD8<sup>+</sup> T cells within CD45<sup>+</sup> leukocytes in FS tumors treated with intratumoral BMS493 or DMSO. (n=5 tumors per group) **D**, Individual growth curves of FS tumors treated with aPD1 (or isotype control) in combination with intratumoral BMS493 (or

DMSO). BMS493 (200ug i.t.) and/or aPD1 (200ug i.p.) were administered at Days 7, 10 and 13. (n=5 tumors per group). **E**, Survival curve of mice bearing FS flank tumors treated with DMSO or BMS493 in combination with isotype control or aPD-1 antibody. Three doses of BMS493 (200ug intratumorally) or Isotype / aPD-1 antibody (200ug i.p.) were given at Days 7, 10 and 13. (n=5 tumors per group). **F**, Relative expression of *Raldh1*, *Raldh2* and *Raldh3* measured by qPCR in FS tumors treated with intratumoral BMS493 or DMSO. Three doses (200ug intratumorally) were given at Days 7, 10 and 13. Expression normalized to *Hprt*. n=4 tumors per group were harvested 15d post-transplant. **G**, Tumor growth curves of *Raldh1/3* DKO or Cas9 Control tumors injected intratumorally with BMS493 or DMSO. Three doses of DMSO or BMS493 (200ug intratumorally) were given at Days 7, 10 and 13. Tumor volume was measured every three days starting at 7d post-implantation (n=5 tumors per group). \*p<0.05, \*\*p<0.01. Two-tailed t test. (E) was analyzed with Kaplan-Meier with log-rank test. All error bars represent SEM. Events shown are pregated on live singlets unless otherwise specified.

### 3.2.2: RAR inhibition synergizes with immune checkpoint blockade selectively in RA producing tumors

We also tested intratumoral RAR inhibition on transplanted UPS and the results were consistent with FS tumors in that RAR blockade synergized with aPD1 therapy (Fig. 3.2.2A and 3.2.2C). Notably, in contrast to our



findings in FS and UPS, RAR blockade did not demonstrate any effect as a monotherapy or in combination with aPD1 in B16-F10 melanoma, which we found to display little to no RA production (Fig. 3.2.2B and 3.2.2D). Together, these results suggested that intratumoral RAR signaling inhibition in RA-rich tumors engenders a stimulatory APC compartment and synergizes with PD-1 blockade.

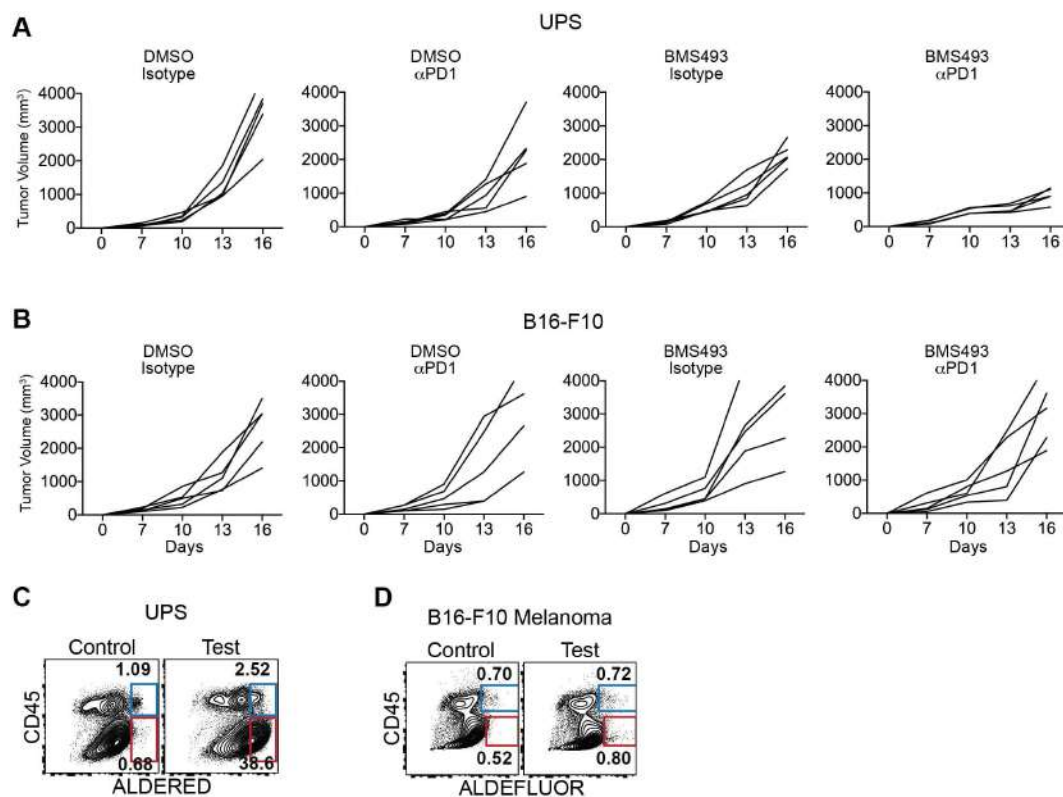


**Figure 3.2.2: RAR inhibition synergizes with immune checkpoint blockade selectively in RA producing tumors. A and B,** Individual growth curves of indicated tumors treated with aPD1 (or isotype control) in combination with intratumoral BMS493 (or DMSO). BMS493 (200ug i.t.) and/or aPD1 (200ug i.p.) were administered at Days 7, 10 and 13. (n=5

tumors per group). **C**, ALDERED assay performed on transplanted UPS tumors. Representative contour plot of Aldh<sup>+</sup> cells. n=5 tumors per group were harvested 14d post-implantation. Data are representative of two independent experiments. **D**, ALDEFLUOR assay performed on B16-F10 melanoma tumors. n=3 tumors per group were harvested at 14d post-implantation. Data are representative of two independent experiments. Events shown are pregated on live singlets unless otherwise specified.

### 3.2.3: Additional models to validate the effects of RAR inhibition on intratumoral APCs and anti-tumor immune responses

The aforementioned effects of RAR signaling inhibitors raise exciting translational possibilities, but were shown in syngeneic transplant-based systems using intratumoral injections. Hence, we next tested the effects of systemic delivery of BMS493 in autochthonous mouse models of SS and UPS. Notably, the effects of systemic BMS493 on increasing intratumoral stimulatory myeloid cells and T cells in these two distinct mouse models of sarcomas were consistent with the findings in syngeneic transplants (Fig. 3.2.3A, 3.2.3B, 3.2.3C and 3.2.3D).

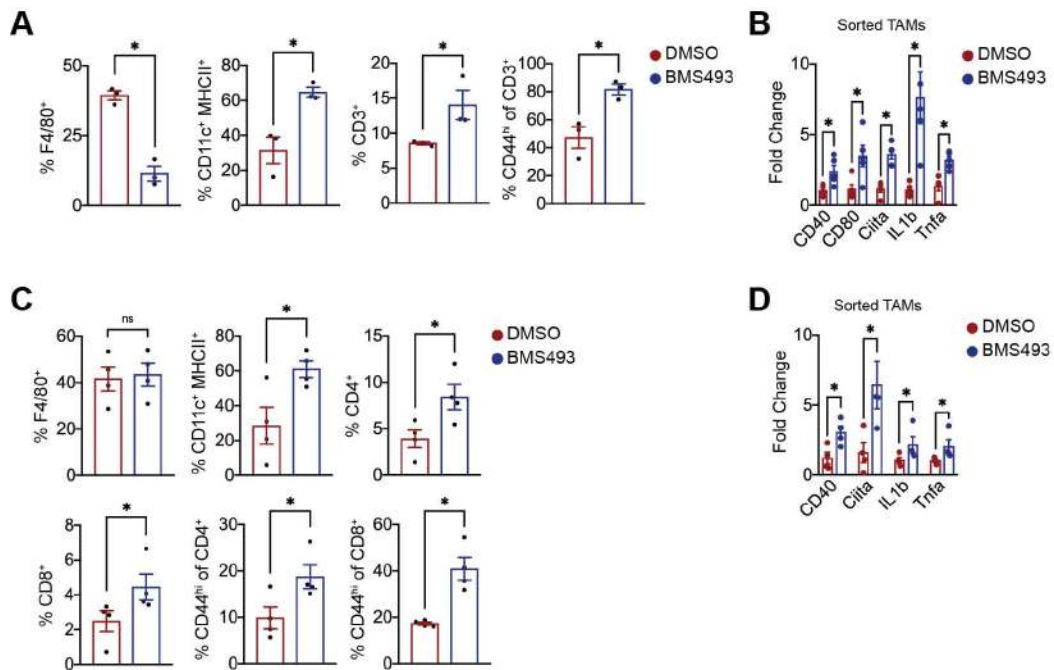


**Figure 3.2.3: Additional models to validate the effects of RAR inhibition on intratumoral APCs and anti-tumor immune responses. A,** Mice bearing established SS tumors (autochthonous model) were treated with DMSO or BMS493 i.p. (3 doses of 200ug at Days 1,3,5; mice euthanized on Day 7). Shown are frequencies of specified myeloid and lymphoid populations in SS tumors (n=3 per group). **B,** Relative expression of *Cd40*, *Cd80*, *Ciita*, *Il1b*, *Tnfa* in FACsorted tumor associated macrophages (TAMs) from DMSO or BMS493 treated SS tumors (n=3 per group). **C,** Mice bearing established UPS tumors (autochthonous model) were treated with DMSO or BMS493 i.p. (3 doses of 200ug at Days 1,3,5; mice euthanized on Day 7). Shown are frequencies of specified myeloid and lymphoid populations in UPS tumors (n=4 per group). **D,** Relative expression of *Cd40*, *Ciita*, *Il1b*, *Tnfa* in sorted TAMs from autochthonous UPS tumors in DMSO or BMS493 treated mice (n=3 per group). Each dot

represents an individual mouse tumor (n=4 per group). Normalized to *Hprt* expression. \*p<0.05. Two-tailed t test. Events shown are pregated on live singlets unless otherwise specified.

### 3.2.4: Monocyte-specific RAR inhibition increases intratumoral DC and augments anti-tumor immunity

Thus far, we have shown that reducing RA in TME promotes monocyte differentiation into immunostimulatory APCs and enhances anti-tumor T cell responses. To further examine the link between these two observations, we devised a monocyte-transplant experiment whereby monocytes isolated from LysM<sup>Cre</sup>: Rosa26<sup>tdT</sup> hosts were treated *ex vivo* with DMSO (control) or BMS493 (irreversible RAR blockade), washed, and transplanted into syngeneic FS tumors. The fate of the transplanted monocytes and their impact on tumor growth were monitored. In contrast to control monocytes, a significant fraction of BMS493 treated monocytes differentiated into CD11c<sup>+</sup> MHCII<sup>+</sup> DCs in the TME (Fig. 3.2.4A). Concomitantly, tumors transplanted with BMS493 treated monocytes grew at a significantly slower rate and displayed an immunostimulatory TME with evidence of activated APCs and T cells. (Fig. 3.2.4B and 3.2.4c).

Taken together, these findings provide proof-of-concept for targeting RA-RAR signaling in solid tumor immunotherapy.

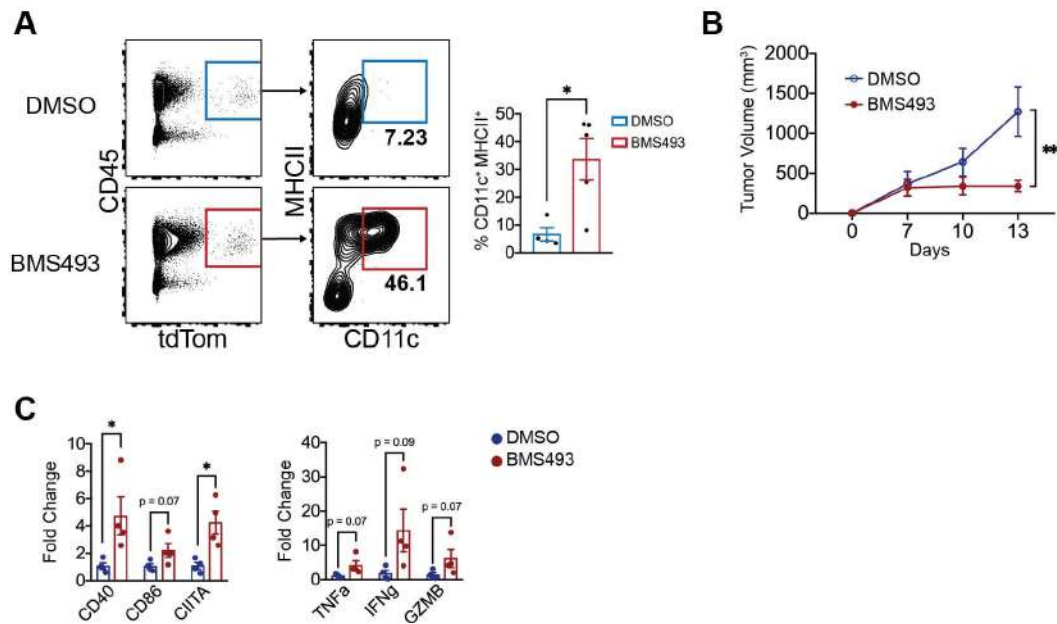


**Figure 3.2.4: Monocyte-specific RAR inhibition increases intratumoral DC and augments anti-tumor immunity. A,** Monocytes were isolated from bone marrow of *Lyz2<sup>Cre</sup>; Rosa26<sup>tdT</sup>* hosts using negative selection on magnetic columns (Miltenyi<sup>TM</sup>). Monocytes were treated with either DMSO or BMS493 (1uM) for one hour and washed twice in PBS. Subsequently, 5 x 10<sup>5</sup> monocytes were injected directly into FS flank tumors (three injections; 7d, 9d and 11d post- transplant). Shown are representative contour plots of tdT<sup>+</sup> cells (derived from transplanted monocytes) and frequencies of CD11c<sup>+</sup> MHCII<sup>+</sup> within the tdT<sup>+</sup> fraction at 13d post tumor implantation. **B,** Tumor growth curve of FS tumors injected with DMSO or BMS493 treated monocytes. Tumor volume was measured every three days starting at 7d post-implantation (n=4 tumors per group and data are representative of three independent experiments). **C,** Relative expression of *Cd40*, *Cd86*, *Ciita*, *Tnfa*, *Ifng*, *Gzmb* in bulk FS tumors transplanted with either DMSO or BMS493 treated monocytes. Normalized to *Hprt* expression. \*p<0.05,

\*\*p<0.01. Two-tailed t test. (B) was analyzed with linear mixed-effects modeling with Tukey's HSD post-test. All error bars represent SEM. Events shown are predated on live singlets unless otherwise specified.

### 3.3: Human tumors display evidence of RA-mediated immunosuppression

#### 3.3.1: Tumor cells upregulate RA producing enzymes in human sarcomas

The data from murine models suggested that increased tumor RA production or heightened RA signaling in MPs can promote tumor immune evasion and contribute to poor clinical outcomes. Levels of RA producing enzymes are known to be elevated in many human cancers (including breast, lung, colon, prostate) and have been associated with poor response to therapy and worse survival (Khoury et al., 2012; Li et al., 2010, 2014; Marcato et al., 2015; Wei et al., 2015; Zhang et al., 2013, p. 3). We found that human UPS expressed higher levels of *RALDH3* compared to non-malignant skeletal muscle (Fig. 3.3.1A). Consistent with murine UPS, ALDEFUOR analysis of human UPS showed that a subset of CD45<sup>-</sup> cells produced the majority of RA (Fig. 3.3.1B). This finding was corroborated in human SS tumors, in which CD45<sup>-</sup> cells expressed significantly higher levels of *RALDH2* and *RALDH3* compared to CD45<sup>+</sup> cells (Fig. 3.3.1C).

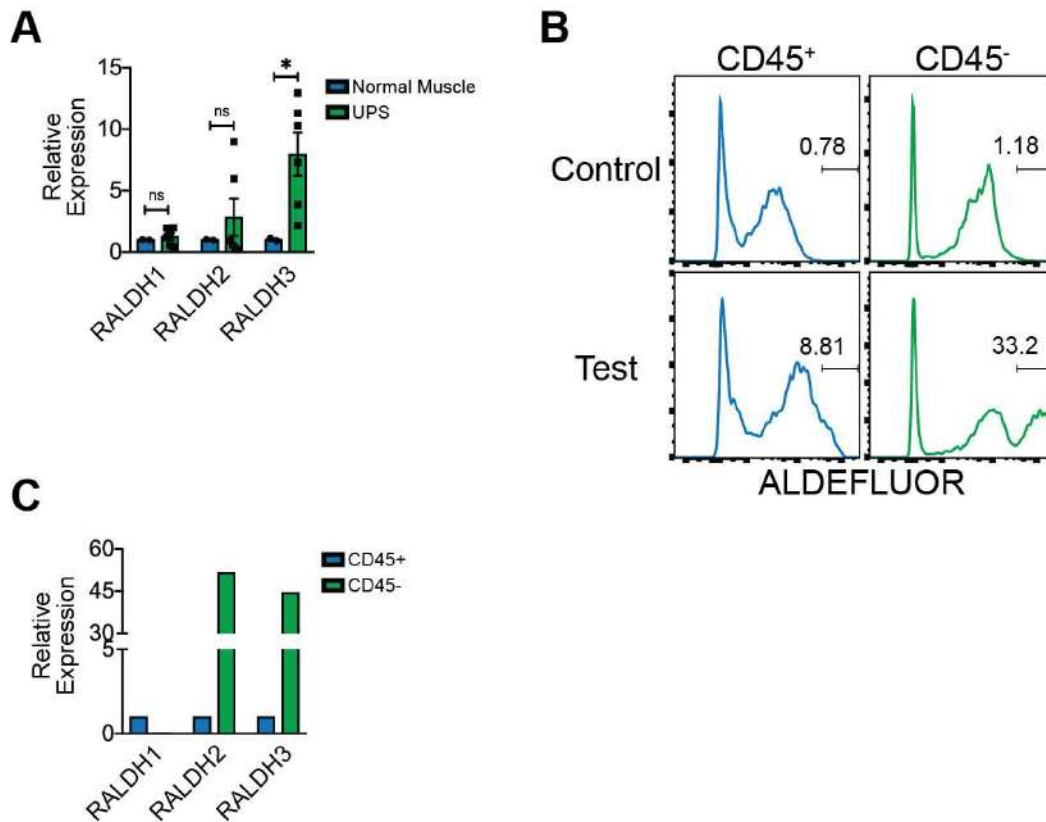


**Figure 3.3.1: Tumor cells upregulate RA producing enzymes in human sarcomas.** **A**, Relative expression of *RALDH1*, *RALDH2* and *RALDH3* measured by qPCR in human UPS compared to human gastrocnemius muscle. Expression normalized to *Hprt*. Each dot represents tissue sampled from a different location of tumor (two tissue samples from n=3 tumors). **B**, ALDEFLUOR assay on primary human undifferentiated pleomorphic sarcoma (UPS). Shown are histograms of “control” and “test” samples pre-gated on CD45<sup>+</sup> (left) or CD45<sup>-</sup> cells (right). Representative of n=2 human UPS. **C**, Relative expression of *RALDH1*, *RALDH2* and *RALDH3* measured by qPCR in sorted CD45<sup>+</sup> compared to CD45<sup>-</sup> cells from primary human synovial sarcoma (SS). Expression normalized to *Hprt*. Representative of n=2 human UPS. \*p<0.05. Two-tailed t test. All error bars

represent SEM. Events shown are pregated on live singlets unless otherwise specified.

### 3.3.2: Analysis of RA production across the TCGA mRNA dataset

Further, analysis of The Cancer Genome Atlas (TCGA) mRNA data revealed that *RALDH* isoforms are expressed in many types of cancers with *RALDH1* and *RALDH3* generally being more highly expressed than *RALDH2* (Fig 3.3.2A). Expression of *RALDH1* or *RALDH3* was significantly negatively correlated with survival in multiple types of human cancer (Fig. 3.3.2B). In sarcoma, subcategorization by Raldh expression was not predictive of poor clinical outcome, but interpretation of these analyses is significantly hampered by small sample sizes and heterogeneity in sarcoma clinical datasets, and will require additional investigation (Fig. 3.3.2C).



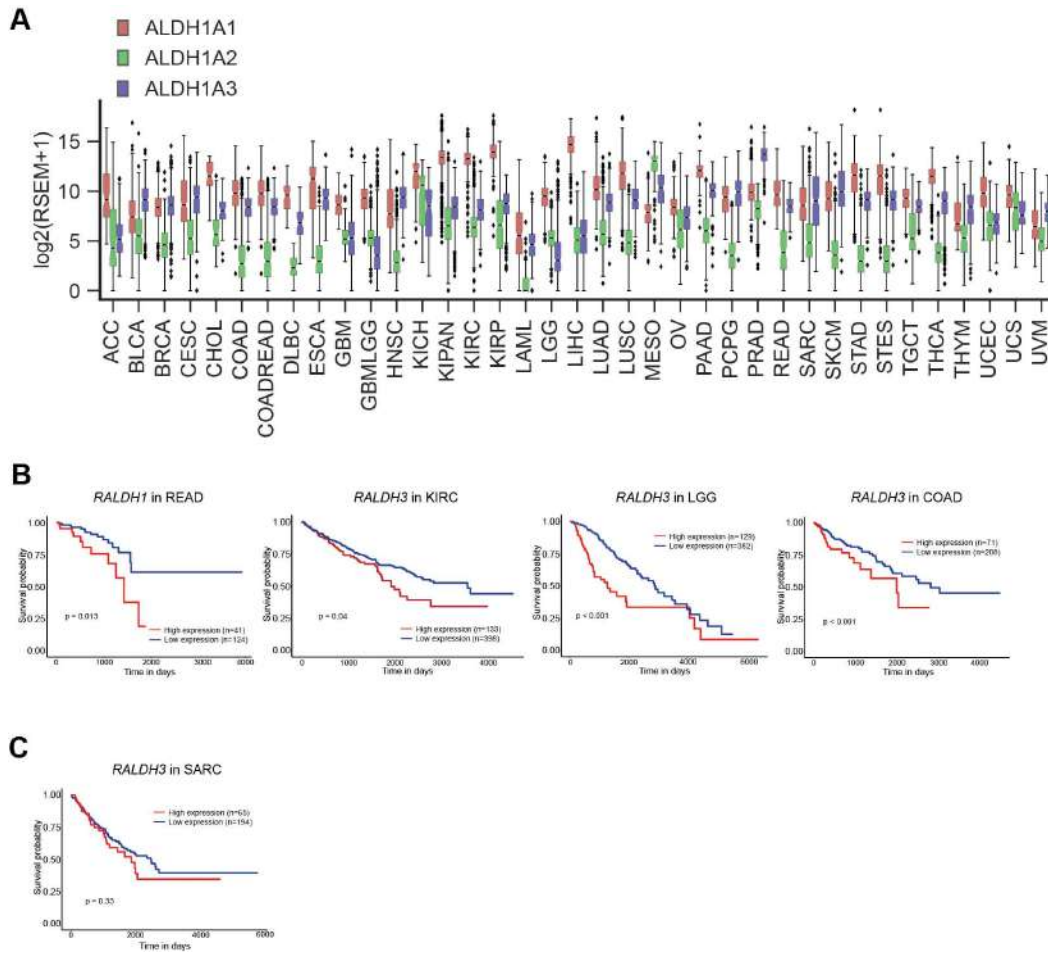


**Figure 3.3.2: Analysis of RA production across the TCGA mRNA dataset. A**, Comparison of *ALDH1A1*, *ALDH1A2* and *ALDH1A3* expression ( $\log_2(\text{RSEM}+1)$ ) expression across all TCGA cancer types. **B and C**, Kaplan-Meier curves showing overall survival partitioned by primary tumor *RALDH1* or *RALDH3* expression in indicated cancer types using TCGA mRNA datasets. READ: rectum adenocarcinoma; KIRC: kidney renal clear cell carcinoma; LGG: low grade glioma; COAD: colon adenocarcinoma; SARC: sarcoma.

### 3.3.3: Generation and analysis of “RA response score” in sarcoma

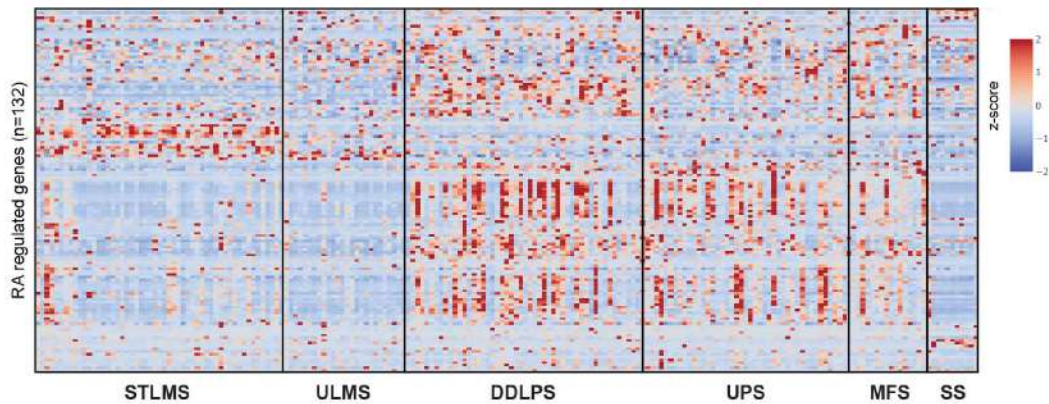
We next wanted to probe whether high levels of RA may drive myeloid mediated immunosuppression in human cancer. To do this, we generated an unbiased list of RA regulated genes from a microarray-based RA-treated human monocyte gene expression profile (Fig. 3.3.3A). Subsequently, we queried for the expression of these genes in the TCGA mRNA database and determined an “RA response score” for individual tumor samples. In TCGA sarcoma dataset, we found that the RA score clustered uniquely within certain sarcoma subtypes, with DDLPS, UPS and MFS having higher average RA scores compared to STLMS, ULMS and SS (Fig. 3.3.3B and 3.3.3C). The RA score was only significantly predictive of survival in ULMS (Fig. 3.3.3D).

**A**

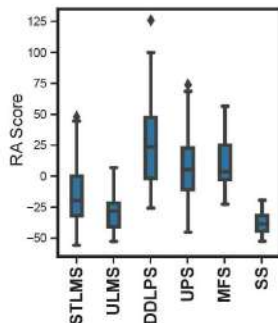
RA regulated genes in human monocytes; 132 genes

JUN	CCL26	IL1R2	CD2AP	NAPSB	LRRRC25	IL7R	ARHGAP31	LRRK2
EPB41L2	SLC7A11	TNFRSF11A	CD1D	PIK3GC	ALOX5AP	TGM2	THBS1	RGL1
MYB	ME1	FFAR4	SIGLEC17P	LY86	PRAM1	ADAM19	CD300LB	NPR1
ITGA6	ADD3	STON2	CCL23	GIMAP4	C1QC	IL31RA	SEMA6B	ABCA6
HIST1H2AK	FAR2	SORL1	SLC30A4	CYTH4	VSIG4	DCSTAMP	FAM124B	ABCA9
NBEAL2	SMAGP	CYP27A1	SCN9A	PTPN22	MS4A4A	MMP12	TCTEX1D1	ITGA9
ALS2CL	ASCM3	DHRS3	GFRA2	CD38	GPR34	CLEC6A	SDC2	CEP112
TBL2	MAP2K6	IL18	AHNAK	P2RY13	ATP8B4	PIM1	LRRRC32	CYP26A1
NFXL1	LRG1	CDA	MYO1C	TIFAB	CCL2	CD1A	HIVEP2	ATP1B2
MLXIPL	RAB20	GALM	FOSL2	IL2RA	LILRA5	FN1	CAMSAP2	TMIE
CTTNBP2	HBEGF	ACVRL1	FLNB	CD300A	PHOSPHO1	VCAN	XYLT1	CXCR5
ZFP69	TRIB1	CAPN2	EMP1	CD300LF	VSTM1	CHST15	PDE4DIP	TNFSF8
TACSTD2	PON2	SLC9A3	CD48	CASS4	CD163	HIC1	FRY	
BT6GALNAC	ANKRD22	SLCO4C1	GAPT	GPR141	CR1	MAFB	DTNA	
	RAP1GAP	NRIP1	RCSD1	TLR8	CXCR2	IL1R1	SOBP	

**B**



**C**



**D**

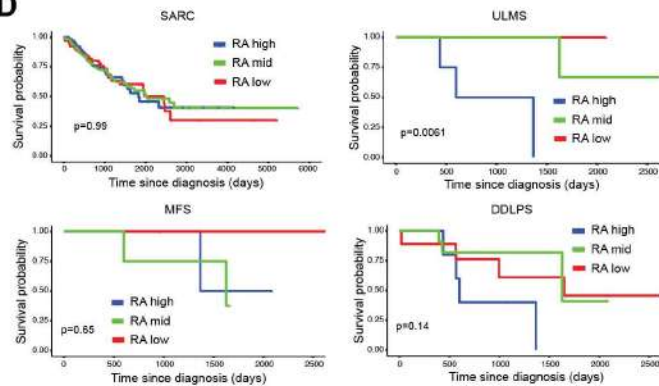


**Figure 3.3.3: Generation and analysis of “RA response score” in sarcoma. A,** List of human monocyte RA regulated genes that were used to build the “RA response score.” **B,** Heatmap of z-scores of human monocyte RA regulated genes (n=132; y-axis) for each tumor sample

(n=259; x-axis) in TCGA SARC (sarcoma) dataset. SARC dataset was further subcategorized into STLMS (soft tissue leiomyosarcoma), ULMS (uterine leiomyosarcoma), DDLPS (dedifferentiated liposarcoma), UPS (undifferentiated pleomorphic sarcoma), MFS (myxofibrosarcoma) and SS (synovial sarcoma). Human monocyte RA regulated gene list was obtained by analyzing microarray data of human monocytes cultured with GM-CSF and IL-4 treated with RA (20 nM) vs DMSO. RA regulated gene list contains genes that were 1) 3-fold up or down regulated after 24h of RA treatment and 2) were present in TCGA mRNA dataset with a median FPKM value >0.5. Z-score for each gene was calculated based on mean FPKM expression across all tumor samples. **C**, Box plots of “RA response score” for samples in SARC TCGA dataset (grouped as described in D). “RA response score” for each tumor sample was calculated by summing over the z-score for all RA regulated genes.

**D**, Kaplan-Meier curves showing overall survival partitioned by RA score (RA high (top quartile), RA mid (middle quartiles) RA low (bottom quartile) in indicated sarcoma types using TCGA mRNA datasets. SARC: sarcoma, ULMS (uterine leiomyosarcoma), MFS (myxofibrosarcoma), DDLPS (dedifferentiated liposarcoma). Analyzed using Kaplan-Meier with log-rank test.

### 3.3.4: Analysis of “RA response score” across TCGA mRNA dataset

Further, the RA score (compared to a “random score”) was enriched in a group of samples across all cancer types in TCGA, suggesting that a subset of human tumors experience heightened RA signaling (Fig. 3.3.4A). We next asked whether the RA score correlates with expression of orthogonal genes that are known to promote immunosuppression in solid tumors. As expected, the RA score was significantly correlated with *RALDH3* expression, providing transcriptional evidence that tumors that produce more RA also respond to higher levels of RA (Fig. 3.3.4B). Importantly, we found that the RA score was significantly correlated with multiple members of TGF $\beta$  and IL-10 signaling pathways, which are known to direct potent immunosuppressive axes in cancer and other settings of inflammation (Fig. 3.3.4B). We found that this association between RA score and TGF $\beta$  and IL-10 signaling was not restricted to sarcoma, but was consistent across a multitude of more common epithelial-derived human cancers including breast invasive carcinoma, lung adenocarcinoma and colon adenocarcinoma (Fig. 3.3.4B). Together, these analyses suggested that multiple types of human solid tumors produce and respond to high levels of RA which may drive an immunosuppressive TME.

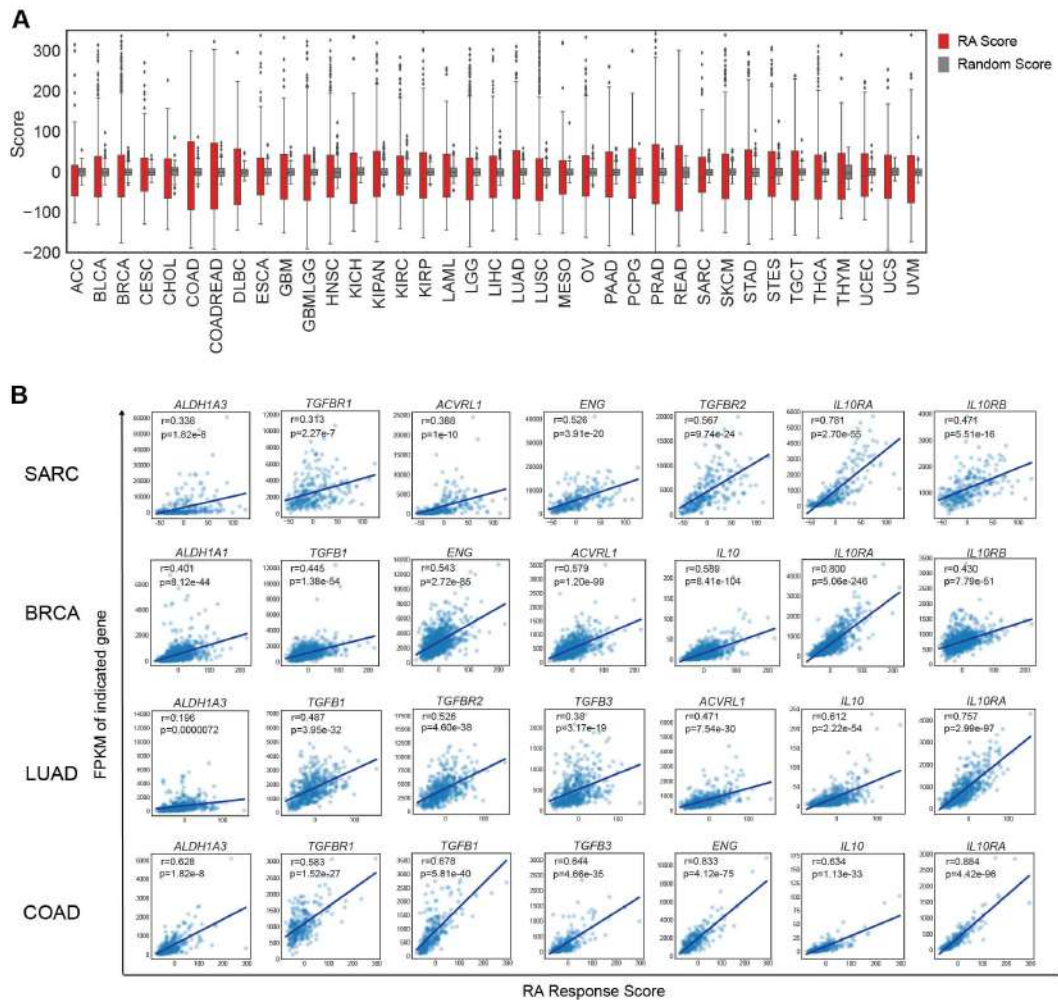


**Figure 3.3.4: Analysis of “RA response score” across TCGA mRNA dataset. A**, Comparison of “RA response score” to a “random response score” in all TCGA cancer types showing heterogeneous distribution of “RA response score.” “RA response score” was computed from the human monocyte RA regulated gene set (n=132 genes), while the “random response score” was computed from a randomly generated gene set (n=132 genes, varying across cancer types) following methods described Materials and Methods. **B**, “RA response score” plotted against FPKM values for each tumor sample for the indicated genes. Detailed explanation

of calculations and methodologies can be found in Materials and Methods. Pearson's correlation analysis was used to determine r and p values. BRCA: breast invasive carcinoma; LUAD: lung adenocarcinoma; COAD: colon adenocarcinoma. Individual p-value for each correlation is listed in Figure 7. All error bars represent SEM.

## CHAPTER 4: DISCUSSION

### 4.1: Targeting myeloid differentiation in the tumor microenvironment

Solid tumors possess an immunosuppressive TME that prevents both spontaneous and treatment-induced anti-tumor immune responses. Myeloid cells are key drivers of this immunosuppressive TME and pathways underlying myeloid immunosuppressive behavior have begun to be elucidated. In this context, the majority of studies have focused on pathways driving *dysfunction* of specific myeloid subsets within tumors. Some examples include PI3K $\gamma$  signaling driving anti-inflammatory function of TAMs, lipid accumulation driving tumor DC dysfunction, and prostaglandin E2 driving suppressive neutrophil functions (Juan R. Cubillos-Ruiz et al., 2015; Kaneda et al., 2016; Veglia et al., 2019). Here, we describe an RA-dependent mechanism of altered myeloid *differentiation* that promotes an immunosuppressive TME and tumor immune escape. Previous work has demonstrated the importance of the transcription factors *Mafb* and *Irf4* in controlling monocyte fate commitment into macrophages and DCs respectively (Goudot et al., 2017). Our work suggests that tumors target this transcriptional circuitry to increase TAMs and reduce DCs. Hence, repolarizing the immune TME from a suppressive to stimulatory milieu may require targeting pathways driving both *dysfunction* and *differentiation* of myeloid cells in the TME. It is important to note that monocytes represent an abundant precursor for both TAMs and DCs. Indeed, monocytes and



macrophages are among the most abundant cell type in the majority of solid tumors. The intratumoral monocyte pool is frequently replenished by the infiltration of circulating monocytes from peripheral blood. Though it is likely that not all monocytes that egress into the tumor microenvironment have the potential to generate stimulatory professional antigen presenting cells, we show in the current study that a significant portion of intratumoral monocytes retain the capacity to differentiate into bona fide dendritic cells, if exposed to the appropriate DC inducing conditions. Hence, therapeutic targeting of monocyte differentiation into stimulatory DCs within the TME may break immunosuppressive barriers and enable immunotherapy of solid tumors. Indeed, we provide proof of concept for this approach by simultaneously targeting both RA signaling and immune checkpoints on T cells to achieve strong synergism. Building on these findings, we envision a multi-pronged approach for solid tumor immunotherapy by: (1) increasing tumor DCs while reducing suppressive TAMs by targeting RA signaling, (2) increasing availability of tumor antigens to DCs by inducing tumor cell death with conventional therapy (cytotoxic or radiation), and (3) overcoming T cell dysfunction via immune checkpoint blockade.

#### 4.2: Dual functions of retinoic acid in tumorigenesis

RA is a well-studied signaling molecule and a powerful morphogen. Decades of research into RA-mediated transcriptional regulation have highlighted its important role in various cell types during development,

homeostasis, and disease. Solid tumors represent a complex niche comprising of many different cell types besides malignant cells. Hence, the overall impact of RA signaling on solid tumors is likely a sum total of its effects on the constituent cells of the TME. It is important to note that high expression of RA producing enzymes, retinaldehyde dehydrogenases (Raldhs) has been reported in many types of solid tumors. Even more, the expression of these enzymes has been correlated with poor survival in human cancers (Khoury et al., 2012; Li et al., 2010, 2014; Marcato et al., 2015; Wei et al., 2015; Zhang et al., 2013, p. 3). However, RA has been shown to have “pro-differentiation” effects on several types of tumor cells and hence can be considered anti-tumor in this context. Indeed, this has been the dominant theme in the field of RA cancer research, as all trans retinoic acid is a powerful therapeutic agent for acute promyelocytic leukemia. The therapeutic effect of RA in this setting is likely imparted by the specific biology driven by the translocation driven event resulting in constitutive expression of the RA receptor. In contrast to the pro-differentiation / anti-tumor effects of RA, we show here that RA drives anti-inflammatory effects in immune cells and can be considered pro-tumor in this context. We focused in this study on the effects of RA on intratumoral myeloid cells, given that they appeared to mediate the majority of RA's effects on tumor immunity in our model, and given that RA is well known to have a short diffusion gradient and likely acts in a paracrine manner. However, it is possible that RA also directly impacts anti-tumor T cells, as

RA has been shown before to control T cell activation, differentiation and effector function. Further, tumor derived RA may impact the biology of tumor draining lymph nodes, which remains to be explored.

Nevertheless, targeting RA signaling for tumor therapy requires a clear understanding of its role in specific tumor types as well as selective targeting of the appropriate cell type within the TME. Our data suggests that inhibition of RA production in tumor cells, and inhibition of RAR signaling in myeloid cells may be effective translational approaches. Though potent commercially available compounds to specifically inhibit RA synthesis do not exist, there are inhibitors to inhibit the parent family of aldehyde dehydrogenase enzymes (e.g. Citral). One can also envision an *in vivo* gene editing approach to delete RA producing enzymes in human tumors, given that an effective delivery method exists. In terms of inhibiting RAR signaling, it is exciting to imagine the possibility of delivering RAR inhibitors such as BMS493 specifically to myeloid cells, such as tumor associated macrophages. In this regard, it may be possible to utilize lipid or polymer-based compounds (such as lipid nanoparticles) as delivery vehicles for RAR inhibitors.

We have attempted to identify tumor types where the RA-dependent myeloid pathway may play a role in immune evasion by computing a monocyte “RA response score”. The overarching intent is to identify

appropriate patient populations for potential clinical trials based on RA-targeting for tumor immunotherapy. It is important to note that the “RA response score” was generated by treating normal donor human monocytes with RA. To probe the specificity of the RA response score, it may be useful to treat cancer cells with RA and query the expression of differentially expressed genes in human mRNA datasets. The hypothesis here is that the transcriptional response of human cancer cells to RA is significantly different from that of human monocytes, and ultimately may help to disentangle the effects of RA on the immune vs tumor cell compartments in solid tumors. Thinking more translationally, it may eventually be useful to determine a “monocyte specific” and “tumor cell specific” RA response score for individual patients, a balance of which may determine the scientific rationale and clinical efficacy of RA blockade in human cancer.

#### 4.3: Ontological specificity of metabolic control of differentiation

DCs can originate from “hardwired” HSC-derived DC precursors (cDCs) or from monocytes (moDCs). In this study, we primarily focused on the effects of RA on moDCs given that monocytes are vastly more abundant than dedicated DC precursors and because monocytes continuously infiltrate solid tumors to differentiate into immunosuppressive TAMs. Furthermore, precursors of cDCs are thought to have already committed to the cDC lineage prior to entering the tissue microenvironment. Nonetheless, previous studies have examined the role of RA on splenic and intestinal

cDC development, finding that RA can actually promote the development of cDC2s (Klebanoff et al., 2013). Though outside the scope of the current manuscript, we also observed that RA did not suppress cDC development in FLT3 culture systems, in which we cultured mouse bulk bone marrow for 7 days with FLT3. Though RA did not suppress DC development as assessed by Zbtb46-GFP expression, RA did induce detectable transcriptional and protein level changes in DC activation markers such as CD40, CD80 and CD86 (data not shown). This was in contrast to the effects of RA we observed on moDC development when using GM-CSF or GM-CSF and IL-4 culture systems. These seemingly opposing findings of the effects of RA may highlight the fact that the effects of RA on DCs may depend on ontogeny. This is an intriguing concept with implications for tumor immunotherapy, and we are currently examining the contextual relevance and molecular basis for this selective impact of RA on DC lineage.

#### 4.4: Varied roles of Th2 cytokines in solid tumor biology

An intriguing observation in our studies was the induction of tumor cell RA production by IL-13 in the TME. It is interesting to note that the related Th2 cytokine IL-4, also induced tumor cell RA production but to a lesser extent. Many previous studies have shown a link between Th2 cytokine milieu and immunosuppressive TME, although the underlying pathways are not fully understood (Fridman et al., 2012; McCormick and Heller, 2015; Suzuki et al., 2015; Zou, 2005). Our findings provide a mechanistic explanation for

this observation. Most of the literature involving Th2 cytokines in tumor immunology focus on the roles of these cytokines on immune cells such as T cells or myeloid cells.

Notably, both IL-4 and IL-13 play a role in the differentiation of monocytes into DCs and M2-polarized macrophages. Indeed, the well-established *in vitro* differentiation system to generate DCs from bone marrow monocytes involves the use of GM-CSF and IL-4. Induction of tumor cell RA production via these cytokines blocks DC differentiation while allowing M2 macrophages to develop from monocytes, which represents an interesting pathway by which tumor cells sense and respond to 'immune pressure'. This may represent a novel immune mechanism by which tumor cells prevent the formation of stimulatory APCs and thereby thwart anti-tumor T cell responses. However, it is very likely that there are other factors besides these cytokines that regulate RA production in solid tumors. One factor that we have briefly tested is hypoxia, which is known to be associated with immunosuppression and tumorigenesis. However, *in vitro* hypoxia treatment with 2% oxygen did not induce RA production in fibrosarcoma cells (data not shown). Further, it is also unclear whether tumor cells are the only RA-producing cells within the TME of *all* tumor types. Though we found that almost all of the RA is produced by tumor cells in sarcoma, given the pro-differentiation effects of RA, other non-malignant cells of TME, such as fibroblasts, may be the primary source of RA in some types of tumors. We

anticipate future work to provide further clarity into these questions, which will help optimize efforts to develop therapeutic approaches targeting RA signaling for tumor immunotherapy.

In summary, our study identifies an RA-dependent immune evasion pathway in solid tumors, provides proof of concept for targeting this pathway for solid tumor immunotherapy, and describes a method to potentially identify human tumors in which this pathway is active and hence amenable to RA-targeted therapeutic approaches.

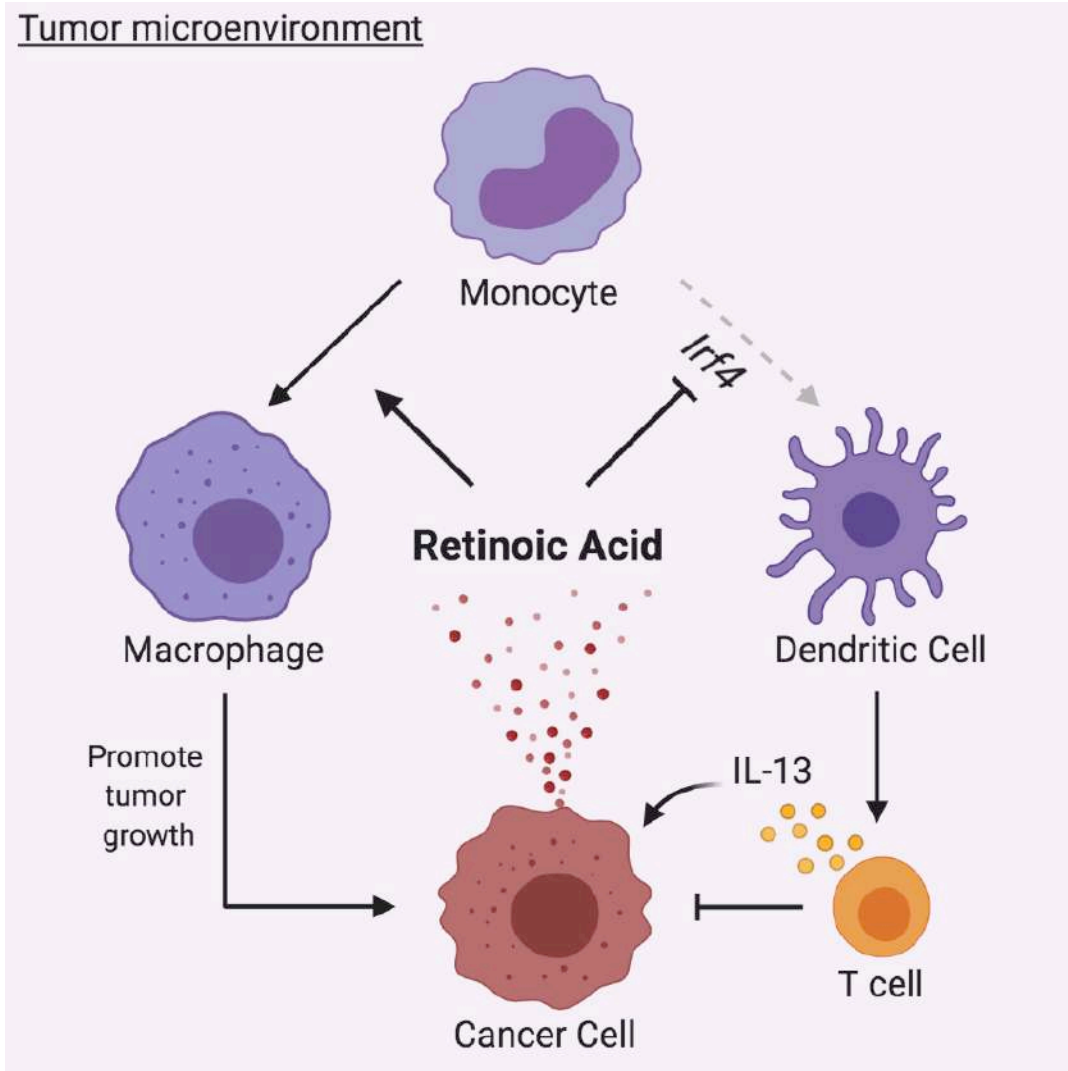


**Figure 4.1.1: Unifying model of findings described in Devalaraja et al. 2020.** Within the tumor microenvironment, T cells produce the cytokine IL-13, which induces tumor cells to produce retinoic acid. Retinoic acid production by tumor cells alters the differentiation trajectory of intratumoral monocytes. Retinoic acid promotes immunosuppressive macrophage but inhibits immunostimulatory DC differentiation from intratumoral monocytes. Mechanistically, retinoic acid suppresses *Irf4*, a transcription factor that is required for monocyte to DC differentiation. Macrophages promote tumor



growth, whereas DCs enhance anti-tumor T cell immunity. In summary, tumor cell production of retinoic acid represents a novel immune evasion mechanism utilized by solid tumors.

## CHAPTER 5: MATERIALS AND METHODS

### 5.1: Experimental models and subject details:

#### 5.1.1: Mouse models

**Tumor models:** Two GEMMs were used in these studies: Rosa26<sup>syt-ssx</sup>: Catnb<sup>lox(e3)</sup> mice (generated as previously described(Barrott et al., 2015)) and Kras<sup>G12D</sup>: Trp53<sup>lox</sup> mice (a generous gift from David Kirsch)(Kirsch et al., 2007). Oncogenesis was initiated by local injection of Cre protein (TAT-Cre, Millipore) in the hind limb musculature to minimize immune response to virus. Syngeneic fibrosarcoma flank tumors were established in C57BL/6 mice purchased from Jackson Laboratories.

**Mononuclear phagocyte models:** Zbtb46<sup>GFP</sup> mice were a generous gift from Kenneth Murphy(Satpathy et al., 2012, p. 46). Ccr2<sup>-/-</sup> mice were obtained from Jackson Laboratories and bred to Kras<sup>G12D</sup>: Trp53<sup>lox</sup> mice. LysM<sup>Cre</sup> mice were obtained from Jackson Laboratories and bred to 1) Rosa26<sup>LSL-tdT</sup> 2) Irf4<sup>lox</sup> or 3) Rosa26<sup>Cas9-eGFP</sup> mice. Batf3<sup>-/-</sup> mice were obtained from Jackson Laboratories and/or bred in house for experimental use.

Sex (both male and female) and aged matched mice between 6-8 weeks were used for these studies. Mice were bred and maintained in specific pathogen free facilities at the University of Pennsylvania. All animal procedures were conducted according to National Institutes of Health guidelines and approved by the Institutional Animal Care and Use Committee at the University of Pennsylvania.

### 5.1.2: Tumor cells

C57BL/6 syngeneic fibrosarcoma cell line was a generous gift from Robert Schrieber at Washington University in St. Louis and was used for experimentation as previously described (Gubin et al., 2018). Kras<sup>G12D</sup>: Trp53<sup>flox</sup> sarcoma cell line was a generous gift from Sandra Ryeom and B16-F10 melanoma cell line was a generous gift from Andy Minn. Tumor cell lines were cultured in DMEM with 10% FBS, 1% Pen/Strep and 2mM glutamine. Low passage (<P15) cell lines were used for *in vitro* and *in vivo* experimentation. All cells were confirmed to be negative for mycoplasma contamination as assessed by MycoAlert Mycoplasma Detection Kit (Lonza).

### 5.1.3: Human samples

Human undifferentiated pleomorphic sarcoma, synovial sarcoma, or non-malignant muscle samples were obtained from surgically resected tumors from patients (de-identified) undergoing therapeutic surgical resection in accordance with protocol approved by the Institutional Review Board at the University of Pennsylvania. Single cell suspensions from human tumor samples were generated using methods described in sections below. Similarly, ALDEFLUOR assay, cell sorting and qPCR analyses were performed as described below.

## 5.2: Method details:

### 5.2.1: “RA response score” computation and TCGA analysis

**(a) RA response gene signature:** We performed differential expression analysis, using DESeq2 (10.1186/s13059-014-0550-8), on microarray data of human monocytes treated with RA or DMSO. Genes up or down-regulated by at least three-fold (with false discovery rate q-value  $<0.05$ ) were collected and assigned to the RA response gene signature that contained a total of 146 genes. For analysis of TCGA mRNA datasets, only genes that were expressed with a FPKM value  $>0.5$  across all patient samples in a cancer group were retained. This reduced the total number of genes in the RA response gene signature to  $n=132$  for the SARC, BRCA, LUAD, and COAD datasets.

**(b) Cancer and patient specific RA response score:** From the TCGA mRNA expression data, we computed the FPKM z-score for the  $n=132$  RA response signature genes and hierarchically ranked them as shown in Fig. 7D. The RA response score for every patient sample, in a given cancer, for a given gene set, was taken to be the z-score summed over all genes. In order to evaluate the heterogeneity in the RA response score, we also computed a random response score employing a randomly generated gene set ( $n=132$  genes) as described above. To identify the genes in a specific cancer that may be regulated by the RA response score, we performed a genome-wide correlation between the patient RA response score and the

corresponding FPKM values and quantified the degree of correlation using a linear regression model.

Additionally, Kaplan-Meier analyses based Raldh mRNA substratification in selected TCGA datasets was performed using UALCAN(Chandrashekar et al., 2017). High expression indicates the top quartile, while low expression indicates the bottom quartile.

### 5.2.2: Analysis of microarray

Microarray services were provided by the UPENN Molecular Profiling Facility, including quality control tests of the total RNA samples by agilent bioanalyzer and nanodrop spectrophotometry. All protocols were conducted as described in the Affymetrix WT Pico Reagent Kit Manual and the Affymetrix GeneChip Expression Analysis Technical Manual. Gene expression data were normalized and values modeled using ArrayStar4 (DNASTAR). The unprocessed data for microarray reported in this manuscript are being deposited in GEO.

### 5.2.3: Implantation of tumor cells, tumor growth measurements and survival analyses

Cultured tumor cells were detached using 0.05% trypsin (GIBCO), washed once with DMEM media and once with 1x PBS, and counted in preparation for implantation. Tumor cells were propagated *in vitro* for two passages prior to implantation and injected cells were greater than 90% viable.  $1 \times 10^6$

tumor cells were implanted subcutaneously (s.c.) into shaved flanks of recipient mice. Tumor dimensions were measured using a caliper starting at Day 7 and every three days thereafter; volume was calculated by using formula  $(ab^2)\pi/2$ , where a is the longest measurement and b is the shortest. Tumor volumes of 1000mm<sup>3</sup> were used as endpoints for survival analyses. Waterfall plots were generated by comparing tumor volume at the start of treatment to tumor volume 11d later. For re-challenge experiments with tumor cell lines, tumor cells were injected into mice cured of primary tumors for >60 days.

#### 5.2.4: Flow cytometry of murine samples

Tumors were harvested and minced at indicated time points post-implantation for analysis. Single cell suspensions were generated by digestion with collagenase B and DNase I for 45 minutes at 37°C and filtration through 70µM cell strainer. Mouse blood was collected in EDTA tubes and RBCs were lysed using ACK lysing buffer. Samples were incubated for 5 minutes at room temperature with anti-mouse CD16/32 Fc Block, and subsequently stained on ice with primary-fluorophore conjugated antibodies for identification of cell populations by FACS. 7AAD (BioLegend) was used for dead cell discrimination. Flow cytometry was performed on an LSR II Flow Cytometer (BD Biosciences) and analyzed using FlowJo software (Treestar). List of antibodies can be found in table above.

### 5.2.5: T cell IFN $\gamma$ *ex vivo* assay

Single cell suspensions generated from mouse tumors were incubated for 4 hours at 37°C with PMA (50ng/mL; Sigma), Ionomycin (750ng/mL; Sigma) and GolgiStop (5ug/mL; BD). Intracellular staining was performed using a fixation/permeabilization kit (eBiosciences) according to manufacturer's instructions.

### 5.2.6: *In vitro* tumor cell proliferation assay

After tumor cells were propagated for two weeks *in vitro*,  $5 \times 10^4$  of indicated tumor cell lines were plated in triplicate. Viable and non-viable cell numbers were counted each day for five days.

### 5.2.7: ALDEFLUOR assay

The ALDEFLUOR assay (STEMCELL Technologies) was performed according to manufacturer's instructions to identify cells with Aldh activity. In brief, single cell suspensions generated from indicated tumors were incubated with a fluorescently tagged substrate of the Aldh enzyme; the fluorescent product accumulates in cells proportional to their Aldh activity. DEAB, a potent inhibitor of Aldh, was used as a negative control for each sample. Cells were subsequently stained with surface antibodies and fluorescence was quantified by flow cytometry. Gates for Aldh<sup>+</sup> cells were drawn relative to baseline fluorescence as determined by DEAB negative control. To avoid spectral overlap, ALDERED assay (STEMCELL

Technologies) was performed in lieu of ALDEFUOR assay for samples with endogenous GFP fluorescence.

#### 5.2.8: Cell sorting

Cells were sorted on MoFlo Astrios or FACS Jazz at the Children's Hospital of Philadelphia (CHOP) Flow Cytometry Core Laboratory. For measurement of gene expression in sorted cells, RNA was isolated from sorted cell pellets and qPCR performed as described elsewhere. For T cell suppression assays, tumor APCs were sorted into complete RPMI media and T cell suppression assay performed as described elsewhere.

#### 5.2.9: LC-MS for ATRA

*All-trans* retinoic acid was extracted from snap frozen mouse tumors or normal muscle as described (Kane et al., 2008). Quantification of ATRA was performed by the Children's Hospital of Philadelphia Metabolomics Core using liquid chromatography tandem mass spectrometry (LC-MS).

#### 5.2.10: Bone marrow monocyte isolation

Monocytes were isolated from bone marrow of indicated mice using the Mouse BM Monocyte Isolation Kit (Miltenyi Biotec) according to manufacturer's instructions. Viability and purity of negative selection monocyte isolation was assessed by flow cytometry to be >90%.



### 5.2.11: Intratumoral monocyte transfer

Monocytes were isolated (as described above) from mouse bone marrow of LysM<sup>Cre</sup>: Rosa26<sup>tdT</sup>: Zbtb46<sup>GFP</sup> mice. Subsequently, 5 x 10<sup>5</sup> monocytes were resuspended in 50uL 1x PBS and injected directly into established FS flank tumors at 7 days post implantation. Tumors were harvested at specified time points and analyzed by flow cytometry to track tdT<sup>+</sup> monocytic progeny.

### 5.2.12: *In vitro* and *ex vivo* mouse and human monocyte differentiation assays

Mouse monocytes (isolated from bone marrow or sorted from LysM<sup>Cre</sup>: Rosa26<sup>tdT</sup>: Zbtb46<sup>GFP</sup> tumors) were cultured with GM-CSF (20ng/mL) & IL-4 (20ng/mL), GM-CSF & IL-13 (20ng/mL), GM-CSF alone, or M-CSF alone (20ng/mL). Normal donor human monocytes (obtained the Human Immunology Core at the University of Pennsylvania) were cultured with GM-CSF (50ng/mL) & IL-4 (50ng/mL), or M-CSF (50ng/mL). Murine or human cytokines were purchased from PeproTech. RA (100nM for mouse and 20nM for human monocytes) or DMSO was added at specified time points for indicated differentiation assays. Cellular identity and function of differentiated monocytes was assessed by a combination of unbiased transcriptional analyses, flow cytometry based protein analyses, and functional T cell suppression assays.

### 5.2.13: Mouse and human T cell suppression assays

Mouse splenic T cells were isolated from a non-tumor bearing C57BL/6 mouse using Pan T Cell Isolation Kit (Miltenyi Biotec). Viability and purity of negative selection T cell isolation was assessed by flow cytometry to be >95%. Normal donor human T cells were obtained from the Human Immunology Core at the University of Pennsylvania.  $8 \times 10^4$  mouse or human T cells were labeled with CFSE and cultured for 3 days at 37°C with 2uL of aCD3/28 beads (Dynabeads Mouse or Human T-Activator CD3/28, Gibco) along with 30U recombinant human IL-2. Mononuclear phagocytes generated under various *in vitro* differentiation conditions (or sorted from mouse tumors) were co-cultured with stimulated T cells. T cell proliferation and activation was measured by flow cytometry to quantify mononuclear phagocyte suppressive ability.

### 5.2.14: Depletion of CD4<sup>+</sup> or CD8<sup>+</sup> T cells *in vivo*

200ug of clone GK1.5 (CD4<sup>+</sup> T cell depletion), clone 2.43 (CD8<sup>+</sup> T cell depletion), or clone LTF-2 (isotype control) antibody was administered i.p. starting three days prior to tumor implantation and repeated every three days until mouse sacrifice. All antibodies were purchased from BioXCell. CD4<sup>+</sup> and CD8<sup>+</sup> depletion was confirmed in peripheral blood and within tumors by flow cytometry.

### 5.2.15: *In vivo* reagents

200ug of aPD1 monoclonal blocking antibody (clone RMP 1-14, BioXCell) or isotype control antibody (clone 2A3, BioXCell) was administered i.p. at Days 7, 10 and 13 post tumor implantation. 200ug of BMS493 (Torcis) was administered intratumorally at Days 7, 10 and 13 post tumor implantation. BMS493 was dissolved in 10uL DMSO and diluted to a final volume of 50uL in 1x PBS for intratumoral injection. As a vehicle control, 10uL DMSO in a final volume of 50uL was injected intratumorally.

#### 5.2.16: RNA isolation and qPCR analysis for gene expression

Total RNA was isolated using GenElute Mammalian Total RNA Miniprep Kit (Sigma). Reverse transcription was performed using High Capacity RNA to cDNA Kit (Life Technologies). qRT-PCR was performed using ViiA7 Real-Time PCR machine and TaqMan probes used for gene specific amplification (purchased from ThermoFisher Scientific) are listed below.

*Arg1* (Mm00475988\_m1), *Hprt* (Mm03024075\_m1), *Tnfa* (Mm00443258\_m1), *Il1b* (Mm00434228\_m1), *Cd40* (Mm00441891\_m1), *Cd80* (Mm00441891\_m1), *Cd86* (Mm00444543\_m1), *Raldh1* (Mm00657317\_m1), *Raldh2* (Mm00501306\_m1), *Raldh3* (Mm00474049\_m1), *Irf4* (Mm00516431\_m1), *Zbtb46* (Mm00511327\_m1), *Raldh1* (Hs00946916\_m1), *Raldh2* (Hs00180254\_m1), *Raldh3* (Hs00167476\_m1), *Irf4* (Hs01056533\_m1), *Zbtb46* (Hs01008168\_m1), *Hprt* (Cat #4333768).

### 5.2.17: CRISPR mediated gene deletion in tumor cells

LentiCRISPRv2 vector was a gift from Feng Zhang (Addgene plasmid #52961). In brief, the vector was transfected into 293T cells using polyethylenimine (PEI) along with lentivirus packaging plasmids. Lentivirus supernatant was collected 48 hours later and passed through a 40uM filter. Subsequently, tumor cells were transduced and selected on 3ug/mL of puromycin for two weeks. Clones were generated using single cell sorting and knockout efficiency determined by genomic sequencing and gene-specific qPCR analysis. CRISPR sequences were identified using mouse Geckov2 library (Feng Zhang): *Raldh1*: TAA-ATC-CGA-CAA-GTA-TGC-AT; *Raldh3*: TAC-TTA-CAG-CCA-GGA-TCG-CT; *IL13Ra1*: GAG-ACG-CTC-AAA-TTC-GTC-AC. *In vivo* knockout efficiency of *Raldh1/3* DKO cell line was determined by qPCR for *Raldh1* and *Raldh3* gene expression in bulk tumor tissue, by ALDEFUOR assay measuring functional enzymatic activity on tumor single cell suspension, and by liquid chromatography / mass spectrometry for *all-trans* retinoic acid in tumor tissue.

### 5.2.18: Overexpression of target genes in tumor cells

*Raldh2*-GFP ORF expression clone was purchased from GeneCopoeia (Cat # EX-Mm21038-M61) and transfected into Cas9 Control or *Raldh1/3* DKO FS cell lines using electroporation and nucleofection (Amaza Nucleofector II, Lonza). After three days, cell lines were sorted based on GFP expression using a BD FACS Jazz instrument and subsequently

cultured for two weeks *in vitro* prior to s.c. implantation. *In vivo* confirmation of overexpression was determined by qPCR for *Raldh2* and maintenance of GFP expression in bulk tumor tissue.

#### 5.2.19: Single cell sequencing preparation

Cas9 Control or *Raldh1/3* DKO tumors (n=4 per group) were harvested on Day 11 (as described elsewhere) and CD45+ live cells were FACS sorted. Subsequently, 10x Genomics Controller and the v3 Library and Gel Bead kit (10x Genomics) were used to obtain single-cell emulsions. 10x 3' v3 kit protocol was followed as described to generate RNA sequencing libraries. The generated libraries were sequenced using an Illumina NovaSeq SP.

#### 5.2.20: Single cell RNA sequencing analysis

Downstream analysis of the single-cell RNA-sequenced samples was performed using Seurat (v. 3.1.0) in R (v. 3.6.0) (CITE SEURAT). Genes expressed in less than three cells were removed. Cells that expressed less than 500 genes or had over 14% mitochondrial content were filtered out. The four samples were merged and counts for all genes were log2 normalized and scaled (*NormalizeData* and *ScaleData*). Principal components (PCs) were determined using the 2000 most variable genes (*FindVariableFeatures*). Subsequently, the top 50 PCs were used for graph-based cluster identification and dimensionality reduction by t-distributed stochastic neighbor embedding (t-SNE). Myeloid clusters were subsetted

out using *Adgre1*, *Lyz2*, *S100a9*, *Itgax* and negative for lymphoid markers and re-analyzed as described above. Genes separating TAM\_1 and TAM\_2 clusters were determined using the default Wilcoxon Rank Sum test in the *FindMarkers* function.

### 5.2.21: Quantification and statistical analysis

Statistical significance was calculated between two groups by student's unpaired t test. One-way ANOVA with Tukey's HSD post-test was used to calculate statistical significance between multiple groups. Significance for survival was calculated by Kaplan-Meier with long-rank analysis. Analyses were performed using GraphPad Prism 8. Error bars represent SEM and  $p < 0.05$  was considered statistically significant (\* $p < 0.05$ , \*\* $p < 0.01$ , \*\*\* $p < 0.001$ ).

## REFERENCES

- Abram, C.L., Roberge, G.L., Hu, Y., Lowell, C.A., 2014. Comparative analysis of the efficiency and specificity of myeloid-Cre deleting strains using ROSA-EYFP reporter mice. *J Immunol Methods* 408, 89–100. <https://doi.org/10.1016/j.jim.2014.05.009>
- Balkwill, F., Mantovani, A., 2001. Inflammation and cancer: back to Virchow? *The Lancet* 357, 539–545. [https://doi.org/10.1016/S0140-6736\(00\)04046-0](https://doi.org/10.1016/S0140-6736(00)04046-0)
- Barrott, J.J., Illum, B.E., Jin, H., Zhu, J.-F., Mosbrugger, T., Monument, M.J., Smith-Fry, K., Cable, M.G., Wang, Y., Grossmann, A.H., Capecchi, M.R., Jones, K.B., 2015.  $\beta$ -catenin stabilization enhances SS18-SSX2-driven synovial sarcomagenesis and blocks the mesenchymal to epithelial transition. *Oncotarget* 6, 22758–22766.
- Bauer, R., Udonta, F., Wroblewski, M., Ben-Batalla, I., Santos, I.M., Taverna, F., Kuhlencord, M., Gensch, V., Päsler, S., Vinckier, S., Brandner, J.M., Pantel, K., Bokemeyer, C., Vogl, T., Roth, J., Carmeliet, P., Loges, S., 2018. Blockade of Myeloid-Derived Suppressor Cell Expansion with All-Trans Retinoic Acid Increases the Efficacy of Antiangiogenic Therapy. *Cancer Res* 78, 3220–3232. <https://doi.org/10.1158/0008-5472.CAN-17-3415>
- Benci, J.L., Xu, B., Qiu, Y., Wu, T.J., Dada, H., Twyman-Saint Victor, C., Cucolo, L., Lee, D.S.M., Pauken, K.E., Huang, A.C., Gangadhar,

T.C., Amaravadi, R.K., Schuchter, L.M., Feldman, M.D., Ishwaran, H., Vonderheide, R.H., Maity, A., Wherry, E.J., Minn, A.J., 2016. Tumor Interferon Signaling Regulates a Multigenic Resistance Program to Immune Checkpoint Blockade. *Cell* 167, 1540-1554.e12. <https://doi.org/10.1016/j.cell.2016.11.022>

Bhatt, S., Qin, J., Bennett, C., Qian, S., Fung, J.J., Hamilton, T.A., Lu, L., 2014. All-trans Retinoic Acid Induces Arginase-1 and Inducible Nitric Oxide Synthase–Producing Dendritic Cells with T Cell Inhibitory Function. *The Journal of Immunology* 192, 5098–5108. <https://doi.org/10.4049/jimmunol.1303073>

Bhattacharya, N., Yuan, R., Prestwood, T.R., Penny, H.L., DiMaio, M.A., Reticker-Flynn, N.E., Krois, C.R., Kenkel, J.A., Pham, T.D., Carmi, Y., Tolentino, L., Choi, O., Hulett, R., Wang, J., Winer, D.A., Napoli, J.L., Engleman, E.G., 2016. Normalizing Microbiota-Induced Retinoic Acid Deficiency Stimulates Protective CD8 + T Cell-Mediated Immunity in Colorectal Cancer. *Immunity* 45, 641–655. <https://doi.org/10.1016/j.immuni.2016.08.008>

Binnewies, M., Roberts, E.W., Kersten, K., Chan, V., Fearon, D.F., Merad, M., Coussens, L.M., Gaborit, D.I., Ostrand-Rosenberg, S., Hedrick, C.C., Vonderheide, R.H., Pittet, M.J., Jain, R.K., Zou, W., Howcroft, T.K., Woodhouse, E.C., Weinberg, R.A., Krummel, M.F., 2018. Understanding the tumor immune microenvironment (TIME)



for effective therapy. *Nature Medicine* 24, 541.

<https://doi.org/10.1038/s41591-018-0014-x>

Blay, J.-Y., Ray-Coquard, I., 2016. Sarcoma in 2016: Evolving biological understanding and treatment of sarcomas. *Nature Reviews Clinical Oncology* 14, 78–80. <https://doi.org/10.1038/nrclinonc.2016.200>

Briseño, C.G., Haldar, M., Kretzer, N.M., Wu, X., Theisen, D.J., Kc, W., Durai, V., Grajales-Reyes, G.E., Iwata, A., Bagadia, P., Murphy, T.L., Murphy, K.M., 2016a. Distinct Transcriptional Programs Control Cross-Priming in Classical and Monocyte-Derived Dendritic Cells. *Cell Reports* 15, 2462–2474.

<https://doi.org/10.1016/j.celrep.2016.05.025>

Briseño, C.G., Haldar, M., Kretzer, N.M., Wu, X., Theisen, D.J., Kc, W., Durai, V., Grajales-Reyes, G.E., Iwata, A., Bagadia, P., Murphy, T.L., Murphy, K.M., 2016b. Distinct Transcriptional Programs Control Cross-Priming in Classical and Monocyte-Derived Dendritic Cells. *Cell Reports* 15, 2462–2474.

<https://doi.org/10.1016/j.celrep.2016.05.025>

Broz, M.L., Binnewies, M., Boldajipour, B., Nelson, A.E., Pollack, J.L., Erle, D.J., Barczak, A., Rosenblum, M.D., Daud, A., Barber, D.L., Amigorena, S., van't Veer, L.J., Sperling, A.I., Wolf, D.M., Krummel, M.F., 2014. Dissecting the Tumor Myeloid Compartment Reveals Rare Activating Antigen-Presenting Cells Critical for T Cell

Immunity. *Cancer Cell* 26, 638–652.

<https://doi.org/10.1016/j.ccell.2014.09.007>

Broz, M.L., Krummel, M.F., 2015. The Emerging Understanding of Myeloid Cells as Partners and Targets in Tumor Rejection. *Cancer Immunol Res* 3, 313–319. <https://doi.org/10.1158/2326-6066.CIR-15-0041>

Chandrashekar, D.S., Bashel, B., Balasubramanya, S.A.H., Creighton, C.J., Ponce-Rodriguez, I., Chakravarthi, B.V.S.K., Varambally, S., 2017. UALCAN: A Portal for Facilitating Tumor Subgroup Gene Expression and Survival Analyses. *Neoplasia* 19, 649–658. <https://doi.org/10.1016/j.neo.2017.05.002>

Chen, D.S., Mellman, I., 2013. Oncology Meets Immunology: The Cancer-Immunity Cycle. *Immunity* 39, 1–10. <https://doi.org/10.1016/j.immuni.2013.07.012>

Chiba, T., Skrypnik, N.I., Skvarca, L.B., Penchev, R., Zhang, K.X., Rochon, E.R., Fall, J.L., Paueksakon, P., Yang, H., Alford, C.E., Roman, B.L., Zhang, M.-Z., Harris, R., Hukriede, N.A., Caestecker, M.P. de, 2016. Retinoic Acid Signaling Coordinates Macrophage-Dependent Injury and Repair after AKI. *JASN* 27, 495–508. <https://doi.org/10.1681/ASN.2014111108>

Coley, W.B., 1891. CONTRIBUTION TO THE KNOWLEDGE OF SARCOMA. *Annals of Surgery* 14, 199–220.

Cubillos-Ruiz, Juan R., Silberman, P.C., Rutkowski, M.R., Chopra, S., Perales-Puchalt, A., Song, M., Zhang, S., Bettigole, S.E., Gupta,

D., Holcomb, K., Ellenson, L.H., Caputo, T., Lee, A.-H., Conejo-Garcia, J.R., Glimcher, L.H., 2015. ER Stress Sensor XBP1 Controls Anti-tumor Immunity by Disrupting Dendritic Cell Homeostasis. *Cell* 161, 1527–1538.  
<https://doi.org/10.1016/j.cell.2015.05.025>

Cubillos-Ruiz, Juan R., Silberman, P.C., Rutkowski, M.R., Chopra, S., Perales-Puchalt, A., Song, M., Zhang, S., Bettigole, S.E., Gupta, D., Holcomb, K., Ellenson, L.H., Caputo, T., Lee, A.-H., Conejo-Garcia, J.R., Glimcher, L.H., 2015. ER Stress Sensor XBP1 Controls Anti-tumor Immunity by Disrupting Dendritic Cell Homeostasis. *Cell* 161, 1527–1538.  
<https://doi.org/10.1016/j.cell.2015.05.025>

Daro, E., Pulendran, B., Brasel, K., Teepe, M., Pettit, D., Lynch, D.H., Vremec, D., Robb, L., Shortman, K., McKenna, H.J., Maliszewski, C.R., Maraskovsky, E., 2000. Polyethylene Glycol-Modified GM-CSF Expands CD11b<sup>high</sup>CD11c<sup>high</sup> But Not CD11b<sup>low</sup>CD11c<sup>high</sup> Murine Dendritic Cells In Vivo: A Comparative Analysis with Flt3 Ligand. *The Journal of Immunology* 165, 49–58.  
<https://doi.org/10.4049/jimmunol.165.1.49>

Duester, G., 2017. Retinoic acid's reproducible future. *Science* 358, 1395–1395. <https://doi.org/10.1126/science.aar6752>

- Duester, G., 2008. Retinoic Acid Synthesis and Signaling during Early Organogenesis. *Cell* 134, 921–931.  
<https://doi.org/10.1016/j.cell.2008.09.002>
- Dunn, G.P., Old, L.J., Schreiber, R.D., 2004. The Three Es of Cancer Immunoediting. *Annual Review of Immunology* 22, 329–360.  
<https://doi.org/10.1146/annurev.immunol.22.012703.104803>
- Ehnman, M., Larsson, O., 2015. Microenvironmental Targets in Sarcoma. *Front Oncol* 5. <https://doi.org/10.3389/fonc.2015.00248>
- Erkelens, M.N., Mebius, R.E., 2017. Retinoic Acid and Immune Homeostasis: A Balancing Act. *Trends in Immunology* 38, 168–180.  
<https://doi.org/10.1016/j.it.2016.12.006>
- Franklin, R.A., Li, M.O., 2016. Ontogeny of Tumor-Associated Macrophages and Its Implication in Cancer Regulation. *Trends in Cancer* 2, 20–34. <https://doi.org/10.1016/j.trecan.2015.11.004>
- Fridman, W.H., Pagès, F., Sautès-Fridman, C., Galon, J., 2012. The immune contexture in human tumours: impact on clinical outcome. *Nature Reviews Cancer* 12, 298–306.  
<https://doi.org/10.1038/nrc3245>
- Fuertes, M.B., Kacha, A.K., Kline, J., Woo, S.-R., Kranz, D.M., Murphy, K.M., Gajewski, T.F., 2011. Host type I IFN signals are required for antitumor CD8<sup>+</sup> T cell responses through CD8 $\alpha$ <sup>+</sup> dendritic cells. *J. Exp. Med.* 208, 2005–2016.  
<https://doi.org/10.1084/jem.20101159>

- Ghosn, M., Rassy, E.E., Kourie, H.R., 2017. Immunotherapies in sarcoma: Updates and future perspectives. *World Journal of Clinical Oncology* 8, 145–150. <https://doi.org/10.5306/wjco.v8.i2.145>
- Ginestier, C., Wicinski, J., Cervera, N., Monville, F., Finetti, P., Bertucci, F., Wicha, M.S., Birnbaum, D., Charafe-Jauffret, E., 2009. Retinoid signaling regulates breast cancer stem cell differentiation. *Cell Cycle* 8, 3297–3302.
- Ginhoux, F., Jung, S., 2014. Monocytes and macrophages: developmental pathways and tissue homeostasis. *Nature Reviews Immunology* 14, 392–404. <https://doi.org/10.1038/nri3671>
- Goudot, C., Coillard, A., Villani, A.-C., Gueguen, P., Cros, A., Sarkizova, S., Tang-Huau, T.-L., Bohec, M., Baulande, S., Hacohen, N., Amigorena, S., Segura, E., 2017. Aryl Hydrocarbon Receptor Controls Monocyte Differentiation into Dendritic Cells versus Macrophages. *Immunity* 47, 582-596.e6. <https://doi.org/10.1016/j.immuni.2017.08.016>
- Greter, M., Helft, J., Chow, A., Hashimoto, D., Mortha, A., Agudo-Cantero, J., Bogunovic, M., Gautier, E.L., Miller, J., Leboeuf, M., Lu, G., Aloman, C., Brown, B.D., Pollard, J.W., Xiong, H., Randolph, G.J., Chipuk, J.E., Frenette, P.S., Merad, M., 2012. GM-CSF Controls Nonlymphoid Tissue Dendritic Cell Homeostasis but Is Dispensable for the Differentiation of Inflammatory Dendritic Cells. *Immunity* 36, 1031–1046. <https://doi.org/10.1016/j.immuni.2012.03.027>

Gubin, M.M., Esaulova, E., Ward, J.P., Malkova, O.N., Runci, D., Wong, P., Noguchi, T., Arthur, C.D., Meng, W., Alspach, E., Medrano, R.F.V., Fronick, C., Fehlings, M., Newell, E.W., Fulton, R.S., Sheehan, K.C.F., Oh, S.T., Schreiber, R.D., Artyomov, M.N., 2018. High-Dimensional Analysis Delineates Myeloid and Lymphoid Compartment Remodeling during Successful Immune-Checkpoint Cancer Therapy. *Cell* 175, 1014-1030.e19. <https://doi.org/10.1016/j.cell.2018.09.030>

Gundra, U.M., Girgis, N.M., Gonzalez, M.A., San Tang, M., Van Der Zande, H.J.P., Lin, J.-D., Ouimet, M., Ma, L.J., Poles, J., Vozhilla, N., Fisher, E.A., Moore, K.J., Loke, P., 2017. Vitamin A mediates conversion of monocyte-derived macrophages into tissue-resident macrophages during alternative activation. *Nat. Immunol.* 18, 642–653. <https://doi.org/10.1038/ni.3734>

Haldar, M., Hancock, J.D., Coffin, C.M., Lessnick, S.L., Capecchi, M.R., 2007. A Conditional Mouse Model of Synovial Sarcoma: Insights into a Myogenic Origin. *Cancer Cell* 11, 375–388. <https://doi.org/10.1016/j.ccr.2007.01.016>

Haldar, M., Kohyama, M., So, A.Y.-L., Kc, W., Wu, X., Briseño, C.G., Satpathy, A.T., Kretzer, N.M., Arase, H., Rajasekaran, N.S., Wang, L., Egawa, T., Igarashi, K., Baltimore, D., Murphy, T.L., Murphy, K.M., 2014. Heme-Mediated SPI-C Induction Promotes Monocyte

- Differentiation into Iron-Recycling Macrophages. *Cell* 156, 1223–1234. <https://doi.org/10.1016/j.cell.2014.01.069>
- Haldar, M., Murphy, K.M., 2014. Origin, development, and homeostasis of tissue-resident macrophages. *Immunol. Rev.* 262, 25–35. <https://doi.org/10.1111/imr.12215>
- Helft, J., Böttcher, J., Chakravarty, P., Zelenay, S., Huotari, J., Schraml, B.U., Goubau, D., Reis e Sousa, C., 2015. GM-CSF Mouse Bone Marrow Cultures Comprise a Heterogeneous Population of CD11c+MHCII+ Macrophages and Dendritic Cells. *Immunity* 42, 1197–1211. <https://doi.org/10.1016/j.immuni.2015.05.018>
- Herber, D.L., Cao, W., Nefedova, Y., Novitskiy, S.V., Nagaraj, S., Tyurin, V.A., Corzo, A., Cho, H.-I., Celis, E., Lennox, B., Knight, S.C., Padhya, T., McCaffrey, T.V., McCaffrey, J.C., Antonia, S., Fishman, M., Ferris, R.L., Kagan, V.E., Gabilovich, D.I., 2010. Lipid accumulation and dendritic cell dysfunction in cancer. *Nature Medicine* 16, 880–886. <https://doi.org/10.1038/nm.2172>
- Hildner, K., Edelson, B.T., Purtha, W.E., Diamond, M., Matsushita, H., Kohyama, M., Calderon, B., Schraml, B.U., Unanue, E.R., Diamond, M.S., Schreiber, R.D., Murphy, T.L., Murphy, K.M., 2008a. Batf3 deficiency reveals a critical role for CD8alpha+ dendritic cells in cytotoxic T cell immunity. *Science* 322, 1097–1100. <https://doi.org/10.1126/science.1164206>

- Hildner, K., Edelson, B.T., Purtha, W.E., Diamond, M., Matsushita, H., Kohyama, M., Calderon, B., Schraml, B.U., Unanue, E.R., Diamond, M.S., Schreiber, R.D., Murphy, T.L., Murphy, K.M., 2008b. Batf3 Deficiency Reveals a Critical Role for CD8 $\alpha$ + Dendritic Cells in Cytotoxic T Cell Immunity. *Science* 322, 1097–1100. <https://doi.org/10.1126/science.1164206>
- Hill, J.A., Hall, J.A., Sun, C.-M., Cai, Q., Ghyselinck, N., Chambon, P., Belkaid, Y., Mathis, D., Benoist, C., 2008. Retinoic acid enhances Foxp3 induction indirectly by relieving inhibition from CD4+CD44hi Cells. *Immunity* 29, 758–770. <https://doi.org/10.1016/j.immuni.2008.09.018>
- Jin, C.-J., Hong, C.Y., Takei, M., Chung, S.-Y., Park, J.-S., Pham, T.-N.N., Choi, S.-J.-N., Nam, J.-H., Chung, I.-J., Kim, H.-J., Lee, J.-J., 2010. All-trans retinoic acid inhibits the differentiation, maturation, and function of human monocyte-derived dendritic cells. *Leukemia Research* 34, 513–520. <https://doi.org/10.1016/j.leukres.2009.10.006>
- Kane, M.A., Folias, A.E., Wang, C., Napoli, J.L., 2008. Quantitative Profiling of Endogenous Retinoic Acid in Vivo and in Vitro by Tandem Mass Spectrometry. *Anal Chem* 80, 1702–1708. <https://doi.org/10.1021/ac702030f>
- Kaneda, M.M., Messer, K.S., Ralainirina, N., Li, H., Leem, C.J., Gorjestani, S., Woo, G., Nguyen, A.V., Figueiredo, C.C., Foubert,



P., Schmid, M.C., Pink, M., Winkler, D.G., Rausch, M., Palombella, V.J., Kutok, J., McGovern, K., Frazer, K.A., Wu, X., Karin, M., Sasik, R., Cohen, E.E.W., Varner, J.A., 2016. PI3K $\gamma$  is a molecular switch that controls immune suppression. *Nature* 539, 437–442.  
<https://doi.org/10.1038/nature19834>

Khoury, T., Ademuyiwa, F.O., Chandraseekhar, R., Jabbour, M., DeLeo, A., Ferrone, S., Wang, Y., Wang, X., 2012. Aldehyde dehydrogenase 1A1 expression in breast cancer is associated with stage, triple negativity, and outcome to neoadjuvant chemotherapy. *Modern Pathology* 25, 388–397.  
<https://doi.org/10.1038/modpathol.2011.172>

Kirsch, D.G., Dinulescu, D.M., Miller, J.B., Grimm, J., Santiago, P.M., Young, N.P., Nielsen, G.P., Quade, B.J., Chaber, C.J., Schultz, C.P., Takeuchi, O., Bronson, R.T., Crowley, D., Korsmeyer, S.J., Yoon, S.S., Hornicek, F.J., Weissleder, R., Jacks, T., 2007. A spatially and temporally restricted mouse model of soft tissue sarcoma. *Nature Medicine* 13, 992–997.  
<https://doi.org/10.1038/nm1602>

Klebanoff, C.A., Spencer, S.P., Torabi-Parizi, P., Grainger, J.R., Roychoudhuri, R., Ji, Y., Sukumar, M., Muranski, P., Scott, C.D., Hall, J.A., Ferreyra, G.A., Leonardi, A.J., Borman, Z.A., Wang, J., Palmer, D.C., Wilhelm, C., Cai, R., Sun, J., Napoli, J.L., Danner, R.L., Gattinoni, L., Belkaid, Y., Restifo, N.P., 2013. Retinoic acid

controls the homeostasis of pre-cDC–derived splenic and intestinal dendritic cells. *Journal of Experimental Medicine* 210, 1961–1976.

<https://doi.org/10.1084/jem.20122508>

Kuhn, S., Hyde, E.J., Yang, J., Rich, F.J., Harper, J.L., Kirman, J.R., Ronchese, F., 2013. Increased Numbers of Monocyte-Derived Dendritic Cells during Successful Tumor Immunotherapy with Immune-Activating Agents. *The Journal of Immunology* 191, 1984–1992. <https://doi.org/10.4049/jimmunol.1301135>

Kuhn, S., Yang, J., Ronchese, F., 2015. Monocyte-Derived Dendritic Cells Are Essential for CD8+ T Cell Activation and Antitumor Responses After Local Immunotherapy. *Front. Immunol.* 6.

<https://doi.org/10.3389/fimmu.2015.00584>

Kumar, S., Sandell, L.L., Trainor, P.A., Koentgen, F., Duyster, G., 2012. Alcohol and Aldehyde Dehydrogenases: Retinoid Metabolic Effects in Mouse Knockout Models. *Biochim Biophys Acta* 1821, 198–205.

<https://doi.org/10.1016/j.bbailip.2011.04.004>

Kumar, V., Cheng, P., Condamine, T., Mony, S., Languino, L.R., McCaffrey, J.C., Hockstein, N., Guarino, M., Masters, G., Penman, E., Denstman, F., Xu, X., Altieri, D.C., Du, H., Yan, C., Gabilovich, D.I., 2016. CD45 Phosphatase Inhibits STAT3 Transcription Factor Activity in Myeloid Cells and Promotes Tumor-Associated

Macrophage Differentiation. *Immunity* 44, 303–315.

<https://doi.org/10.1016/j.immuni.2016.01.014>

- Laoui, D., Van Overmeire, E., Movahedi, K., Van den Bossche, J., Schouppe, E., Mommer, C., Nikolaou, A., Morias, Y., De Baetselier, P., Van Ginderachter, J.A., 2011. Mononuclear phagocyte heterogeneity in cancer: Different subsets and activation states reaching out at the tumor site. *Immunobiology, EMDS Special Issue: Systems Biology of Macrophages and Dendritic Cells in Health and Disease* 216, 1192–1202.  
<https://doi.org/10.1016/j.imbio.2011.06.007>
- Lehtonen, A., Veckman, V., Nikula, T., Lahesmaa, R., Kinnunen, L., Matikainen, S., Julkunen, I., 2005. Differential Expression of IFN Regulatory Factor 4 Gene in Human Monocyte-Derived Dendritic Cells and Macrophages. *The Journal of Immunology* 175, 6570–6579. <https://doi.org/10.4049/jimmunol.175.10.6570>
- Li, T., Su, Y., Mei, Y., Leng, Q., Leng, B., Liu, Z., Stass, S.A., Jiang, F., 2010. ALDH1A1 is a marker for malignant prostate stem cells and predictor of prostate cancer patients' outcome. *Laboratory Investigation* 90, 234–244.  
<https://doi.org/10.1038/labinvest.2009.127>
- Li, X., Xu, Q., Fu, X., Luo, W., 2014. ALDH1A1 overexpression is associated with the progression and prognosis in gastric cancer. *BMC Cancer* 14, 705. <https://doi.org/10.1186/1471-2407-14-705>
- Lim, S.Y., Yuzhalin, A.E., Gordon-Weeks, A.N., Muschel, R.J., 2016. Tumor-infiltrating monocytes/macrophages promote tumor invasion

and migration by upregulating S100A8 and S100A9 expression in cancer cells. *Oncogene* 35, 5735–5745.

<https://doi.org/10.1038/onc.2016.107>

Linch, M., Miah, A.B., Thway, K., Judson, I.R., Benson, C., 2014.

Systemic treatment of soft-tissue sarcoma—gold standard and novel therapies. *Nature Reviews Clinical Oncology* 11, 187–202.

<https://doi.org/10.1038/nrclinonc.2014.26>

Ma, Y., Adjemian, S., Mattarollo, S.R., Yamazaki, T., Aymeric, L., Yang, H., Portela Catani, J.P., Hannani, D., Duret, H., Steegh, K., Martins, I., Schlemmer, F., Michaud, M., Kepp, O., Sukkurwala, A.Q., Menger, L., Vacchelli, E., Droin, N., Galluzzi, L., Krzysiek, R., Gordon, S., Taylor, P.R., Van Endert, P., Solary, E., Smyth, M.J., Zitvogel, L., Kroemer, G., 2013. Anticancer Chemotherapy-Induced Intratumoral Recruitment and Differentiation of Antigen-Presenting Cells. *Immunity* 38, 729–741.

<https://doi.org/10.1016/j.immuni.2013.03.003>

Mach, N., Gillessen, S., Wilson, S.B., Sheehan, C., Mihm, M., Dranoff, G., 2000. Differences in Dendritic Cells Stimulated in Vivo by Tumors Engineered to Secrete Granulocyte-Macrophage Colony-stimulating Factor or Flt3-Ligand. *Cancer Res* 60, 3239–3246.

Marcato, P., Dean, C.A., Liu, R.-Z., Coyle, K.M., Bydoun, M., Wallace, M., Clements, D., Turner, C., Mathenge, E.G., Gujar, S.A., Giacomantonio, C.A., Mackey, J.R., Godbout, R., Lee, P.W.K.,

2015. Aldehyde dehydrogenase 1A3 influences breast cancer progression via differential retinoic acid signaling. *Molecular Oncology* 9, 17–31. <https://doi.org/10.1016/j.molonc.2014.07.010>
- Marigo, I., Zilio, S., Desantis, G., Mlecnik, B., Agnellini, A.H.R., Ugel, S., Sasso, M.S., Qualls, J.E., Kratochvill, F., Zanovello, P., Molon, B., Ries, C.H., Runza, V., Hoves, S., Bilocq, A.M., Bindea, G., Mazza, E.M.C., Bicciano, S., Galon, J., Murray, P.J., Bronte, V., 2016. T Cell Cancer Therapy Requires CD40-CD40L Activation of Tumor Necrosis Factor and Inducible Nitric-Oxide-Synthase-Producing Dendritic Cells. *Cancer Cell* 30, 377–390. <https://doi.org/10.1016/j.ccell.2016.08.004>
- McCormick, S.M., Heller, N.M., 2015. Commentary: IL-4 and IL-13 receptors and signaling. *Cytokine, IL 4/IL 13 family* 75, 38–50. <https://doi.org/10.1016/j.cyto.2015.05.023>
- Menezes, S., Melandri, D., Anselmi, G., Perchet, T., Loschko, J., Dubrot, J., Patel, R., Gautier, E.L., Hugues, S., Longhi, M.P., Henry, J.Y., Quezada, S.A., Lauvau, G., Lennon-Duménil, A.-M., Gutiérrez-Martínez, E., Bessis, A., Gomez-Perdiguero, E., Jacome-Galarza, C.E., Garner, H., Geissmann, F., Golub, R., Nussenzweig, M.C., Guérmonprez, P., 2016. The Heterogeneity of Ly6Chi Monocytes Controls Their Differentiation into iNOS+ Macrophages or Monocyte-Derived Dendritic Cells. *Immunity* 45, 1205–1218. <https://doi.org/10.1016/j.immuni.2016.12.001>

- Merad, M., Sathe, P., Helft, J., Miller, J., Mortha, A., 2013. The Dendritic Cell Lineage: Ontogeny and Function of Dendritic Cells and Their Subsets in the Steady State and the Inflamed Setting. *Annual Review of Immunology* 31, 563–604.  
<https://doi.org/10.1146/annurev-immunol-020711-074950>
- Mildner, A., Jung, S., 2014a. Development and function of dendritic cell subsets. *Immunity* 40, 642–656.  
<https://doi.org/10.1016/j.immuni.2014.04.016>
- Mildner, A., Jung, S., 2014b. Development and Function of Dendritic Cell Subsets. *Immunity* 40, 642–656.  
<https://doi.org/10.1016/j.immuni.2014.04.016>
- Mohty, M., Morbelli, S., Isnardon, D., Sainty, D., Arnoulet, C., Gaugler, B., Olive, D., 2003. All-trans retinoic acid skews monocyte differentiation into interleukin-12-secreting dendritic-like cells. *British Journal of Haematology* 122, 829–836.  
<https://doi.org/10.1046/j.1365-2141.2003.04489.x>
- Motz, G.T., Coukos, G., 2013. Deciphering and Reversing Tumor Immune Suppression. *Immunity* 39, 61–73.  
<https://doi.org/10.1016/j.immuni.2013.07.005>
- Nefedova, Y., Fishman, M., Sherman, S., Wang, X., Beg, A.A., Gaborilovich, D.I., 2007. Mechanism of All-Trans Retinoic Acid Effect on Tumor-Associated Myeloid-Derived Suppressor Cells. *Cancer*

Res 67, 11021–11028. <https://doi.org/10.1158/0008-5472.CAN-07-2593>

Noy, R., Pollard, J.W., 2014. Tumor-Associated Macrophages: From Mechanisms to Therapy. *Immunity* 41, 49–61.  
<https://doi.org/10.1016/j.immuni.2014.06.010>

Okabe, Y., Medzhitov, R., 2014. Tissue-Specific Signals Control Reversible Program of Localization and Functional Polarization of Macrophages. *Cell* 157, 832–844.  
<https://doi.org/10.1016/j.cell.2014.04.016>

Olingy, C.E., Dinh, H.Q., Hedrick, C.C., 2019. Monocyte heterogeneity and functions in cancer. *Journal of Leukocyte Biology* 0.  
<https://doi.org/10.1002/JLB.4RI0818-311R>

Qian, B.-Z., Pollard, J.W., 2010. Macrophage Diversity Enhances Tumor Progression and Metastasis. *Cell* 141, 39–51.  
<https://doi.org/10.1016/j.cell.2010.03.014>

Rich, F.J., Kuhn, S., Hyde, E.J., Harper, J.L., Ronchese, F., Kirman, J.R., 2012. Induction of T cell responses and recruitment of an inflammatory dendritic cell subset following tumor immunotherapy with *Mycobacterium smegmatis*. *Cancer Immunol Immunother* 61, 2333–2342. <https://doi.org/10.1007/s00262-012-1291-8>

Richards, D.M., Hettinger, J., Feuerer, M., 2012. Monocytes and Macrophages in Cancer: Development and Functions. *Cancer*

Microenviron 6, 179–191. <https://doi.org/10.1007/s12307-012-0123-x>

Salmon, H., Remark, R., Gnjatic, S., Merad, M., 2019. Host tissue determinants of tumour immunity. *Nature Reviews Cancer* 19, 215. <https://doi.org/10.1038/s41568-019-0125-9>

Satpathy, A.T., KC, W., Albring, J.C., Edelson, B.T., Kretzer, N.M., Bhattacharya, D., Murphy, T.L., Murphy, K.M., 2012. Zbtb46 expression distinguishes classical dendritic cells and their committed progenitors from other immune lineages. *J Exp Med* 209, 1135–1152. <https://doi.org/10.1084/jem.20120030>

Schreiber, T.H., Podack, E.R., 2009. A critical analysis of the tumour immunosurveillance controversy for 3-MCA-induced sarcomas. *British Journal of Cancer* 101, 381–386. <https://doi.org/10.1038/sj.bjc.6605198>

Segura, E., Amigorena, S., 2013. Inflammatory dendritic cells in mice and humans. *Trends in Immunology* 34, 440–445. <https://doi.org/10.1016/j.it.2013.06.001>

Segura, E., Touzot, M., Bohineust, A., Cappuccio, A., Chiochia, G., Hosmalin, A., Dalod, M., Soumelis, V., Amigorena, S., 2013. Human Inflammatory Dendritic Cells Induce Th17 Cell Differentiation. *Immunity* 38, 336–348. <https://doi.org/10.1016/j.immuni.2012.10.018>



- Spranger, S., Bao, R., Gajewski, T.F., 2015a. Melanoma-intrinsic  $\beta$ -catenin signalling prevents anti-tumour immunity. *Nature* 523, 231–235. <https://doi.org/10.1038/nature14404>
- Spranger, S., Bao, R., Gajewski, T.F., 2015b. Melanoma-intrinsic  $\beta$ -catenin signalling prevents anti-tumour immunity. *Nature* 523, 231–235. <https://doi.org/10.1038/nature14404>
- Suzuki, A., Leland, P., Joshi, B.H., Puri, R.K., 2015. Targeting of IL-4 and IL-13 receptors for cancer therapy. *Cytokine, IL 4/IL 13 family* 75, 79–88. <https://doi.org/10.1016/j.cyto.2015.05.026>
- Tang, X.-H., Gudas, L.J., 2011. Retinoids, Retinoic Acid Receptors, and Cancer. *Annual Review of Pathology: Mechanisms of Disease* 6, 345–364. <https://doi.org/10.1146/annurev-pathol-011110-130303>
- Taylor, B.S., Barretina, J., Maki, R.G., Antonescu, C.R., Singer, S., Ladanyi, M., 2011. Advances in sarcoma genomics and new therapeutic targets. *Nature Reviews Cancer* 11, 541. <https://doi.org/10.1038/nrc3087>
- Theisen, D.J., Davidson, J.T., Briseño, C.G., Gargaro, M., Lauron, E.J., Wang, Q., Desai, P., Durai, V., Bagadia, P., Brickner, J.R., Beatty, W.L., Virgin, H.W., Gillanders, W.E., Mosammaparast, N., Diamond, M.S., Sibley, L.D., Yokoyama, W., Schreiber, R.D., Murphy, T.L., Murphy, K.M., 2018. WDFY4 is required for cross-presentation in response to viral and tumor antigens. *Science* 362, 694–699. <https://doi.org/10.1126/science.aat5030>

van den Boorn, J.G., Hartmann, G., 2013. Turning Tumors into Vaccines: Co-opting the Innate Immune System. *Immunity* 39, 27–37.

<https://doi.org/10.1016/j.immuni.2013.07.011>

Veglia, F., Gabrilovich, D.I., 2017. Dendritic cells in cancer: the role revisited. *Current Opinion in Immunology, Lymphocyte development and activation \* Tumour immunology* 45, 43–51.

<https://doi.org/10.1016/j.coi.2017.01.002>

Veglia, F., Tyurin, V.A., Blasi, M., Leo, A.D., Kossenkov, A.V., Donthireddy, L., To, T.K.J., Schug, Z., Basu, S., Wang, F., Ricciotti, E., DiRusso, C., Murphy, M.E., Vonderheide, R.H., Lieberman, P.M., Mulligan, C., Nam, B., Hockstein, N., Masters, G., Guarino, M., Lin, C., Nefedova, Y., Black, P., Kagan, V.E., Gabrilovich, D.I., 2019. Fatty acid transport protein 2 reprograms neutrophils in cancer. *Nature* 569, 73. <https://doi.org/10.1038/s41586-019-1118-2>

Vellozo, N.S., Pereira-Marques, S.T., Cabral-Piccin, M.P., Filardy, A.A., Ribeiro-Gomes, F.L., Rigoni, T.S., DosReis, G.A., Lopes, M.F., 2017. All-Trans Retinoic Acid Promotes an M1- to M2-Phenotype Shift and Inhibits Macrophage-Mediated Immunity to *Leishmania major*. *Front. Immunol.* 8. <https://doi.org/10.3389/fimmu.2017.01560>

Vinay, D.S., Ryan, E.P., Pawelec, G., Talib, W.H., Stagg, J., Elkord, E., Lichtor, T., Decker, W.K., Whelan, R.L., Kumara, H.M.C.S., Signori, E., Honoki, K., Georgakilas, A.G., Amin, A., Helferich, W.G., Boosani, C.S., Guha, G., Ciriolo, M.R., Chen, S., Mohammed, S.I.,

- Azmi, A.S., Keith, W.N., Bilsland, A., Bhakta, D., Halicka, D., Fujii, H., Aquilano, K., Ashraf, S.S., Nowsheen, S., Yang, X., Choi, B.K., Kwon, B.S., 2015. Immune evasion in cancer: Mechanistic basis and therapeutic strategies. *Seminars in Cancer Biology*, A broad-spectrum integrative design for cancer prevention and therapy 35, S185–S198. <https://doi.org/10.1016/j.semcancer.2015.03.004>
- Wei, D., Peng, J.-J., Gao, H., Zhang, T., Tan, Y., Hu, Y.-H., 2015. ALDH1 Expression and the Prognosis of Lung Cancer: A Systematic Review and Meta-Analysis. *Heart, Lung and Circulation* 24, 780–788. <https://doi.org/10.1016/j.hlc.2015.03.021>
- Zhang, W., Yan, W., You, G., Bao, Z., Wang, Y., Liu, Y., You, Y., Jiang, T., 2013. Genome-wide DNA methylation profiling identifies ALDH1A3 promoter methylation as a prognostic predictor in G-CIMP- primary glioblastoma. *Cancer Letters* 328, 120–125. <https://doi.org/10.1016/j.canlet.2012.08.033>
- Zou, W., 2005. Immunosuppressive networks in the tumour environment and their therapeutic relevance. *Nature Reviews Cancer* 5, 263–274. <https://doi.org/10.1038/nrc1586>